EUROPEAN AVIATION SAFETY AGENCY
AGENCE EUROPÉENNE DE LA SÉCURITÉ AÉRIENNE
EUROPÄISCHE AGENTUR FÜR FLUGSICHERHEIT

Research project EASA.2008/OP13

Studying, sAmpling and Measuring of aircraft ParticuLate Emissions I (SAMPLE I)

23 October 2009

easa.europa.eu

EASA.2008.OP.13

Study on sampling and measurement of aircraft particulate emissions SAMPLE – Final Report

23 October 2009

Lead Authors:

A. Petzold [1] and R. Marsh [2]

Contributing Authors

M. Johnson [3], M. Miller [4], Y. Sevcenco [2], D. Delhaye [5], X. Vancassel [5], A. Ibrahim [1], A. Veira [1], P. Williams [6], H. Bauer [7], A. Crayford [2], S. Morris [2], P. Kay [2], P. Bowen [2], W.D. Bachalo [8], D. Raper [9]

[1] Institute of Atmospheric Physics, DLR Oberpfaffenhofen, 82234 Wessling, Germany

[2] Cardiff University, School of Engineering, Cardiff, UK

[3] Rolls-Royce plc, Derby DE24 8BJ, UK

[4] QinetiQ, Cody Technology Park, Farnborough Hants, GU14 OLX, UK

[5] ONERA, 92320 Chatillon, France

[6] Centre for Atmospheric Science (CAS), University of Manchester, Manchester, M13 9PL, UK

[7] Vienna University of Technology, 1060 Vienna, Austria

[8] Artium Technologies, Sunnyvale, CA 94086, USA

[9] Manchester Metropolitan University, Manchester M15GD, UK

This page is intentionally blank.

Table of Contents

Disclaimer

Acknowledgment

EASA would like to acknowledge the support and collaboration in the SAMPLE project from the UK Department of Transport, the EU FP6 Network of Excellence on Environmentally Compatible Air Transport System (ECATS) and the UK academic partnership OMEGA.

This page is intentionally blank.

Executive Summary

This report covers the work undertaken on the "Study on Sampling and Measurement of Aircraft Particulate Emissions (SAMPLE)" project. Methods for measuring particle mass concentration and composition, particle number concentration and particle size distribution were tested and evaluated under real conditions with respect to their applicability for aircraft engine exhaust certification applications.

The work performed in SAMPLE used the Combustor – Hot End Simulator test rig at Cardiff University, UK, which was initially developed during the European FP5 programme PARTEMIS. This test rig served as a stable aircraft engine simulator providing particles of physical-chemical properties similar to real aircraft engines.

The Combustor - HES operation conditions were designed such that the physico-chemical properties of the generated combustion aerosol cover the widest possible range from low smoke emissions associated with high organic matter emissions to high smoke emissions associated with low organic matter emissions. The operation conditions chosen for the SAMPLE runs do not refer to any real engine ICAO LTO cycle operational conditions.

Key results and conclusions from the SAMPLE study are:

Mass-based methods:

1. Total mass from the gravimetry method exceeds all other mass measurements.
2. Total mass determined from the sum of the major chemical constituents balances the gravimetric mass. The constituents include elemental carbon, organic matter (= organic carbon plus an estimate for oxygen and hydrogen contents of organic matter) and an estimate of sulphate from the fuel sulphur content.
3. In general, total non-volatile carbon from the 2-Step Combustion method agrees well with total non-volatile mass data calculated from the SN equation within FOA 3 (±10%) as long as the organic carbon content is small. However, as this non-volatile part of FOA 3 does not account all of the organic matter, it can underestimate total carbon mass by approx. 40% where particulate matter contains a high organic matter fraction.
4. The non-volatile part of FOA 3 has an even greater underestimation of gravimetric mass (19 to 53%), depending on the organic carbon fraction. Neither the oxygen and hydrogen contributions to organic matter fraction, nor sulphate, are recovered by the non-volatile part of FOA 3.
5. Elemental carbon from 2-Step Combustion and black carbon from absorption photometry (MAAP) are in close agreement. The particulate matter fraction detected by these methods contributes 35 to 70% to total mass from gravimetry. This ratio is a measure for the underestimation of total mass if light-absorbing black carbon or elemental carbon is used as a proxy for non-volatile particulate mass.

6. Multi-Angle Absorption Photometry as an on-line instrument measuring light absorbing carbon (black carbon) proved successful and well applicable to exhaust studies as long as the sample gas prior to the measurement is diluted. The application of high carbon loadings requires instrument modifications by the manufacturer to allow operation at lower flow rates.
7. The laser-induced incandescence technique which is capable of measuring black carbon from either undiluted or diluted exhausts in real time detected the presence of super-micron particles (sampling artefacts see 'Sampling line effects'). The existence of these large particles meant that the BC mass measurement could not be directly compared with other methods. However, statistical inclusion of the super-micron detection incidences did provide good agreement with other methodologies measuring total BC mass (see specific LII report in the Appendix B).
8. Indirect methods for measuring mass concentrations such as differential mobility spectrometers (or other size distribution instruments) appear to be of limited applicability for gas turbine particulate exhaust because they suffer from sampling limitations - inability to distinguish non-volatile/volatile composition and from the need for a priori assumptions of particle effective density and shape. In addition, their size cut-off limits the measurement of the sample line shedding phenomenon.

Number-based methods:

1. Condensation Particle Counter (CPC) based instruments are highly robust tools for the measurement of aerosol number concentrations. Dilution of sample gas prior to the measurement is required.
2. The definition of a standard method requires an agreement on the 50% detection efficiency diameter of the applied instrument. Measured non-volatile particle size distributions indicate a bi-modal size distribution with the smaller mode centred at 15 – 16 nm. Modelling results for the hot sample line indicate a volatile particle mode below 10 nm in diameter. From these results, a 50% detection efficiency diameter of 10 nm appears appropriate.
3. Indirect methods for the measurement of particle number concentrations, such as Differential Mobility Spectrometry, should not be considered as a standard methodology since they show a larger scatter of data than direct methods like condensation particle counters.

Particle size-based methods:

1. Differential Mobility Spectrometry appears to be a well reproducible method for measuring particle size distributions in aircraft engine exhaust.
2. The intercomparison between different instruments using differential mobility spectrometry was not performed within SAMPLE due to the failure of one instrument. The intercomparison of average particle sizes determined with different methods is an open issue for upcoming method evaluation studies.

Sampling line effects:

1. As indicated from sample line model results, entirely volatile particles remain small in diameter (below 10 nm). Measurements proof, that more than 90% of non-volatile combustion particles are larger than 10 nm in diameter.
2. Soot particles are affected in terms of weak particle growth which is dominated by condensation of volatile material. The increase in the particle count median diameter is less than 5 nm.
3. Particle coagulation is not a major process if the sample is sufficiently diluted.
4. Large (super-micron) black carbon particles were detected by several instruments as a function of particle shedding. These mechanically generated particles are a secondary source of soot particles that have deposited on surfaces due to thermophoretic motion and diffusion, and then re-entrained into the sample flow due to flow turbulence. This process will reach some sort of equilibrium but with uncertain shedding frequency. In order to only measure the gas turbine combustion particulates an upper cut-off size would be required to remove these shedding artefacts.

Main recommendations from the SAMPLE study are:

1. Considering the decreasing smoke level of modern aircraft engines, gravimetry as the reference method for total non-volatile PM mass measurement is limited by filter exposure time. Sample exposure times of 40 min (Table 8) and more are not practical for engine testing.
2. Carbon sensitive methods like 2-Step Combustion (off-line, filter exposure time < 15 min) or light absorption photometry (on-line, 1 Hz data resolution) offer modern and highly sensitive alternatives to gravimetry for measuring non-volatile particulate matter.
3. Considering the effect of large mechanically generated particles (shedding), an upper size cut-off limit should be applied. Gas turbine combustion produces soot particles <1 µm, therefore a 1 micron cut-off seems reasonable. However further research is required to assess this issue.
4. Precise instruments for particle number measurements are available. An agreement on the 50% detection efficiency diameter of the applied instruments is required. Based on current experience, a value of 10 nm appears appropriate.
5. Particle size distribution measurement by electrical mobility spectrometers offers a promising way forward. Intercomparison of different instruments and the definition of respective operation conditions are potential remaining issues for further research.
6. Removal of volatile and semi-volatile matter by a hot dilution system followed by a sampling line of sufficient length ensures complete removal of volatile compounds. Details in terms of residence time, i.e., line length and volumetric flow rate have yet to be specified and require further research.
7. Sample dilution is required for suppressing particle coagulation and enabling the application of current particle counting methods, on-line mass-based methods and particle sizing methods. Based on current experience, specifications for sample dilution have to be developed within further research.

This page is intentionally blank.

1 Introduction

The emission of particulate matter from aircraft engines, their potential impacts on Earth's climate and human health, and state-of-the-art methods for measuring particulate matter in aircraft engine exhaust are high up on the agenda of research activities as well as of international bodies such as ICAO, EASA and FAA [*CAEP*, 2007]. At present, the respective measure is the SAE Smoke Number [*SAE*, 1997], which is related to the darkening of particle-loaded filters by the deposited particulate matter.

Historically, the justification came from a visibility criterion for aircraft plumes. The method has been effective for the purpose for which it was developed. However, it is based on a relatively crude filter stain method and does not measure mass, distinguish between particle sizes, capture all the solid particles - especially the smaller ones, nor does it include volatile particles. Along with cleaner engines in terms of smoke and with increasing interest in an environmentally compatible air transportation system, this measure is therefore no longer regarded as appropriate for meeting current needs which focus on particle-related health effects and on climate effects via contrail and cirrus-contrail interactions. The replacement of this out-dated method and an assessment of alternative technologies is one of the key issues of this study.

Significant work has already been performed by the SAE E-31 committee in developing sampling and measurement techniques for non-volatile PM emissions from aircraft engines, including the publication of the Aerospace Information Report (AIR) 5892 [*SAE*, 2004] and the respective Technical Annexes as AIR 6037 [*SAE*, 2009]. These Annexes include detailed descriptions of techniques and methods applicable for the measurement of PM mass, number, and size.

This report covers the work undertaken on the "Study on Sampling and Measurement of Aircraft Particulate Emissions (SAMPLE)" project. The tests were undertaken in March 2009 at the Gas Turbine Research Centre (GTRC) in Port Talbot, Wales. This facility is an off-site research centre owned and operated by Cardiff University, School of Engineering. GTRC consists of two major combustion rigs each designed for detailed investigation of combustion and emissions in gas turbines. The rigs are designed for the study of different facets of the combustion process and are operated at different pressures. This rig is a multi-purpose combustion facility for combustor fundamentals research and development work. An extensive range of state-of-the-art measurement sections are available, some unique, each with different capabilities, all of which are predominately non-intrusive. Exhaust gas samples are collected and transmitted to a comprehensive on-line gas analysis suite.

The work detailed in this report was funded by the European Aviation Safety Agency (EASA). Technical leadership and project management was supplied by Deutsches Zentrum für Luft- und Raumfahrt (DLR) Oberpfaffenhofen, Germany. Project partners included Cardiff University, DLR, QinetiQ, Rolls-Royce, University of Manchester, Manchester Metropolitan University, ONERA and Vienna University of Technology.

2 Aims of SAMPLE

The key purpose of this study was to test and evaluate techniques and methods for particulate matter measurement in the exhaust of aircraft engines at engine exit operational/flight conditions. This study aimed to provide necessary information on instrument applicability and method characteristics under real-world conditions corresponding to engine certification measurements. The consortium of the proposal included associated consultants combining SAE E-31 members with strong expertise in particle measurement, engine manufacturers, and institutions active in coordinating research programmes.

This study involved services requested by EASA with current research work going on in the framework of the European Network of Excellence ECATS (Environmentally Compatible Air Transport System) and within the UK OMEGA project in order to promote European research in this area. Principally, the combustor and Hot End Simulator (HES) were therefore used as a smoke source in order to provide a sample for the measurement partners. This particular assembly was used since it was developed to provide a representative sample from a simulated gas turbine exhaust under typical flight conditions and has a proven track record in this field as it was successfully used to complete a previous research project (PARTEMIS). Thus, the smoke source should be as representative as possible without the complexity or cost of using a full engine.

According to the approach discussed with SAE-E31, this report is focusing on the SAMPLE results on measurement methods for non-volatile particulate matter. For this aerosol type measurement methods are well developed and mature so that methods can be tested under realistic conditions. The study provides results on the precision and reproducibility of methods for measuring particle mass, number, and size of non-volatile combustion particles in the exhaust of gas turbines. The additionally undertaken research on a better characterisation of volatile organic matter emitted from a combustor will be presented as well.

Important Notes:

1. **The operation conditions chosen for the SAMPLE runs DO NOT refer to any ICAO – LTO cycle operation condition of a real engine.**
2. **The Combustor - HES operation conditions were designed such that the physico-chemical properties of the generated combustion aerosol cover the widest possible range from low smoke emissions and associated high organic matter emissions to high smoke emissions and associated low organic matter emissions.**
3. **The results of this study DO NOT represent any emission conditions for real aircraft engines.**
4. **In the context of SAMPLE, volatile and semi-volatile matter is defined as any compound remaining in the particulate phase at temperatures below 350°C.**

3 Experimental Approach

3.1 Rig description

The facility upstream of the rig under consideration comprises of the main air handling and treatment hardware. Air is introduced to the combustion chamber pre-heated and at the required mass flow. Pressure is usually controlled during an experiment by a back-pressurising valve. In the case of this experiment, however, a choke-plate downstream of the combustor was used to maintain the operating pressure, see Figure 1. A compressor transfers the incoming air into a gas-fired non-vitiating heater, where it is raised to the required temperature for the test. The mass flow rate is measured using a Coriolis meter, located upstream of the rig test section.

The rig conditions are monitored and controlled from a control room, which is remote from the rig room for the purposes of safety. The operators have full control over all of the operating parameters in the experiment using a computer controlled Supervisory Control And Data Acquisition (SCADA) system. Rig and plant conditions are logged once per second and stored on the instrumentation and logging systems in the control room. This room also houses the gas analysis apparatus, which measure the gaseous compounds described in Section 3.5.

An overall schematic of the rig is shown in Figure 1 and a photograph is shown in Figure 2. These diagrams show the assembly of the rig, with locations of the combustion section, HES and exhaust gas sampling probes. The flow in the process is from left to right; pressurised, heated air is supplied to the combustion can where fuel is injected and burnt at constant pressure. The pressure in the can was maintained by a choke plate, which is a matrix of holes in a water-cooled assembly that holds the pressure in the upstream section. Details of the components are shown in Figure 3.

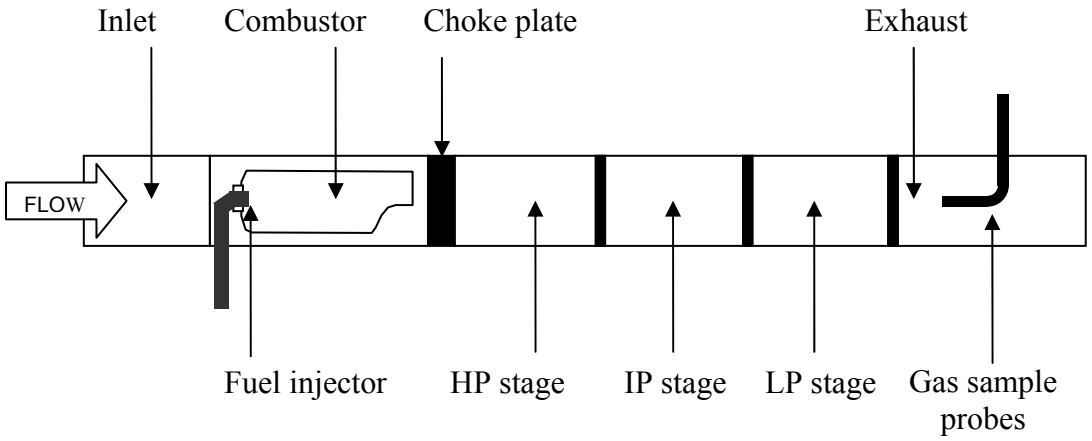

Figure 1. Schematic of the combustor system, HES and location of the two gas sampling probes down stream the exhaust of the HES.

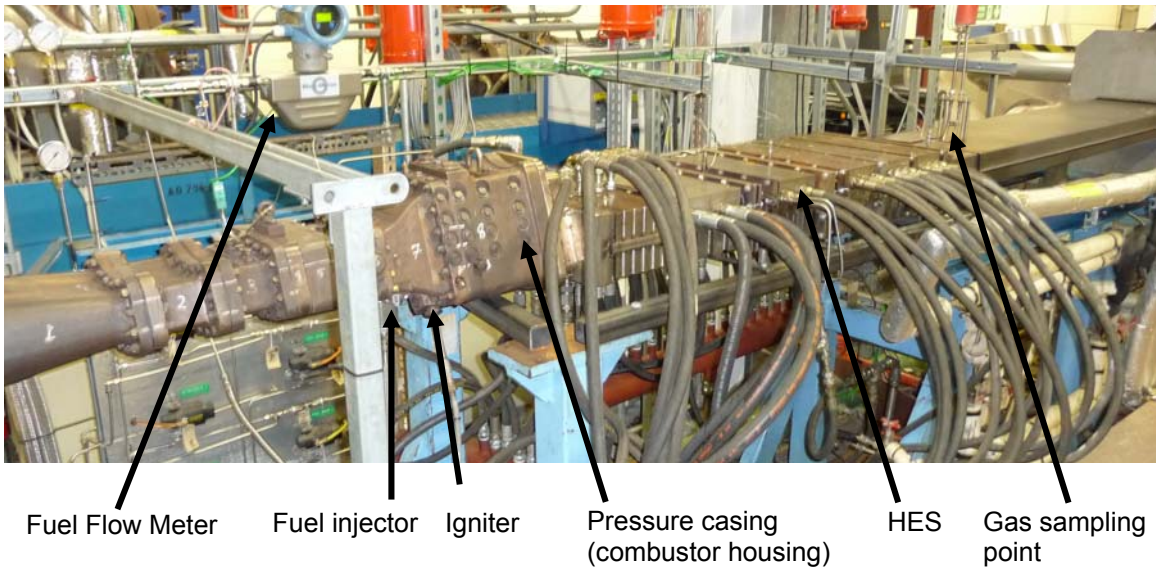

Figure 2. Photograph of the combustor, HES and gas sampling point.

Figure 3. Combustor pressure casing (top, front), combustor can (top back), and HES components (bottom).

For the combustion section of the rig, an aerospace cannular combustion chamber, constructed out of transpiration cooled steel was used for the tests. Fuel was provided into the can via an airblast atomizer, a modified version of the type used in an engine configuration. The fuel used in this trial was aviation grade kerosene, known as AVTUR F-35 also known as Jet A-1. The fuel was analysed for specific energy, density, hydrogen, sulphur and carbon mass fractions, respectively. UK fuel meets the UK fuel specification (DEF 91-91) and the ICAO Annex 16 Volume II Appendix 4 specification with the exception of aromatics and Naphthalene, where about 11% of fuel does not meet the aromatic specifications and about 6% the naphthalene specifications. The fuel analysis conducted by QinetiQ is attached in Appendix A.

The Hot End Simulator (HES) is a facility that sits behind the combustor, mimicking the behaviour of a turbine section in a gas turbine. This component reduces the pressure and temperature of the exhaust gasses by removing heat rather than work from the exit gases. The HES is comprised of three separate heat exchanger stages. Each stage simulates the rotor workload while variation of the cross-sectional area and trimmer plates simulates the pressure stages in a turbine, referred to here as the high, intermediate and low pressure stages. Pressure was maintained in these sections via pressure trim plates, similar to the upstream choke plate, consisting of a matrix of holes, designating the effective blockage ratio.

The assembly was almost identical to that utilized in the PARTEMIS project tests conducted during 2002. More details are given in Wilson et al. [2004] and Petzold et al. [2005a]. For the purposes of this experimental campaign the combustor and HES were used to provide a standard smoke source for the measurement apparatus. The main difference between this and the PARTEMIS tests were that only two gas samples were extracted from the rig. These locations were side-by-side and either side of the HES centreline, 50mm downstream of the low pressure choke plate.

The gas sample probes were manufactured from 7.75 mm internal diameter stainless steel pipes. Where bending or shaping was required the pipes were not subjected to bend radii smaller than 10 internal pipe diameters, thus adhering to ARP 1179 [*SAE*, 1997] on gas sampling. In particular the bend radius of the main sample lines at the probe tip is 87.25mm to the centre of the pipe. This is 11.3 times the internal diameter of the pipe (ID 7.75mm; OD 3/8"; wall thickness 0.035"). The pipes were temperature controlled by trace heating chords, such that the material temperature was kept above 160°C on gas analysis lines and controlled at required temperature on heated sections of smoke sampling lines, see also Section 3.4. The pipe and heating chord were also lagged with a silicone-based tubular insulation sheath.

The location of the gas sample probes was such that they were under only a slight positive static pressure of 1.05 bar plus additional dynamic pressure from the flow of the gas stream. For this reason each partner provided a pump to each sampling apparatus in order to draw the required sample flow through each analyser. Additional pumps at the end of each sample line were facilitated to keep a positive gas sample flow at all times, see Figure 10 for details.

3.2 Test conditions

In total three conditions were selected for the trials. The aim of selecting the three was to provide tangible differences in the composition of the particulates emitted from the smoke source. Of particular interest to the research team was the difference in emissions for cases of varying organic (volatile, semi-volatile and non-volatile) and inorganic (non-volatile) carbon concentrations in the exhaust. The selected conditions are briefly described in the following. A summary is compiled in Table 1.

Condition 1 - low smoke low organic matter (low SN-low OM): Baseline condition with nominal particulates and organic carbon loading.

This condition was chosen since it represented one of the PARTEMIS conditions, and thus there was potential for cross-correlation of data if required. At this point the combustor is operating on the engine line and as such its emissions of both gaseous and particulate should be within normal operating parameters. From the point of view of the experiment in question, the smoke source should be providing particulates with a target Smoke Number of around 13.

Condition 2 – low smoke high organic matter (low SN-high OM): Condition for low particulates and high organic carbon loading:

This condition involved operating the combustor at reduced temperature and pressure conditions when compared to the baseline case. The aim of this condition was for the smoke source to produce comparatively lower quantities of particulates but higher amounts of unburned hydrocarbons in the exhaust. The target Smoke Number for this condition was 5.

Condition 3 – high smoke low organic matter (high SN-low OM): Condition for high particulates and low organic carbon loading.

This condition involved operating the combustor at a richer AFR and increased temperature and pressure conditions when compared to the baseline case. The aim of this condition was for the smoke source to produce comparatively higher quantities of particulates but lower amounts of unburned hydrocarbons in the exhaust. The target Smoke Number for this condition was 20.

Table 1. Operation conditions of the Combustor HES during the SAMPLE trials.

Condition	Air flow kg s^{-1}	Combustor inlet temperature T_{in}, K	Combustor inlet pressure (abs), kPa	AFR	Target SN
low SN-low OM	2.0	566	705	66	13
low SN-high OM	1.0	400	350	65	5
high SN-low OM	2.6	660	1000	54	20

3.3 Sample line and instrumentation

According to AIR 5892 [*SAE*, 2004], the instrumentation applied during the study consists of methods for the measurement of particle mass, particle number, and particle size. The applied methods are briefly described. Details are given in AIR 6037 "Aircraft Exhaust Nonvolatile Particle Matter Measurement Method Development" [*SAE*, 2009]. The working principles and instruments are summarised in Table 2.

3.3.1 Particle mass measurement

Non-volatile PM mass measurement methods can be divided into three general approaches:

- ▹ gravimetric methods which measure total particulate mass (TM = OC + EC + inorganic compounds);
- ▹ carbon-burn off methods which measure total carbon (TC = OC + EC) and elemental carbon (EC) particulate mass; and
- ▹ optically-based methods which rely on light absorption by particles to measure the black carbon (BC) particulate mass, e.g., absorption photometry, laser-induced incandescence.

Table 2. – Selected Methods for the Measurement of Particle Mass Concentrations in an Aircraft Engine Exhaust

Measurement Method	Measurement	Instrument / Reference
Smoke Number	smoke	ARP 1179 [*SAE*, 1997]
Gravimetric Analysis	total particulate mass (TM_{GRAV})	off line, filter samples
2-step combustion of filter samples	total carbon (TC) elemental carbon (EC)	off line, filter samples [*Schmid et al.*, 2001]
Thermo-Gravimetry (TG): Continuous combustion of filter samples	organic carbon (OC), elemental carbon (EC),	off line, filter samples [*Schmid et al.*, 2001]
Multi-Angle Absorption Photometry (MAAP)	Black carbon (BC), BC ≅ EC	THERMO ELECTRON Model 5012 MAAP [*Petzold et al.*, 2005b]
Laser Induced Incandescence (LII)	Black carbon (BC)	Artium Technologies LII 200 http://artium-temp.com/products/lii

Gravimetric Analysis

Time-averaging methods are used to sample the emitted particles on appropriate fibrous filters or membrane filters. Common practice is to use glass fibre, quartz fibre, or Teflon filters for exhaust particle sampling that show a filtration efficiency of >99% in the size range relevant for particulate matter emitted from gas turbines, i.e. for $10\ nm < D_p < 500\ nm$. Applying gravimetry, the sampled particle matter is analyzed gravimetrically by weighing the filter before and after loading, which yields the total particle mass. The accumulated exhaust volume penetrating the filter is recorded for each sample in order to obtain a mass concentration measurement [*SAE*, 2009] .

2-Step Combustion
Pre-conditioned quartz fibre filters are used for sampling exhaust particle matter. Particle-laden filters are analysed for the carbon content in a two-step combustion process. During the two-step combustion process the organic carbon is oxidized for 42 min at 340 °C in a pure oxygen atmosphere. The remaining carbon, defined as elemental carbon, is then determined at 650 °C (32 min) by a total organic carbon analyzer based on non-dispersive IR absorption of the evolving CO_2 [*Schmid et al.*, 2001].

Thermo-Gravimetry
Pre-conditioned quartz fibre filters are used for sampling exhaust particle matter. Particle-laden filters are analysed for the carbon content in a continuous combustion process. In an oxygen atmosphere, the sample is heated from room temperature to 1000°C using a gradient of 20K/min. The evolving CO_2 is detected by non-dispersive infrared absorption. Simultaneous to the heating of the filter, a laser beam is directed through the filter sample and records the change in filter transmission. The transmission of a clean particle-free filter is 1.0; increasing aerosol loading reduces filter transmission towards 0.0. Elemental carbon oxidation is assumed to start as soon as the filter transmission increases from its initially very low value according to the black particle-laden filter [*Schmid et al.*, 2001].

Multi-Angle Absorption Photometry (MAAP)
Aerosol absorption photometry analyzes the modification of filter optical properties as transmittance or reflectance caused by the particles deposited on a filter matrix. Optical absorption methods are highly suitable for the measurement of combustion particles because the key component black carbon is a very efficient absorber of light in the visible spectral range. Since any particulate matter contains also a fraction of non-absorbing, i.e. light-scattering aerosol components, absorption photometry cannot be used for the measurement of total particle mass. The THERMO Model 5012 MAAP uses a multi angle absorption photometer approach to analyze the modification of radiation fields in the forward and back hemispheres of a glass-fibre filter caused by deposited particles. The MAAP data inversion algorithm is based on a radiation transfer method and compensates for the cross-sensitivity of aerosol absorption photometry to light-scattering aerosol components (Figure 4). [*Petzold and Schönlinner*, 2004; *Petzold et al.*, 2005b].

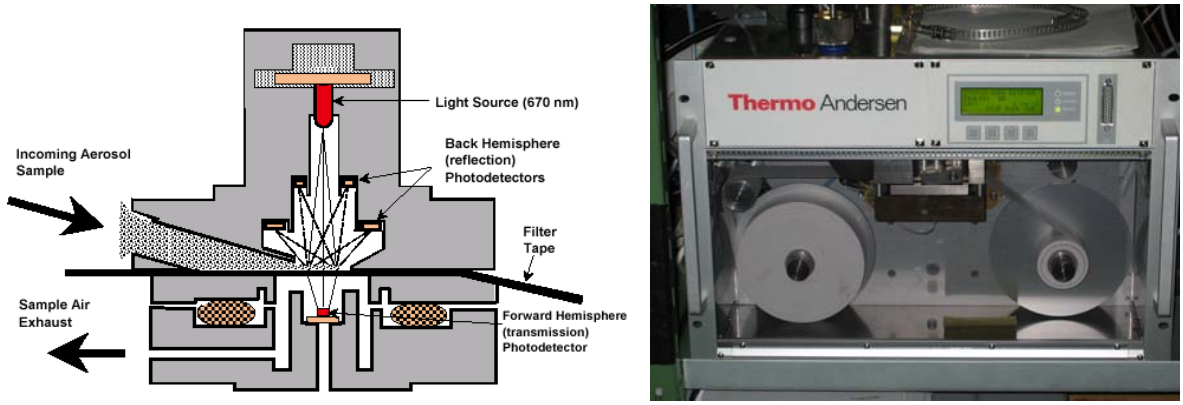

Figure 4. Optical unit of the THERMO Model 5012 Multi-Angle Absorption Photometer MAAP (left) and complete instrument (right).

The principal measure of any absorption photometer is the aerosol absorption coefficient σ_{ap}, given in units of 1/m. The conversion of an absorption coefficient measurement into a black carbon mass measurement requires the assumption on a mass-specific absorption cross-section for black carbon, B_{BC}. For the MAAP the value B_{BC} = 6.6 m²/g was determined from calibration studies for the operation wavelength λ = 630 nm [*Petzold and Schönlinner*, 2004].

Using these values, the BC mass concentration is given as

$$BC = \frac{\sigma_{ap}}{B_{BC}} \quad . \qquad (1)$$

Laser Induced Incandescence

Laser-induced incandescence (LII) is performed by measuring the thermal emission (incandescent light) emitted from particles heated by a pulsed laser to temperatures in the 2500 K to 4500 K range [*Snelling et al.*, 2005]. LII is highly selective, responding only to the presence of black carbon, making it decidedly appropriate for measuring the non-volatile particles produced as a combustion emission. This selectivity is due to the fact that the non-volatile particles are primarily black carbon. BC absorbs laser radiation over a broad spectral range, and is refractory, so that the nanoparticles survive heating to the temperatures necessary for the incandescence to be detected. At these temperatures, all volatile components that may have been condensed on the BC particles will be promptly evaporated, and most other non-carbonaceous particles will have also evaporated or undergone sublimation. Due to this selectivity, LII cannot be used for the measurement of total particle mass.

This method has a dynamic range of greater than 1000000:1 and can therefore measure either raw or diluted exhaust. Analysis of the LII signals results in the determination of the mass concentration, volume concentration, active surface area, and primary particle diameter of the particle emissions. LII data is converted from the volume fraction to mass concentration by applying a determined particle material density of 1.90 g /cm³ [*Snelling et al.*, 2005]. Figure 5 shows the scheme of the LII instrument deployed in SAMPLE.

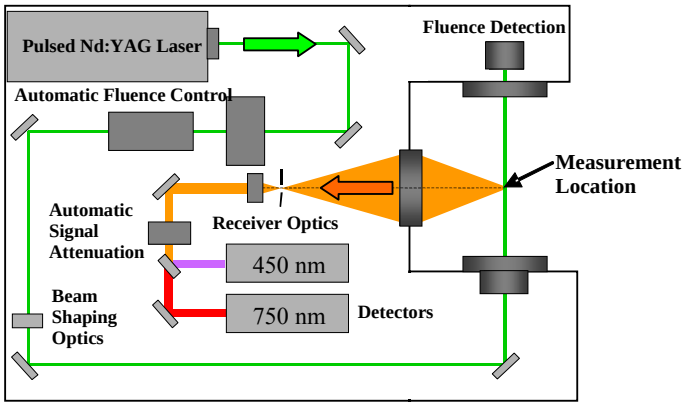

Figure 5. Schematic of LII 200 instrument optics layout, showing path of laser beam and detected particle incandescence.

Mass Fractionation – Organic Matter

The total particulate mass (TM) emitted from a gas turbine is composed of organic carbon (OC), inorganic or elemental carbon (EC) and of inorganic species like sulphate (S). The distribution between organic carbon and elemental carbon depends on the operating conditions of the engine [*Petzold and Schröder*, 1998]. Since organic matter is composed of organic carbon with minor contributions of oxygen and hydrogen, the ratio of organic matter to organic carbon is calculated from the ratio of oxygen to carbon by [*Aiken et al.*, 2008]

$$\frac{OM}{OC} = 1.26 \times \frac{O}{C} + 1.18 \quad . \tag{2}$$

For fuels with an O to C ratio of less than 1.0 weight-%, this relationship can be rewritten as

$$OM \cong 1.20 \times OC \quad . \tag{2a}$$

Mass Fractionation – Particulate Sulphate

According to the First Order Approximation (FOA) Version 3 [*CAEP*, 2008], ε = 2.4 wt-% of the fuel sulphur is converted into particulate sulphate. This result is in agreement with PARTEMIS results [*Petzold et al.*, 2005a]. Knowing the sulphur content of the fuel was 0.030 wt%, the sulphate emission index (in g / kg) is estimated as

$$EI_{SO4-FOA3} = 10^3 \left[\frac{FSC \times \varepsilon \times MW_{SO4}}{MW_S} \right] \tag{3}$$

with molecular weights MW_{SO4} = 96 g per mole and MW_S = 32 g per mole. This approach assumes that all gaseous sulphuric acid is converted into particulate sulphate. From the comparison of non-volatile matter emission indices calculated by means of FOA 3 and elemental carbon values obtained during PARTEMIS using similar equipment as in SAMPLE it was shown that $EI_{nonvol\text{-}FOA} \cong EI_{EC}$ (EASA APE Task 3 – Report, 2009). At conditions typical for gravimetric measurements (RH = 40%, T = 25°C), sulphate exists in its hydrated form as ($H_2SO_4 \bullet 6.5H_2O$) [*Agrawal et al.*, 2008]. Combining these findings and using the equivalence of FOA non-volatile matter emission index $EI_{nonvol\text{-}FOA3}$ and elemental carbon emission index EI_{EC} the hydrated sulphate contribution to total aerosol mass is estimated as

$$SO4 \bullet 6.5H2O = \frac{EI_{SO4-FOA3}}{EI_{nonvol-FOA3}} \times EC \times \left[1 + \frac{6.5\, M_{H2O}}{M_{H2SO4}} \right] \tag{4}$$

Mass Fractionation – Total Particulate Matter

Total particulate matter is calculated from the sum of the single components as

$$TM_{SUM} = OM + EC + SO4 \bullet 6.5\, H2O \tag{5}$$

Mass Fractionation – Black Carbon

The light absorbing carbonaceous material (smoke), termed black carbon (BC), is strongly correlated to the EC fraction of the aerosol, and thus to the key traceable compound of the non-volatile fraction of the gas turbine exhaust aerosol, i.e.

$$BC \cong EC \quad . \tag{6}$$

3.3.2 Particle number measurement

The operating principle of the saturator-condenser type CPC is depicted in Figure 6. Details of the CPC method are given in Appendix B of AIR 6037 [*SAE*, 2009]. With respect to the saturator, particle laden sample air is continuously passed through a tube where a liquid (the so-called working fluid) evaporates into the air until the air is almost saturated with vapour. Upon entering the condenser, the sample air becomes supersaturated by cooling or heating (depending on the working fluid) the walls of the tube, and this leads to condensation of vapour onto the particles to form droplets which grow to sizes suitable for optical detection. The minimum size of particles which are detectable by this method depends on the supersaturation realized in a single instrument according to the Kelvin equation (7) [*Baron and Willeke*, 2001; *Hinds*, 1999]

$$\ln S^* = \frac{4\,\sigma_{liquid}\,M_{liquid}}{RT\rho_{liquid}\,D_p^*} \quad ; \quad S^* \geq 1 \quad ; \quad D_p^* \propto \frac{1}{\ln S^*} \tag{7}$$

S^* – critical supersaturation
M_{liquid} – liquid molar mass
σ_{liquid} – liquid surface tension
ρ_{liquid} – liquid density
D_p^* – minimum particle diameter for activation at S^*

After the sample flow has left the condenser the droplets are passed through an illuminated region and the light scattered by the droplets is detected with a photodetector, which converts the scatted light into an electrical pulse that is electronically recorded as a particle count. The flow rate through the CPC is controlled by the flow control system typically consisting of a pump combined with a critical orifice or a flow controller.

Table 3 summarises the CPC used in the SAMPLE trials. For each model two identical instruments were operated in parallel. Please note that the applied instruments differ significantly in the minimum detectable particle diameter.

Table 3. Condensation particle counters (CPC) applied during SAMPLE.

Manufacturer	Website	Model	$D_{p,\,min}$
TSI Incorporated	http://www.tsi.com/	CPC 3760	14 nm
TSI Incorporated	http://www.tsi.com/	CPC 3010	10 nm
Grimm Aerosol Technik	http://www.grimm-aerosol.com/	CPC 5.400	5 nm

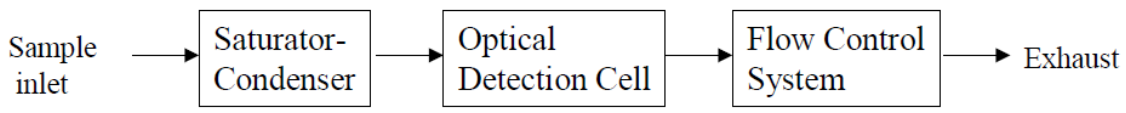

Figure 6. Schematic of a saturator-condenser type CPC [*SAE*, 2009].

3.3.3 Particle size measurement

Electrical mobility analysis is a well-established technique for sizing aerosol in the sub-micrometer size range. This method exposes charged aerosol particles to an electrostatic force resulting in a particle migration speed (proportional to electrical mobility Z), which depends among other parameters on particle size [*Baron and Willeke*, 2001; *Hinds*, 1999]. Hence, electrical mobility can be used for particle sizing. The electrical mobility of a charged particle, Z, is linked to particle size via the relationship

$$Z = \frac{n\,e\,C_C(D_m)}{3\,\pi\,\eta_g\,D_m} \qquad (8)$$

ne – charge of particle
C_c – slip correction factor
η_g – viscosity of carrier gas
D_m – particle mobility diameter

For spherical particles, the electrical mobility diameter D_m is identical to the geometric diameter D_g (as measured by electron microscopy). The operation principle of mobility sizing methods is shown in Figure 7. The Differential Mobility Spectrometer DMS 500, Differential Mobility Analysers DMA/DMPS and the Engine Exhaust Particle Sizer (EEPS) are based on this method. As an example, the DMS is described with more detail.

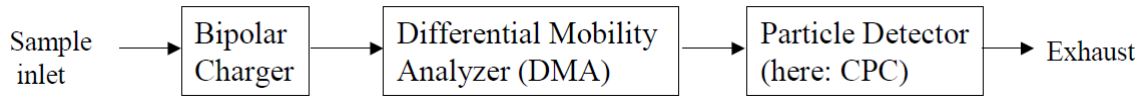

Figure 7. Schematic of a DMA coupled with a CPC-based detector [*SAE*, 2009].

Differential Mobility Spectrometer

The DMS500 uses a classifier column (Figure 8) operating at sub-atmospheric pressure. Sample flow is drawn into the instrument through a conductive rubber sample tube. The DMS uses a cyclone that prevents particles larger than 1µm entering the sampling tube and the instrument. To measure the particles in the 5–1000 nm diameter range, steel restrictors with holes of 1.00 mm were placed upstream of the cyclones to maintain a flow rate of 8 standard litres/min (SLPM) and a pressure of 0.25 bar (the same as the instrument's classification column) inside the sampling tube. This reduced pressure discourages particle agglomeration by reducing residency times [*Symonds et al.*, 2007] and helps isolate the instrument from fluctuating sample pressure. The sample gas passes through a corona discharge charger into the classifier column.

The charged particles flow within a particle-free sheath flow which is a uniform, cylindrical laminar column of air designed to carry the charged particles in a predictable manner. The particles are then deflected towards grounded electrometer rings by their repulsion from a central high voltage rod. Their landing position is a function of their charge and their aerodynamic drag. The particles yield their charge to the electrometer amplifiers and the resulting currents are translated by the instrument's user-interface into particle number and size data. Using a 5 m sample line, a 300 ms response can be achieved.

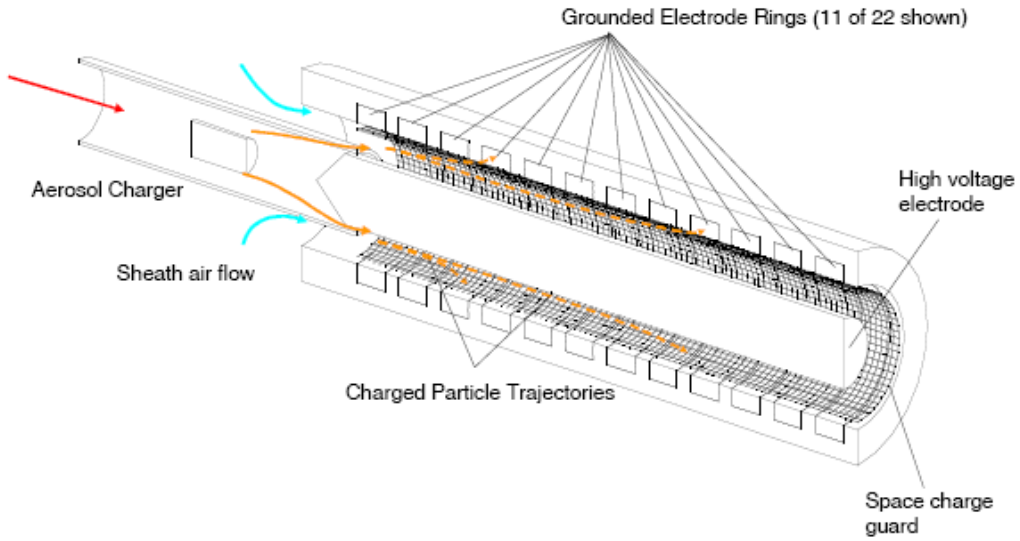

Figure 8. The Differential Mobility Spectrometer.

The use of PTFE tubing allows sampling temperatures as high as 200 ºC. It requires an external supply of clean, dry compressed air at 3 bar gauge, for primary dilution of compressed air, up to 4:1 ratio. A precipitator inside the instrument removes charged particles below approx. 30nm in diameter. The charger consists of a corona discharge wire suspended along the major axis of a perforated cylinder. The corona discharge produces a large number of positive ions. These ions collide with and charge the incoming particles.

The classifier separates the charged particles according to their electrical mobility. Although the classifier is operated at reduced pressure the aerodynamic drag of the particles is significant, it classifies by charge to drag ratio, or by electrical mobility i.e. using the diameter of a spherical particle with the same charge to drag ratio as the particle being measured. The main advantage of the DMS is the real-time (up to 10Hz) sampling capability allowing immediate analysis of the data, which is of prime concern as expensive rig running may be reduced if erroneous data points are observed early in the test. However, the particle morphology and density will affect the mobility, thus assumptions of these parameters is required to extract useful measurement data.

3.3.4 SAMPLE equipment overview

The measurement partners and equipment are summarised in Table 4. The information given below is to explain the configuration of the measurements made and outline the expertise brought by each group to the project. Additional to the particulate characterisation measurements, Cardiff University supplied a suite of gas analysis, measuring CO, CO_2, THC, NO_X and O_2. Take-off points were available for each gas sample line, and were activated using ball valves controlled by the test manager.

Table 4. Overview of instruments and methods used in the trials.

Instrument / method	Acronym	Partner	Sample type
Standard gas analysis	GA	Cardiff Univ.	Undiluted, 160°C
Gravimetry	GRAV	QinetiQ	Undiluted, 70°C
AECD Smoke meter	AECD	QinetiQ	Undiluted, 70°C
Smoke Number	SN	QinetiQ	Undiluted, 70°C
Thermogravimetry	TG	DLR/VUT	Undiluted, 70°C
2-Step Combustion	2SC	DLR/VUT	Undiluted, 70°C
Mini - Impactors	MI	ONERA	Undiluted, 70°C
Laser Induced Incandescence	LII	Rolls-Royce/Artium	Undiluted, 70°C
Aerosol Mass Spectrometer	AMS	Manchester Univ.	Undiluted, 70°C
Differential Mobility Spectrometer	DMS 500	Cardiff Univ.	All
Multi Angle Absorption Photometer	MAAP	DLR	Hot diluted, 20°C
Condensation Particle Counter	CPC	DLR	Hot diluted, 20°C
Optical Particle Counter	OPC	DLR	Hot diluted, 20°C
Scanning Mobility Particle Sizer	SMPS	Rolls-Royce	Hot diluted, 20°C
Engine Exhaust Particle Sizer	EEPS	Rolls-Royce/TSI	Hot diluted, 20°C
Condensation Particle Counter	TSI 3025A	DLR	Cold diluted, 20°C
Optical Particle Counter	OPC	DLR	Cold diluted, 20°C
Multi Angle Absorption Photometer	MAAP	DLR	Cold diluted, 20°C

3.4 Gas sample distribution system

The gas sample distribution system was manufactured for the tests within this project. In total two gas sample lines were used; these are shown as a photograph in Figure 9 and a schematic in Figure 10 (this also gives details of the locations of partner's analysers). Two lines were used mainly to provide sufficient space for all of the partners to connect to the sample, but also to separate the analysis into diluted and undiluted samples, as shown in Table 4. The samples were drawn through the sampling pipes via a positive displacement pump located at the end of each line. These were used to keep the sample flowing on occasions when the total quantity flowing through the system was low. The pumps ran continuously during the tests. During the trials it was found that the continuously operating on-line methods were showing results that were dependent on the total gas sample flow rate through the system. Thus, some periods were designated as 'constant flow' where none of the partners were allowed to adjust the rate of sample flow through the system via the modulation of sample pumps. These periods are shown in detail within Section 3.5.

For the diluted line, two separate dilution systems were used:

- A 'hot' dilution system was constructed making use of a DEKATI pressurised dilution air heater and ejector diluter (DI-1000). This apparatus was operated at 400°C and diluted the sample 10:1. The hot diluter was followed by a 3/8 inch line of 2655 mm length and 9.78 mm inner diameter kept at 360°C. At the downstream end of the heated line a Palas VKL 10 E stainless steel injection diluter was operated that diluted the sample with cold air by approx. 10:1. The principle of the hot diluter was to allow any volatile carbon species to be evaporated into the vapour phase and be effectively removed from the non-volatile particulates during the dilution process. Personal correspondence with the PMP "Golden Engineer" (Jon Andersson from Ricardo) specified that an 'evaporation tube' residence time should be >0.2 seconds to ensure effective removal of volatile aerosol (experience from automotive particulate measurements). At a maximum flow rate of 50L/min this equates to a minimum residence time of 0.24 seconds.
- A 'cold' dilution system was constructed out of two Palas VKL 10 in series. Once the gas sample passed into this train it was no longer heated and allowed to cool to ambient conditions. The principle of this was to allow any volatile carbon species to condense onto solid particulates during the dilution process.
- A CPC dilution system was constructed out of one Palas VKL 100 diluter which diluted the sample from the hot dilution system by another factor of 1:100 upstream the CPC.
- A thermal denuder (TD) consisting of a heated sampling line followed by an activated charcoal sink [*Burtscher et al.*, 2001] was operated upstream of a set of CPC in order to investigate the volatile matter removal efficiency of the applied hot diluter system.

For both diluters, the GTRC gas analysis system was used to periodically determine the dilution ratios. This was performed every 2 hours and reported back to the measurement group. For the calibration of the GTRC CO_2 detectors, two low-concentration span gases (799 ± 4 ppm and 380.3 ± 1.9 ppm) were supplied by DLR.

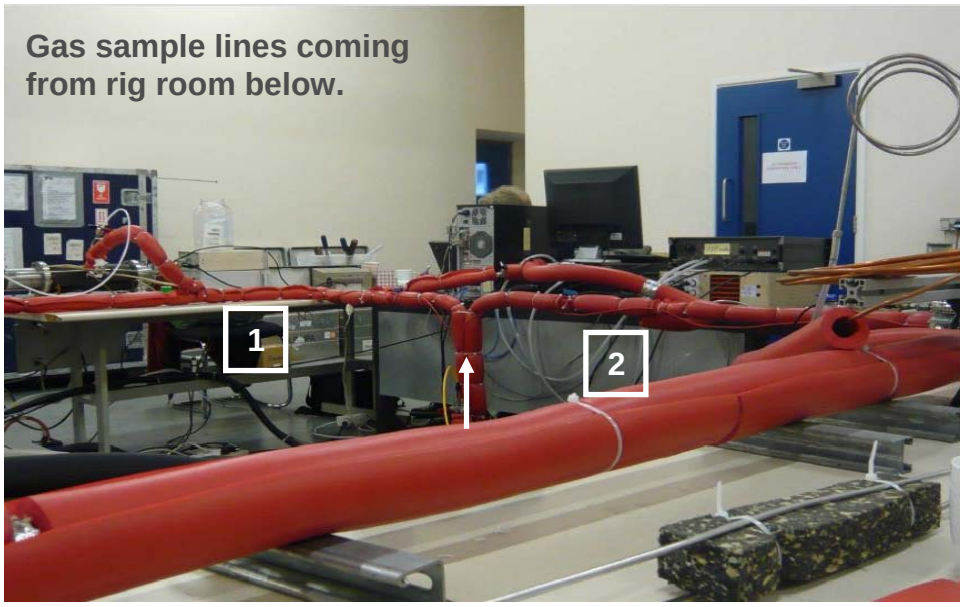

Figure 9. Photograph inside the analysis room. Heated sample lines are shown wrapped in the red-coloured silicon foam insulation. 1 = undiluted line; 2 = diluted line.

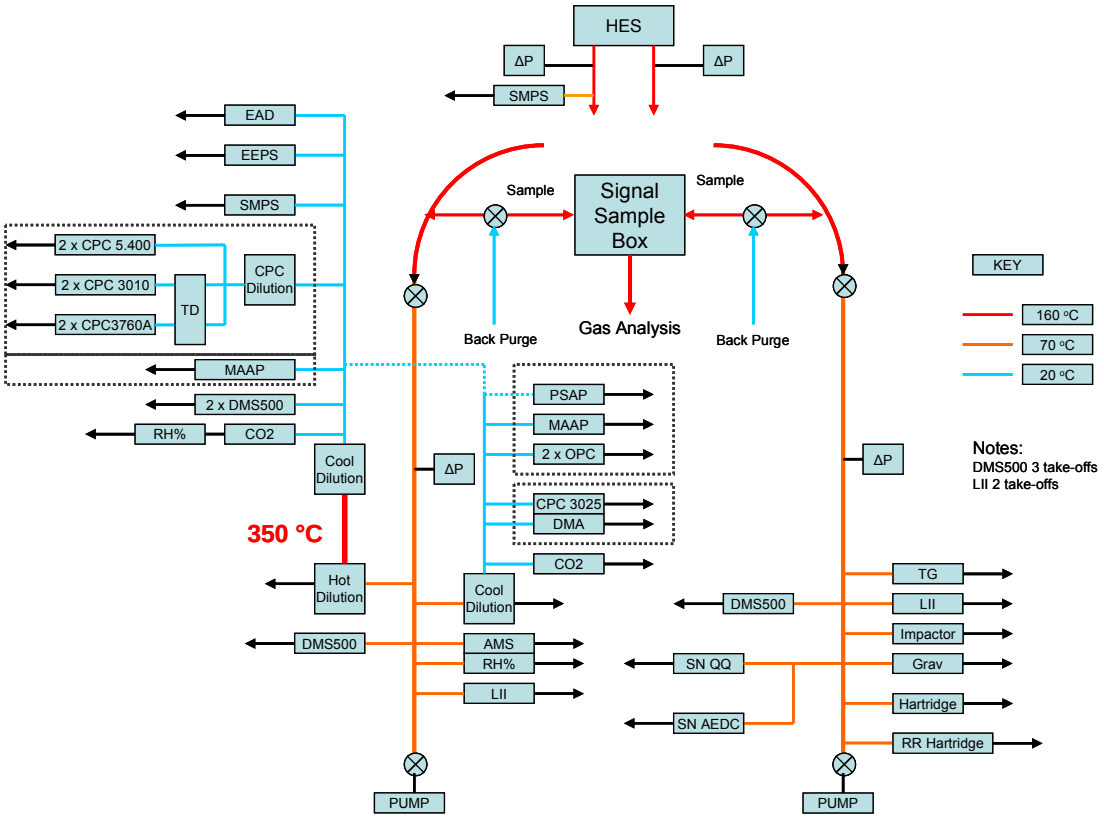

Figure 10. Schematic of the gas analysis system and the analysers connected to it.

The flow through the system was measured via two static pressure tappings in each sample line, spaced four metres apart over a straight vertical section of the system; these were located upstream of the sample distribution system. The tappings were used to measure the pressure difference over this distance, which was then used to calculate sample mass flow rate via a calibration test performed just before the tests. An UKAS accredited calibrated rotameter flow meter was connected to the end of each line and the pressure differences between the tappings were calibrated over a range of flows using compressed air to simulate the sample flow. Sample flow rate was logged once per second with the rig data.

3.5 Rig conditions during the tests

The conditions measured during the tests are summarised in this section (see also Table 1 in Section 3.2). This data also includes gas analysis results, which is summarised in tabular form within Table 5. In all, the following rig operating conditions are reported: air mass flow rate (kg/s), fuel mass flow rate (g/s) inlet pressure (Bar abs), rig inlet temperature (K), undiluted sample flow rate and diluted sample flow rate (both standard l/min). All times are quoted as British Summer Time (BST). Please note that during the dates in question, BST is exactly 1 hour ahead of Greenwich Mean Time (GMT), e.g. 10am GMT = 11am BST.

Figure 11 shows the rig conditions during Condition 1 in Session 1. The data proves that the intended conditions as described earlier in this report were satisfied and that the rig maintained stable operation throughout the session. The gas sample flow through the diluted and undiluted lines appeared to be sporadic in nature, which was due to the measurement partners drawing sample at different times during the test. This behaviour of the flow rates

appeared particularly during the first half of the session. It was noted and attempts were made to provide for steadier conditions in subsequent sessions. For this reason, Condition 1 was repeated in Session 2. In the undiluted line a fairly steady period occurred between 17:45 and 18:30. Peaks in the flow rate were associated to changes of filter sample holders. For the diluted line, conditions were quite stable for the same period of time. Any analyses for Condition 1 refer to this sequence.

Figure 12 shows the rig conditions during Condition 1 in Session 2. The conditions were approximately identical to that in Session 1, but this test allowed for a steady 'constant flow' condition in the diluted sampling line between 11:50 and 13:05, where the gas flow rate was just greater than 50 litres per minute. This constant behaviour was not deemed necessary for the undiluted line since the analysers, unlike those on the diluted line, were not showing any variability in results. In the undiluted sampling line peaks of the flow rate were again associated to changes of filters sample holders while the flow in the diluted line remained stable as intended by the steady 'constant flow' condition.

Figure 13 shows the rig conditions during Condition 2. As noted previously, there were no significant variations in the rig performance. A problem was detected some time after the session as to the flow rates through the sample lines. On closer inspection of the data it can be seen that the diluted and undiluted lines appear to have similar flow rates and near identical dynamic responses in flow demand. This was attributed to an unintentional transfer of gas through a cross-linkage between the two lines. This linkage is normally kept close and only open during back-purging of the system.

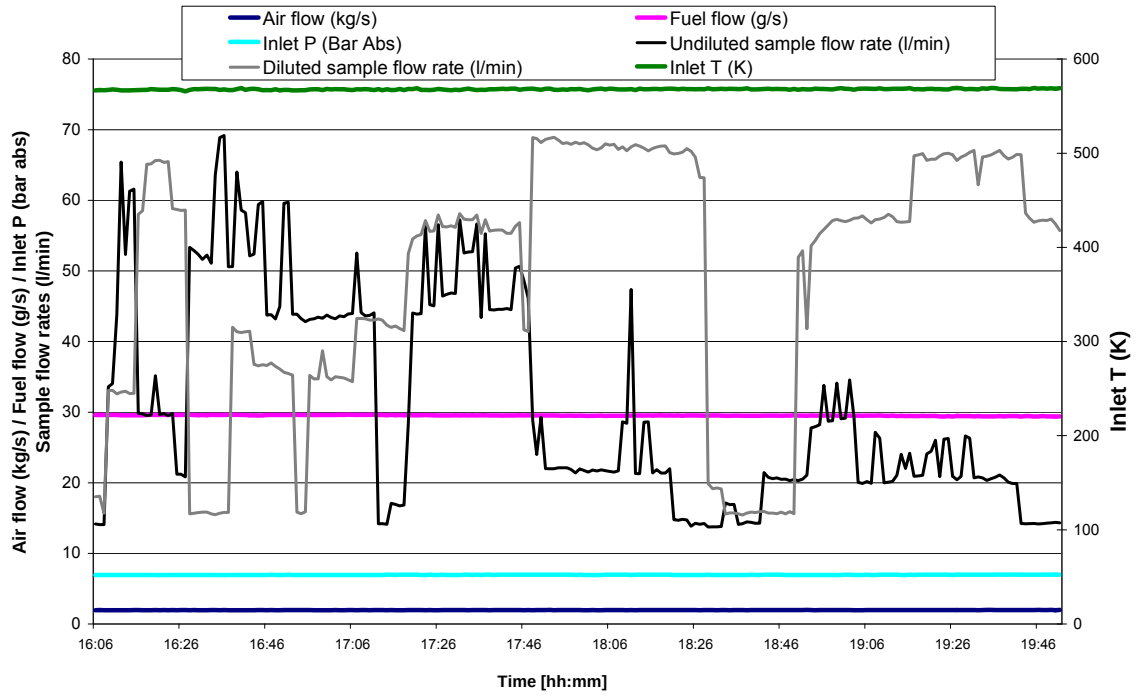

Figure 11. Rig data for Condition 1 (*low SN-low OM*) – Session 1, performed on 30 March 2009.

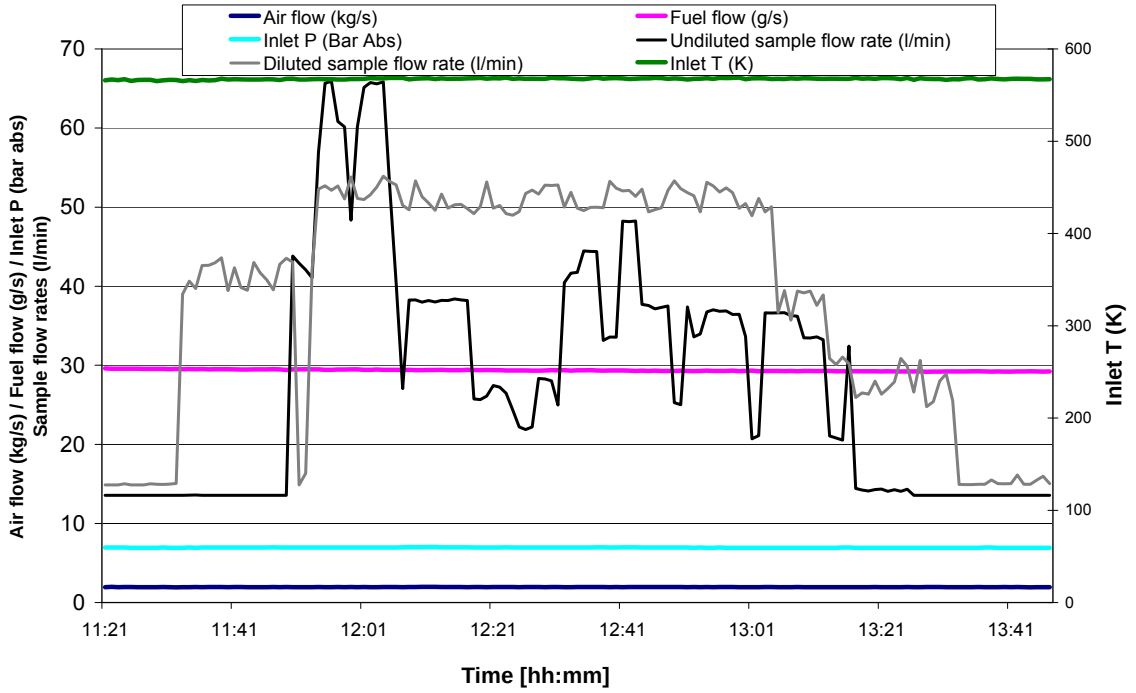

Figure 12. Rig data for Condition 1 ((*low SN-low OM*) – Session 2, performed on 01 April 2009. Note the steady flow rate in the diluted gas sample line (grey colour) at 11:50 - 13:05.

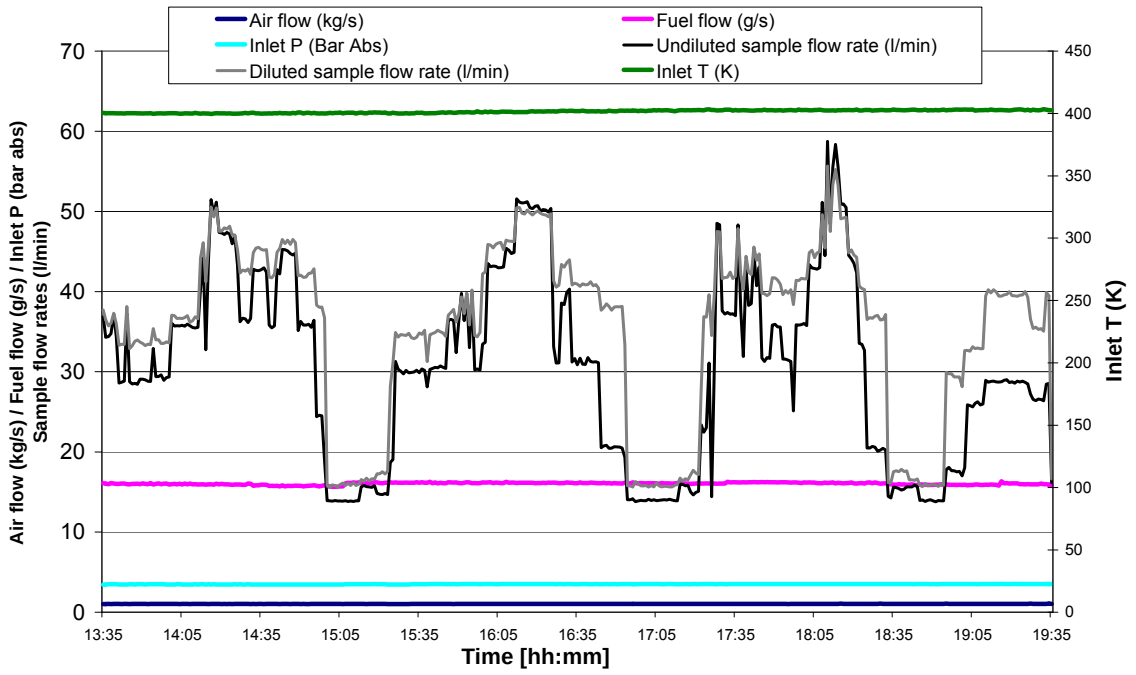

Figure 13. Rig data for Condition 2 (*low SN-high OM*), performed on 31 March 2009. Note the similarity between undiluted (black colour) and diluted (grey colour) sample line flow rates. This has been attributed to a cross-leakage between the two sample lines during this run only.

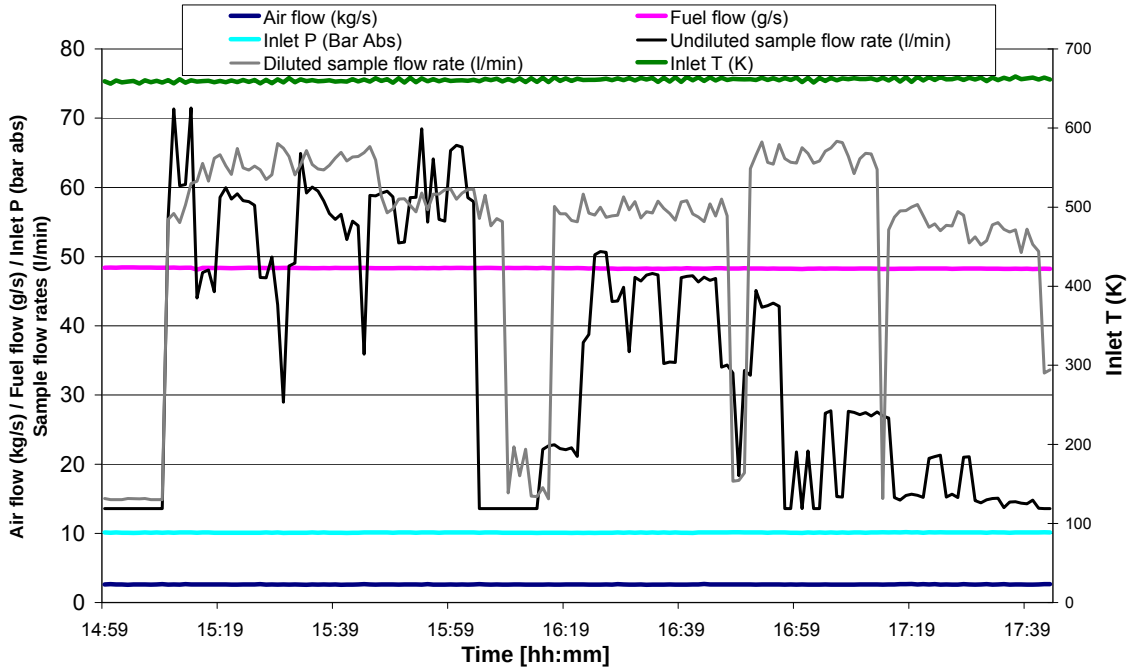

Figure 14. Rig data for Condition 3 (*high SN-low OM*), performed on 01 April 2009. Note the steady flow rate in the diluted gas sample line (grey colour) on 3 distinct occasions during the tests.

The operators are confident that this cross-leakage between the lines was minimal, and caused no significant affect on the sample integrity and did not introduce air or other contamination into the sample flow. This was confirmed with gas analysis results, showing that measured and calculated AFRs were within expected values.

The effect of this cross-leakage is therefore assumed to having no impact on results, but it means that the individual flow rate of each sample line is not known during this session. However, the total sample flow rate is known from the sample line section upstream to the bifurcation into the two branches, and a safe approximation would be that the flow in each line was the average of this total value at any time during the session. It should be stressed that this problem occurred during this session only and not elsewhere during the trial.

Figure 14 shows the rig conditions and sample line flow rates during Condition 3. The rig behaved in a consistent and steady manner throughout the session and the gas analysis was more constant, due to more stringent management of the measurement partners with respect to instrument switching. A number of 'constant flow' conditions were imposed, shown by the distinct plateaus in the diluted line sample flow.

Table 5 summarises the averaged gas analysis results for the conditions tested. These values are averages of the entire sessions. The data shows that when compared to the baseline case Condition 1:

- Condition 2 produced higher quantities of CO and THC with lower NO_X (hence the combustion process was less efficient at this condition).
- Condition 3 produced lower quantities of CO and THC with higher NO_X (hence the combustion process was more efficient at this condition).

Table 5. Averaged gas analysis data for the four conditions under consideration.

Condition	Session	CO_2 (%)	CO (ppm)	THC (ppm)	NO_X (ppm)
1 – *low SN-low OM*	#1	3.3	57.9	4.1	84.2
1 – *low SN-low OM*	#2	3.3	63.3	4.3	79.3
2 – *low SN-high OM*	n.a.	3.3	456.4	48.8	33.7
3 – *high SN-low OM*	n.a.	4.1	27.9	1.7	218.3

Table 6. Dilution ratios in the hot and cold sample lines.

Condition	Session	Date	Time (BST)	HOT	COLD
1 – *low SN-low OM*	#1	30 March 2009	20:21:00	39.8	100.2
2 – *low SN-high OM*	n.a.	31 March 2009	15:21:00	36.5	173.7
2 – *low SN-high OM*	n.a.	31 March 2009	17:20:00	38.3	156.1
2 – *low SN-high OM*	n.a.	31 March 2009	18:37:00	33.2	155.3
1 – *low SN-low OM*	#2	01 April 2009	11:53:00	31.0	129.4
3 – *high SN-low OM*	n.a.	01 April 2009	14:00:00	34.4	106.5

This gas analysis therefore provides evidence that the conditions chosen were representative of their target criteria in terms of quantities of volatile carbon emitted as combustion products. In addition to this analysis, the two sample lines were tested independently throughout the trials and it was shown that the gas composition in both sample lines was considered identical, thus providing evidence that the two sampling probes were seeing near identical samples.

Table 6 shows the dilution ratios as measured by the gas analysis system at GTRC. For the data analysis individual dilution ratios were used for the respective sampling lines and sampling times. The data shows that dilution in the hot system was on average 34.6 ± 3.9 for the whole of the trials, indicating a variation of approx. 11%. The dilution in the cold system was on average 132.6 ± 29.5 (22%) for the whole of the trials.

4 Results

The procedure followed in analyzing the data is defined as follows:

Mass

- Mass-based instruments are evaluated against gravimetry and Smoke Number. Statistical methods are used to quantify the recovery of total mass when analysing the total carbon loading.
- MAAP (BC) results are analysed against gravimetry (OC + EC + inorganic compounds) and thermogravimetry (EC) to evaluate the under-determination of particulate mass when only light absorbing black carbon compounds are considered.
- Analyses of the OC/EC split from thermogravimetry for various operation conditions are used to estimate the under-determination of particulate mass when only non-volatile carbonaceous compounds (EC + non-volatile OM) are considered.
- Laser-Induced Incandescence will be evaluated against thermogravimetry and against MAAP which both (MAAP and LII) separate the light absorbing carbonaceous fraction (BC) from the total aerosol.

Number

- Condensation particle counters were operated in parallel to assess the uncertainty in the measured data depending on instrument performance like variations in instrument flow and lower detection diameters.
- A thermodenuder which heated the sample to 350°C prior to the measurement was applied to characterise the removal efficiency of the hot dilution system.

Size

- The sizing instruments based on electrical mobility measurements are evaluated against each other to study the accuracy of this method for this application.

4.1 Particle mass measurement

The results from the mass-based methods are summarised as test condition average values in Table 7. Details for certain time slots are compiled in Table 8. All data refer to standard temperature and pressure (STP) conditions which are defined as T = 273.15 K and p = 1013.25 hPa. Figure 15 illustrates the structure of particles under investigation.

Total mass was approached by several methods, see also Section 3.3.1:

TM_{GRAV} : total mass determined by gravimetric analysis;

TM_{SUM} : total mass given as the sum of chemical components by Eq. (4);

TM_{FOA3} : total mass of non-volatile matter calculated from the measured SN, using the ICAO approved First Order Approximation Version 3 FOA 3 [*CAEP*, 2008];

TM_{MOB}: total mass calculated from particle mobility spectra using spherical particle shape and unit density of 1000 kg / m³.

Total mass

Gravimetry (TM_{GRAV}) was determined from filter papers. TM_{SUM} was determined from the sum of all chemical components including estimated contributions from sulphate and organic matter according to Eq. (4). DMS 500 mobility size distributions (TM_{MOB}) assume an effective particle density of 1000 kg / m³. The mobility diameter was measured with compensation made for the number of charges as suggested in the data processing respective to the DMS500 and the EEPS. This is important for mass calculation because the volume of a non-spherical particle is not the same as that of the mobility equivalent sphere. Furthermore, for accumulation mode particles, the ratio of actual volume to equivalent sphere volume varied with particle diameter.

Total carbon and elemental carbon

Total carbon (TC) and elemental carbon (EC) were determined by a two-step combustion process. During sampling the flow through the filters was fixed by a critical orifice providing a constant volumetric flow rate of 10.68 – 10.98 l/min. Values varied according to the respective pressure and temperature conditions during sampling. Day to day variations of the flow rates were recorded and corrected.

Black carbon

Black carbon is determined by multi-angle absorption photometry, and by laser induced incandescence, see Section 3.3.1.

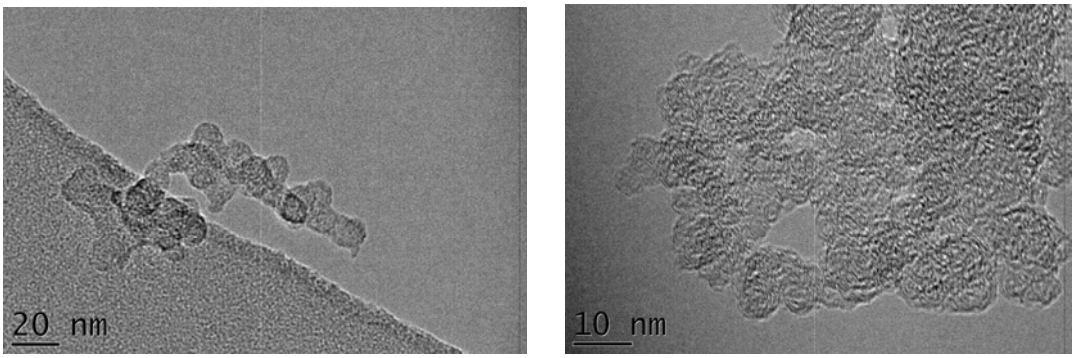

Figure 15. Transmission electron microscopy images of gas turbine exhaust soot particles.

Table 7. Summary of particle mass measurements; values in parentheses correspond to one standard deviation of the average. All mass concentrations are given in mg / m³ STP.

Date	Condition	ARP 1179	FOA3	Grav.	2-STEP COMB		MAAP	DMS	EEPS	LII
		SN	TM_{FOA3}	TM_{GRAV}	TC	EC	BC	TM_{MOB}	TM_{MOB}	BC
30/03/09	*low SN-low OM*	11.7 (1.6)	1.44 (0.20)	1.79 (0.10)	1.35 (0.05)	1.14 (0.16)	1.17 (0.06)	3.17	0.60	0.35
31/03/09	*low SN-high OM*	8.8 (1.6)	1.02 (0.19)	2.18 (0.81)	1.40 (0.29)	0.76 (0.24)	0.72 (0.19)	0.89	0.64	0.06
01/04/09	*low SN-low OM* [#]	10.5 (1.2)	1.26 (0.14)	2.0	1.29	0.85	1.07	1.68	0.52	0.30
01/04/09	*high SN-low OM*	26.4 (2.9)	3.94 (0.43)	5.10 (0.26)	3.86 (0.29)	3.50 (0.39)	1.83 (0.02)	2.70	1.83	1.55

[#] For this condition only one filter sample or time slot, respectively, was available.

Table 8. Details of particle mass measurements.

Date	Time GMT		Condition	Paper #	Exposure time	GRA T_{GRA}	DMS50 TM_{MOB}	Filter #	Exposure time	2-STEP COMB TC	2-STEP COMB EC	MAAP BC
	Start	Finish			min	mg/m^3 STP			min	mg/m^3 STP		
30/03/09	15:12:00	16:12:00	*low SN-low OM*	2	60	1.852	1.12	23	80	1.412	0.964	
30/03/09	16:22:00	17:22:00	*low SN-low OM*	3	60		1.85	22	15	1.318	1.256	1.128
30/03/09	17:25:00	18:45:00	*low SN-low OM*	4	80	1.992		27	10	1.318	1.207	1.217
31/03/09	12:24:00	13:58:00	*low SN-high OM*	5	94	1.854	0.77	26	18	1.422	0.651	
31/03/09	14:27:00	15:27:00	*low SN-high OM*	6	60	3.113	0.83	10	15	1.850	1.117	0.854
						3.113		9	15	1.468	0.877	
31/03/09	16:25:00	17:25:00	*low SN-high OM*			1.557		8	15	1.143	0.570	0.583
						1.557		11	15	1.138	0.571	
01/04/09	10:51:00	12:17:00	*low SN-low OM*	7	60	2.001	1.68	3	10	1.289	0.852	1.074
01/04/09	14:05:00	15:05:00	*high SN-low OM*			5.473	2.96	18	5	3.669	3.626	1.845
						5.473		19	5	3.882	3.626	
				8	86	5.473		20	5	4.586	4.427	
				9	60	5.473		21	7.5	3.873	3.379	
						5.473		24	5	4.190	3.358	
01/04/09	15:16:00	15:58:00	*high SN-low OM*			5.185		16	5	3.789	3.453	1.821
						5.185		25	5	3.703	2.745	
						5.185		15	7.5	3.701	3.546	
						5.185		14	5	3.590	3.310	
01/04/09	16:05:00	16:43:00	*high SN-low OM*	10	42	4.798	2.68	13	7.5	3.789	3.453	
						4.798		12	8	3.671	3.592	

Table 9. Ratios of total mass from various methods to total mass from gravimetry (GRAV) and to total mass from SN data (FOA3); the ratio of black carbon to elemental carbon supports the expected equivalency of both metrics.

Condition	TM_{SUM}/ TM_{GRAV}	TM_{FOA3}/ TM_{GRAV}	TC/ TM_{GRAV}	EC/ TM_{GRAV}	BC/ TM_{GRAV}	TM_{MOB}/ TM_{GRAV}	TC/ TM_{FOA3}	TM_{MOB}/ TM_{FOA3}	EC/ TC
low SN-low OM S1	1.18	0.81	0.75	0.64	0.66	1.02	0.93	1.26	0.85
low SN-high OM	1.02	0.47	0.64	0.35	0.33	0.37	1.38	0.79	0.54
low SN-low OM S2	0.99	0.63	0.64	0.43	0.54	0.84	1.02	1.33	0.66
high SN-low OM	0.96	0.77	0.76	0.69	0.36	0.55	0.98	0.72	0.91

Detailed data on the relative behaviour of the different mass-based metrics against the reference value of total mass determined from SN data according to the FOA 3 methodology and against the values from gravimetry are compiled in Table 9 as average values with respect to the operation conditions. The subset of data referring to TM_{FOA3} is shown graphically in Figure 16. The column of Table 9 referring to the ratio of EC/TC proofs the variation in the split of organic carbon and elemental carbon as intended by the different operation conditions. However, it has to be noted that the particles emitted during Session 2 of Condition 1 contained a significantly higher organic fraction compared to the particles emitted during Session 2 of Condition 1, although the rig operation conditions compared well.

Summarising, for total mass measurement methods systematic trends become obvious:

$$TM_{GRAV} \cong TM_{SUM}$$

$$TM_{GRAV} > TM_{FOA3} \text{ by } 19 - 53\%$$

$$TM_{GRAV} > TC \text{ by } 25 - 36\%$$

Total mass from gravimetry exceeds all other mass measurements. The difference between TM_{GRAV} and TC can be explained by the estimated contributions from sulphate and from the assumed difference between OM and OC, see Eq. (4). Total carbon and total mass from SN agree well with the exception of high OM conditions, where FOA 3 differs from total carbon mass by approx. -40%, see column TC / TM_{FOA3} in Table 9.

The left panel of Figure 17 shows the comparison of black carbon (BC) from MAAP and elemental carbon (EC) from the 2-Step Combustion method (340°C threshold). It has to be noted that for the high loading conditions the MAAP instrument was operated beyond its upper limit which led to frequent filter spot changes and causes an underestimation of BC, i.e.

$$BC / EC = 0.92 \pm 0.12, \text{ except for high SN where } BC / EC = 0.52$$

The right panel of Figure 17 shows the comparison of total mass from the DMS 500 instrument and total mass from gravimetry. Interestingly, total mass from DMS 500 deviates strongest from total mass from gravimetry for the highest load conditions, similar to the deviation of BC from MAAP from EC from 2-step combustion. Note that both MAAP and DMS 500 sample online from the exhaust gas while gravimetry and EC are determined from filter samples. The systematic deviation of on-line methods from filter methods for high load conditions requires further investigation.

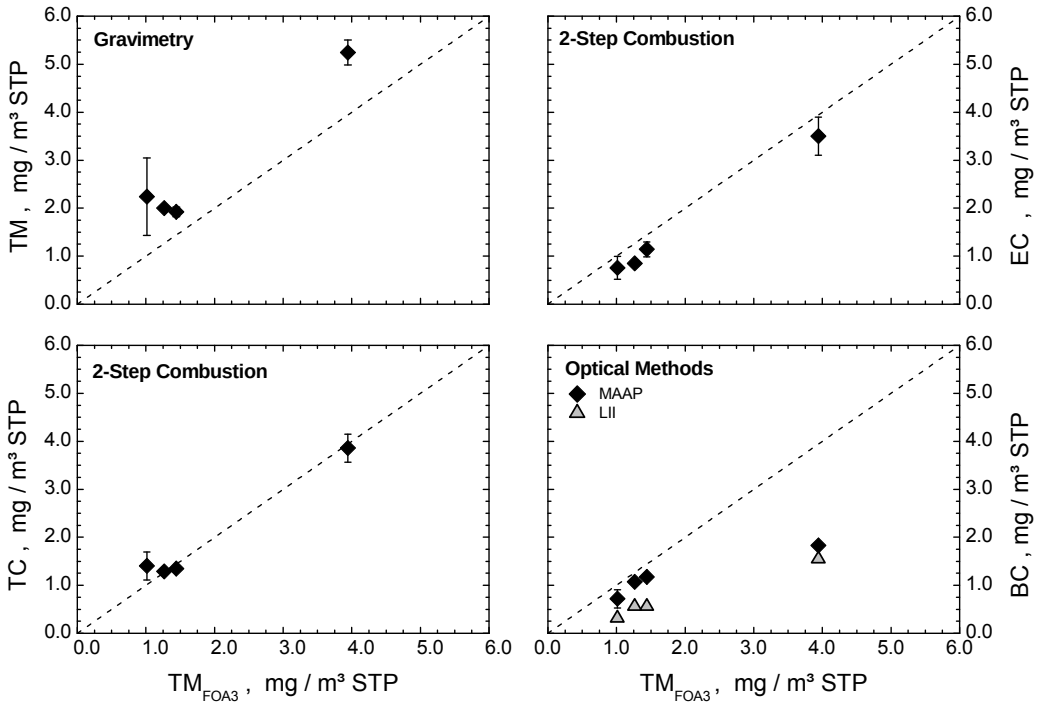

Figure 16. Left column: total mass from gravimetry and total carbon from 2-Step Combustion vs. total mass from SN data; right column: elemental carbon from 2-Step Combustion and black carbon from LII and MAAP vs. total mass from SN. The dashed line indicates the 1:1 – relationship.

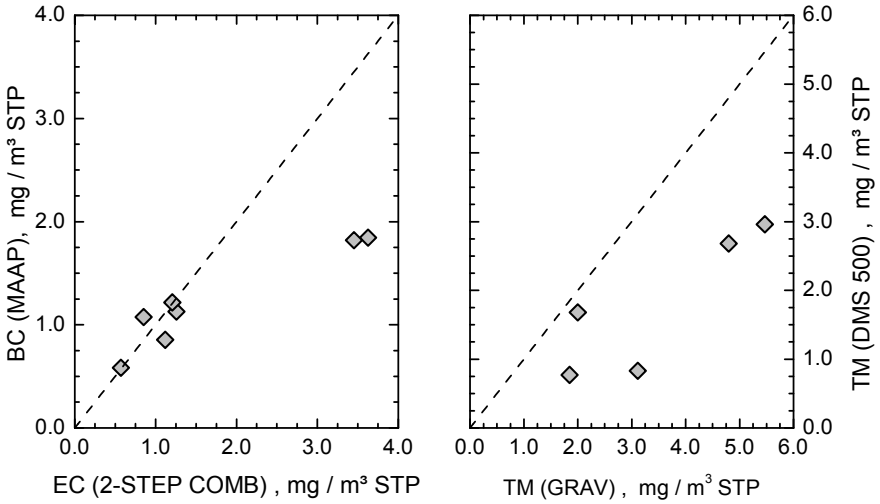

Figure 17. Black carbon from MAAP vs. elemental carbon from the carbon burn-off method; the dashed line refers to the 1:1 relationship.

Instrument precision

Instrument precision is determined from the parallel operation of two identical instruments sampling from the same source. With respect to mass-based methods this was possible for the DMS 500. For MAAP and LII instruments respective results from studies outside of SAMPLE are referenced.

During SAMPLE two Cambustion DMS500 instruments were running, most often split between the different lines or under different dilution regimes. However for each condition the two instruments serial numbers M44 and M45 were run simultaneously on the Hot Diluted line. The DMS500 logs at 10Hz the number concentration of particles over the range 5 nm to 1µm, of which is split into 38 bins. For the purposes of comparative measurements – and to show repeatability between different instruments, a regression analysis was carried out on both the size distribution and number concentration (N/cm³) over time. Figure 18 shows this for all the investigated rig conditions.

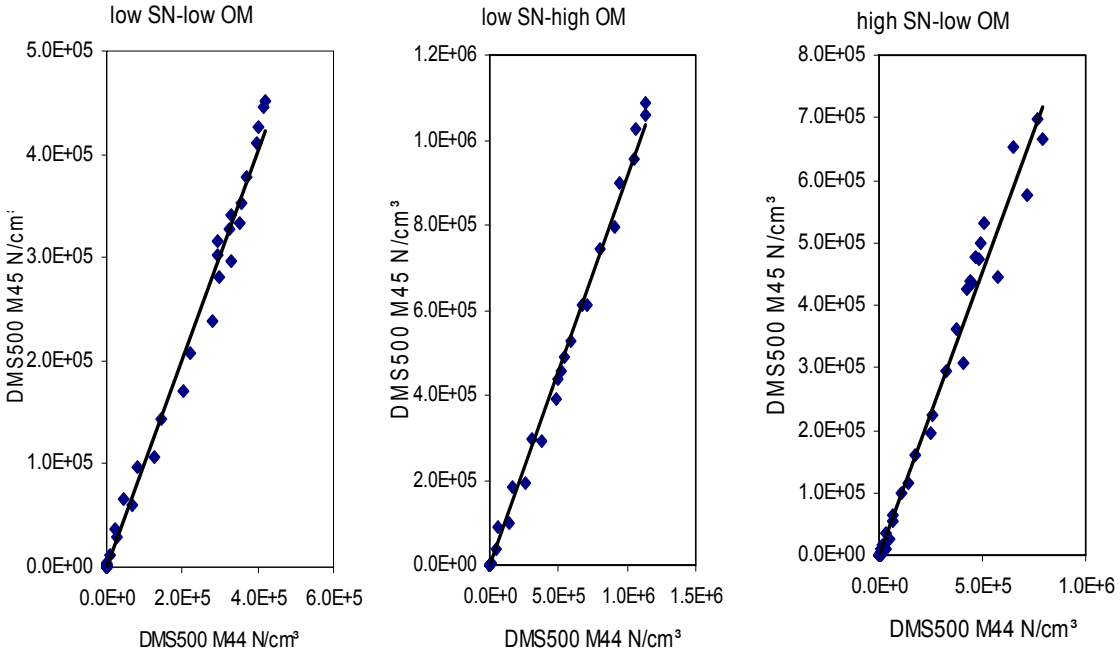

Figure 18. Correlation between the number concentration of particles from 5nm to 1µm between two DMS500 analysers running on identical sampling conditions. The HES simulator was ran at different SN/OM conditions on aviation grade kerosene.

For the Low-Organic Low-Smoke condition there was a 1:1 correlation with less than 3% deviation for the majority of the data over the measured range. However for the other two conditions there was a 9-10% bias in number towards the ser. M45 DMS500. Using regression analysis the confidence level was 95% for these conditions. Overall there was less than 12% deviation over the test points recorded over the range up to 500nm.

For the MAAP instrument, data from an instrument intercomparison undertaken in the framework of the Global Atmospheric Watch programme of the World Meteorological Organisation are shown in Figure 19. During this study five MAAP instruments operated within a relative deviation of 3.5% from the average (one standard deviation). From these extensive studies it is known that the MAAP is a robust method for measuring black carbon.

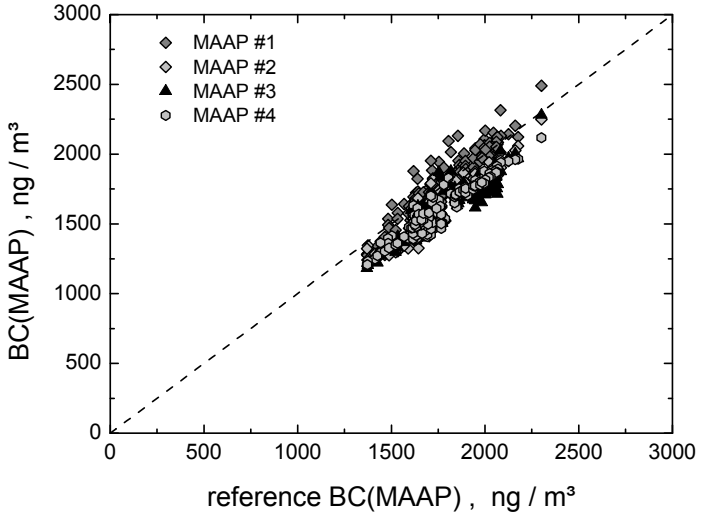

Figure 19. Correlation of four different MAAP instruments operated parallel to on reference instrument during an instrument intercomparison study at Institute for Tropospheric Research in Leipzig in November 2005.

For the LII instrument data from an instrument intercomparison is shown in Figure 20. Comparative measurements to demonstrate the agreement between identical Artium LII-200 instruments were performed, investigating black carbon concentrations produced from a kerosene burner. There was a 1:1 correlation with less than 2% deviation for the majority of the data over the measured range of concentrations (from less than 0.1 mg/m3 to over 10 mg/m3). This linearity was demonstrated to hold over two orders of magnitude, including the lowest concentrations measured.

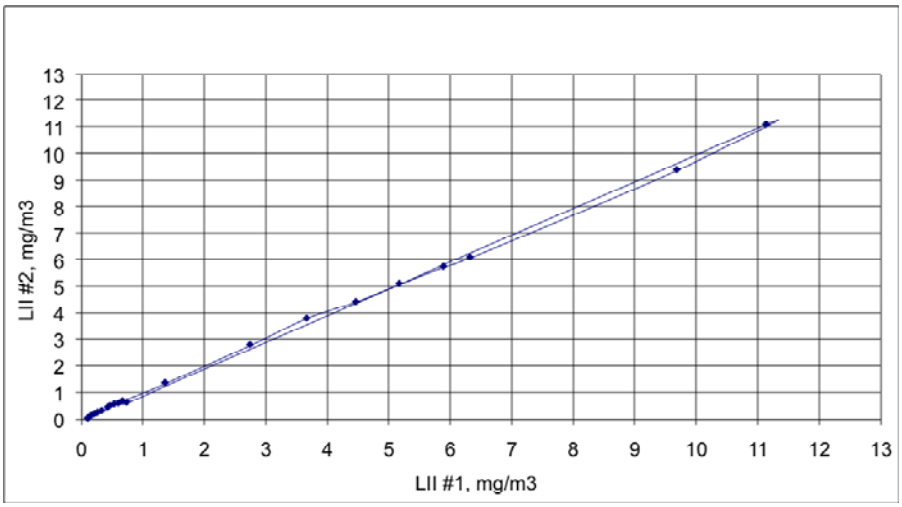

Figure 20. Correlation between black carbon concentration measurements performed in parallel with two identical LII instruments. The source of black carbon was soot produced by kerosene combustion during a study performed in September 2007.

4.2 Organic and volatile matter measurement

4.2.1 Thermogravimetry

The contribution of organic carbon to total carbon and to the non-volatile particulate matter fraction was investigated using thermogravimetry. FOA 3 was used for estimating the contribution of hydrated sulphate to total particle mass, see Eq. (4). The equivalence of BC and EC from 2-Step-Combustion is proven in Figure 17 with the constraints discussed there.

Thermogravimetry was used for the investigation of the organic fraction of the sampled aerosol. Figure 21 shows examples of thermograms for the four sessions conducted during SAMPLE. Elemental carbon burn-off starts at approx. 600 °C. The threshold is monitored by a laser beam directed through the filter paper. When the initially dark filter starts to get brighter again, the onset of elemental carbon oxidation is identified [*Schmid et al.*, 2001]. Fitting a 5-modal Gaussian distribution to the measured thermograms gives access to different carbon fractions being present in the samples. The fitting procedure yielded that a number of five Gaussian modes can reproduce all measured thermograms best. The detailed positions of the Gaussian peaks with respect to the combustion temperature varied for the single samples.

The data analysis procedures for the analysis of the thermal properties of the organic matter fraction are illustrated in Figure 22. In summary, for each quartz fibre filter sample, the following data are available:

TC and EC from 2-Step Combustion;
Thermograms from Thermogravimetry;
Laser transmission signal from Thermogravimetry;
5-Peak Gaussian fit to Thermogram.

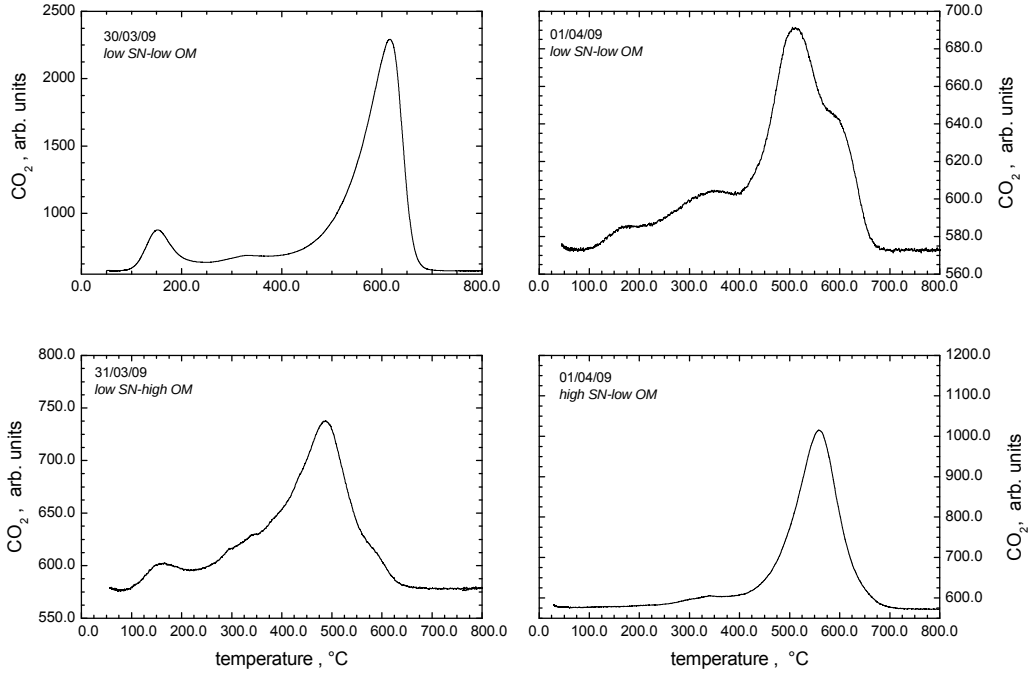

Figure 21. Examples of thermograms for the four sessions conducted during SAMPLE; respective EC / TC ratios are 80%, 70%, 66%, and 91% (from top left to bottom right).

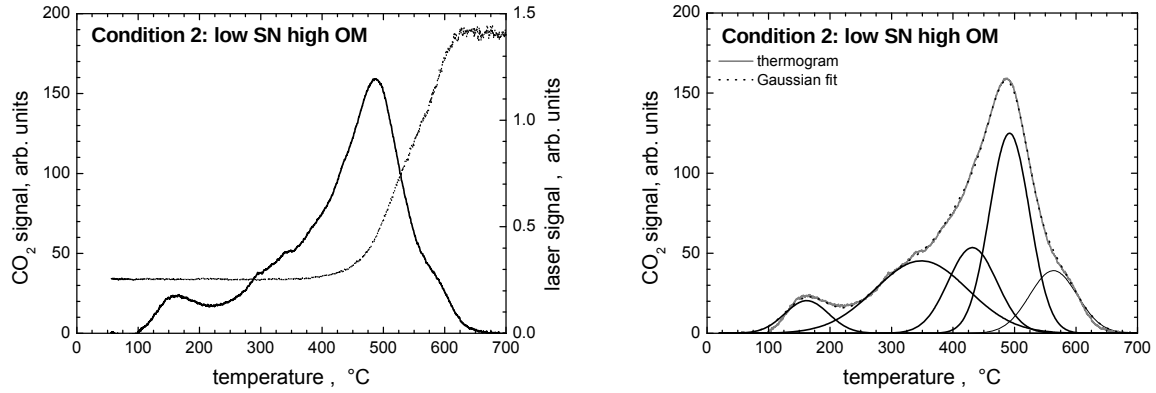

Figure 22. Thermogram for *low SN – high OM* conditions including the laser transmission signal (top panel) and the Gaussian fit for five carbonaceous matter fractions (bottom panel).

Table 10. Average fractions of EC, BC, and non-volatile matter of TC ($TC_{Non\text{-}Vol}$), and average volatilisation temperature T_{OC}; standard deviations are added in parentheses.

	2-Step Comb EC / TC	MAAP BC / TC	TG laser $TC_{Non\text{-}Vol}$ / TC	TG Fit	T_{OC} , °C
low SN - low OM	0.85 (0,16)	0.87 (0.06)	0.78 (0.07)	0.81 (0.09)	425 (13)
low SN - high OM	0.54 (0.06)	0.51 (0.17)	0.69 (0.04)	0.67 (0.03)	400 (31)
high SN - low OM	0.91 (0.08)	n.a.	0.69 (0.10)	0.91 (0.03)	393 (30)

TC from 2-Step Combustion was selected as the reference for the carbonaceous material because this parameter can be determined with highest precision [*Schmid et al.*, 2001]. The relative split of EC and OC and the relative contributions of OC fractions of different volatility were analysed from the thermograms.

EC is defined by different approaches:

1 2-Step Combustion determines EC from the carbonaceous fraction remaining after the 340°C combustion step.

2 Thermogravimetry combined with laser filter transmission monitoring measures EC when the laser transmission signal exceeds the average value for temperatures < 350°C by 3 standard deviations (99% statistical significance level).

3 Gaussian fitting interprets non-volatile carbonaceous matter as the fraction which vaporises at temperatures > 350°C, i.e. peaks no. #3, #4, and #5 (counting starts from left), see the bottom panel of Figure 22 for details.

Table 11. Non-volatile fraction of TC from different approaches, see text for details.

Condition	Filter #	2-Step Comb	TG laser	TG Fit	T_{OC} , °C
low SN – low OM S1	22	0.953	0.752	0.871	412
low SN – low OM S1	27	0.916	0.865	0.858	426
low SN – low OM S2	3	0.661	0.731	0.705	437
low SN – high OM	10	0.604	0.647	0.657	391
low SN – high OM	9	0.597	0.733	0.658	435
low SN – high OM	8	0.498	0.721	0.656	411
low SN – high OM	11	0.502	0.657	0.725	363
high SN – low OM	18	0.969	0.685	0.910	374
high SN – low OM	19	0.934	0.672	0.850	437
high SN – low OM	20	0.965	0.834	0.915	386
high SN – low OM	21	0.872	0.618	0.911	389
high SN – low OM	24	0.801	0.849	0.879	439
high SN – low OM	16	0.998	0.693	0.954	350
high SN – low OM	25	0.741	0.673	0.909	408
high SN – low OM	15	0.958	0.643	0.900	419
high SN – low OM	14	0.922	0.815	0.911	375
high SN – low OM	13	0.911	0.617	0.965	358
high SN – low OM	12	0.978	0.515	0.946	390

Table 10 summarises average relative fractions of EC, BC, and $TC_{Non\text{-}Vol}$ with respect to TC from the applied methods and permits an estimation of the recovery rates of different methods for non-volatile matter using total carbon as reference metric. The non-volatile fractions of TC resulting from the different approaches are summarised in Table 11 for the entire set of analysed quartz fibre filter samples.

For *high SN – low OM* and for *high SN – low OM* conditions the peak at T ≅ 600°C dominates the thermogram, indicating that the carbonaceous fraction is composed predominantly of elemental carbon with a high thermal stability. 2-Step Combustion and Gaussian fitting agree well for reported values for EC fractions of TC while the laser transmission method overcorrects the OC contribution for heavily loaded filters and thus underestimates $TC_{Non\text{-}Vol}$. BC / TC ratios agree well with EC / TC and with $TC_{Non\text{-}Vol}$ / TC for low SN conditions. For those cases, elemental carbon, black carbon and non-volatile carbon are of equal value.

For the *low SN - high OM* condition a significant fraction of carbonaceous material volatilises at temperatures < 350°C. BC / TC agree well with EC / TC while $TC_{Non\text{-}Vol}$ / TC (TG Fit) exceed these values significantly, indicating that approx. 15% of non-volatile matter can be associated to non-volatile organic compounds of so far unknown composition. For particles containing a large fraction of OM, EC and BC – sensitive methods tend to underestimate non-volatile mass.

The temperature T_{OC} defines the transition between volatile and semi-volatile OC on one hand and non-volatile OC and EC on the other hand. This transition is defined by the local minimum of the thermogram around 400°C. Figure 21 demonstrates that all thermograms showed such a local minimum. Furthermore this local minimum is close to the OC-EC separation temperature of 340°C applied in the 2-Step Combustion method.

Analysing the volatilisation temperature T_{OC} and the respective non-volatile fraction of TC provides the results listed in Table 10 for session averages and in Table 11 for each sample. The average volatilisation temperature T_{OC} is slightly higher than the temperature of 350°C defined in AIR 5892 [*SAE*, 2004] but rather constant. Referring to T_{OC} as the temperature separating volatile and non-volatile matter indicates that for the investigated conditions from 9% (*high SN, low OM*) to 33% (*low SN, high OM*) of the total carbon mass are volatile.

Summarising, the volatility properties of the carbonaceous fraction of gas turbine exhaust particle can be characterised by 5 modes wit different volatilisation temperatures. Averaging over the entire SAMPLE data set, volatilisation temperatures are:

Peak #1:	255 ± 78 °C
Peak #2:	360 ± 82 °C
Peak #3:	510 ± 39 °C
Peak #4:	570 ± 38 °C
Peak #5:	630 ± 39 °C

Identifying peaks #3 to #5 as non-volatile carbonaceous matter provides good agreement with simultaneous BC measurements, see Table 10. Thus, the temperature threshold for the determination of non-volatile PM might be increased from currently 350°C [*SAE*, 2004] to 400°C in order to provide good agreement between non-volatile carbonaceous matter and light absorbing black carbon. This increase of the temperature threshold is still within the limits set by AIR 5892 which defines non-volatile particles as “particles that exist at engine exit plane temperature and pressure conditions” [*SAE*, 2004].

4.2.2 Aerosol Mass Spectrometry

During SAMPLE, a High Resolution Time-of-Flight Aerosol Mass Spectrometer (HR-ToF-AMS) was successfully deployed to measure the none-refractory (volatile and semi-volatile), sub-micron aerosol composition. This includes the total organic mass (OM) and inorganic species such as sulphate and nitrate. Substances such as Black Carbon are not measured by the HR-ToF-AMS. The HR-ToF-AMS is manufactured by Aerodyne Research Inc (http://www.aerodyne.com/). The University of Manchester owns three different AMS and there are approximately 70 worldwide.

The HR-ToF-AMS can measure either a complete mass spectrum from 0 to 550 mass-to-charge ratios (m/z) with a high signal to noise or the chemical composition as a function of size. The HR-ToF-AMS measures particles in the size range 60 – 600 nm with 100% transmission efficiency. Above or below these sizes and the transmission efficiency falls to zero. The two main advantages of using this instrument are: the quantifiable nature of the HR-ToF-AMS and the real time measurements. A full description of the HR-ToF-AMS can be found at http://cires.colorado.edu/jimenez-group/wiki/index.php?title=ToF-AMS_Main, which also includes all the resources available to all AMS users.

Results

Figures 23 shows the time trends of total OM and some of the inorganic species as measured by the HR-ToF-AMS. Top panel of Figure 23 (30/03) shows the time trends before and after switching from the diluted to the undiluted lines. All measurements 'on condition' were taken from the undiluted line. Bottom panel of Figure 23 (01/04) only shows OM and SO_4 as these dominate the total mass. The periods marked Condition 3 (1-3) are different sampling periods on the same condition. Condition 3-2 was defined as the stable rig condition and is used in any averaging to represent the Rich condition.

Figure 24 shows the average mass distribution of SO_4 and OM from Conditions 1, Condition 2, and Condition 3. All 4 graphs show that under Conditions 2 and 3 the OM was higher than under Condition 1. The SO_4 loadings for Conditions 2 and 3 are approximately the same, but under Condition 2 conditions the SO4 is approximately the same as the organic loading (Condition 3 SO_4 is plotted on the left hand axis). Figure 24 also shows that there is a shift in size, with Condition 2 producing the smallest particles, Condition 3 the largest and Condition 1 sitting in between.

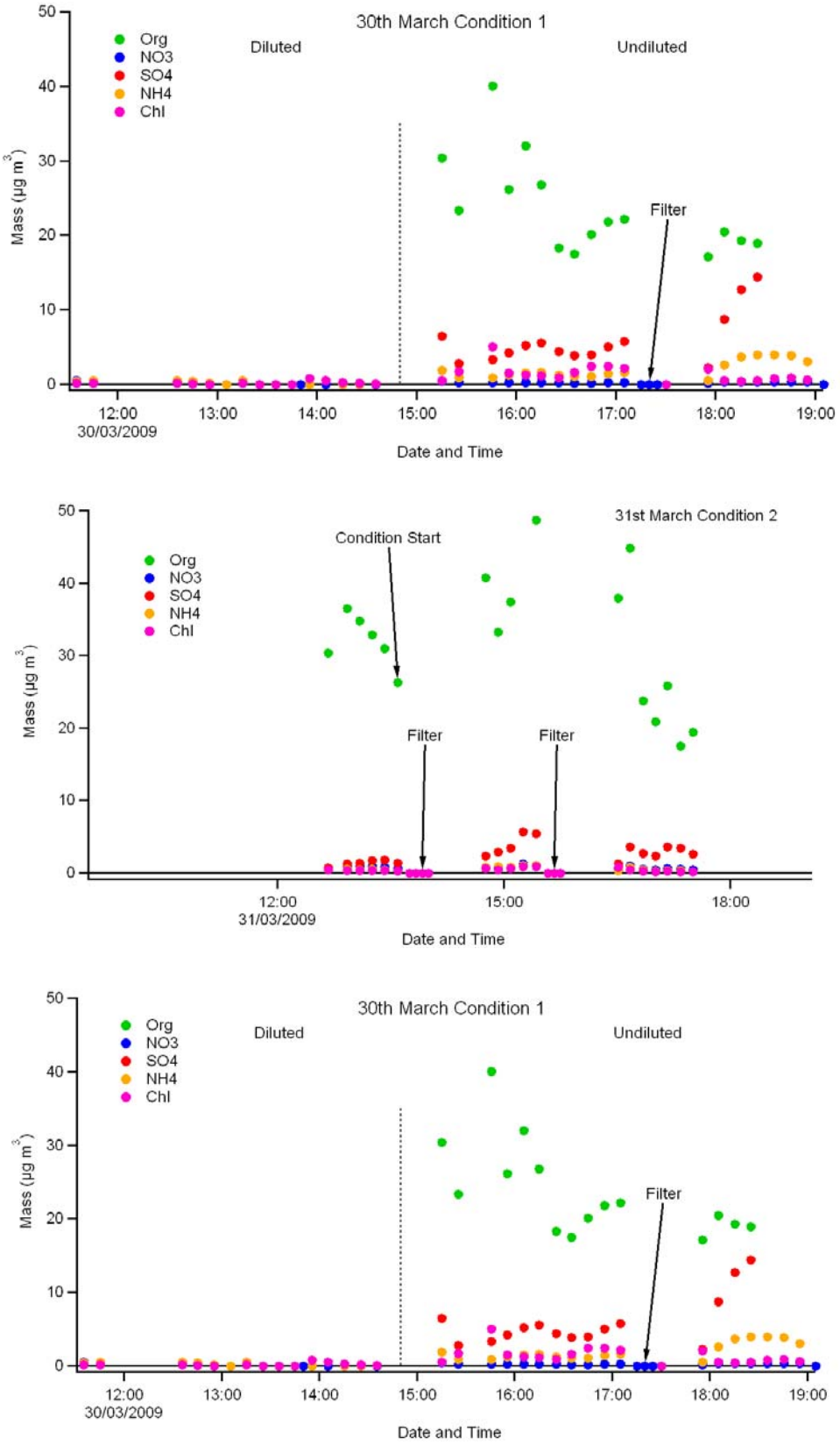

Figure 23. Time series of total OM and some of the inorganic species as measured by the HR-ToF-AMS; top panel: Condition 1 (*low SN - low OM Session 1*); mid panel: Condition 2 (*low SN - high OM*l); bottom panel: Condition 1 (*low SN - low OM Session 2*) and Condition 3 (*high SN - low OM*).

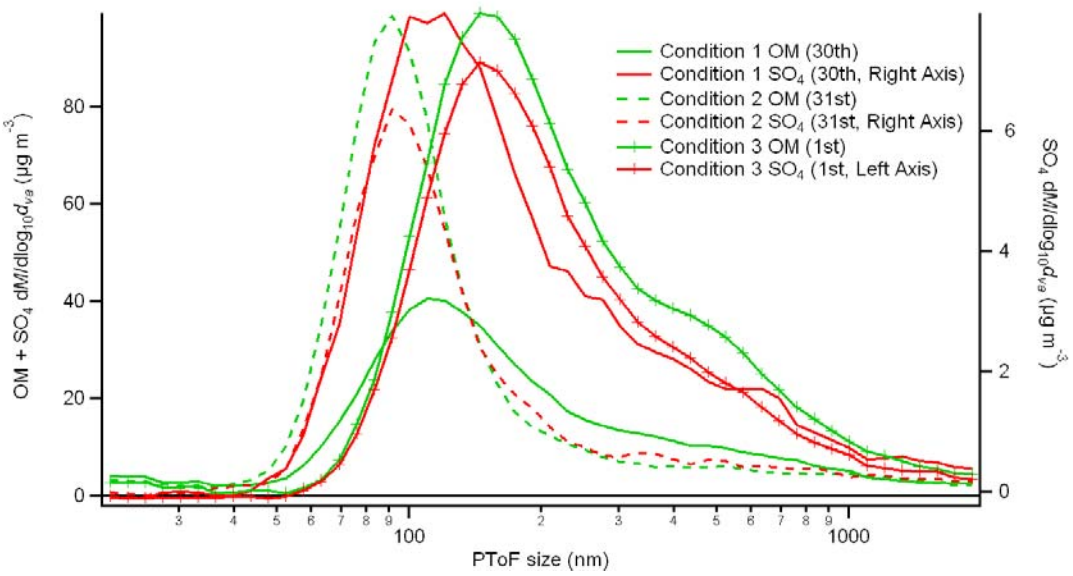

Figure 24. Average mass distribution of SO_4 and OM from Conditions 1, Condition 2, and Condition 3.

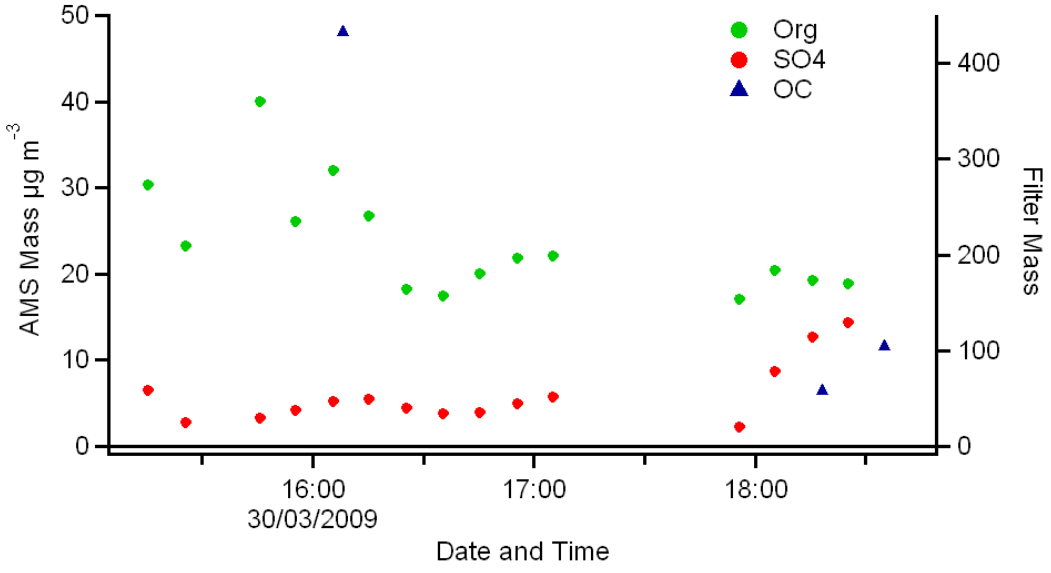

Figure 25. Comparison of the HR-ToF-AMS OM with filter based measurements of OC.

Comparison with other methods

Figure 25 shows the comparison of the HR-ToF-AMS OM with filter based measurements of OC. Although OM and OC are not the same, the theoretical conversions from one to another in the literature are less than an order of magnitude, see Eqs. (2) and (2a) for clarification. This shows that the HR-ToF-AMS is under measuring the mass when compared with filters. Comparison of the HR-ToF-AMS mass with a convolved mass distribution from the DMS-500 (assuming a density of 1000 kg / m³) shows that the DMS-500 measures more mass, which is to be expected as it does not distinguish volatile from semi-volatile. The comparison shows that there is mass below 60 nm not seen by the HR-ToF-AMS, although it is impossible to say how much of that is black carbon and how much is organic matter.

One possible explanation for this missing mass comes from the analysis of the LII data. It was found that 1 in every 150 events was a relatively large, super-micrometer sized particle. If the HR-ToF-AMS is measuring a peak particle size of 100nm and a 1000nm particle comes through, which the HR-ToF-AMS does not sample efficiency, that is a factor of 10 in diameter, which is a factor of 1000 in mass (mass proportional to Dp^3). If 1 in 150 particles are these larger agglomerates, then approximately there is 1000/150 times more mass on the filters that the HR-ToF-AMS does not see. i.e $\cong$ 6.67. Scaling the filter mass by this factor and the HR-ToF-AMS are in better agreement.

In summary, the application of aerosol mass spectrometry to a quantitative analysis of the organic fraction of the particles emitted form a gas turbine is not straight forward. Caused by the large number fraction of particles smaller than 60 nm in diameter, particle sampling is an important issue. Recalling the great potential of aerosol mass spectrometry for the on-line chemical analysis of particulate matter, further studies are suggested in order to improve the applicability of aerosol mass spectrometry for the measurement of volatile matter in gas turbine exhaust particles.

4.3 Particle number measurement

Three different models of CPC were operated in parallel during the trials in order to provide intercomparison data for two identical instruments. Furthermore, one instrument of each of the CPC models TSI 3010 and TSI 3760A were connected to a thermodenuder (TD) which was operated at 350 °C. This thermodenuder was used to test whether or not the hot dilutor removes all volatile material from the exhaust particulate matter. In order to test the instrument response without a thermodenuder connected to the CPC all instruments were operated during a dedicated sequence on laboratory air. Additional to the CPC, the total number concentration of particles was derived from the mobility spectra of the DMS 500 instrument.

Table 12 summarises the average number concentrations measured by the different CPC instruments for the rig operation conditions. According to the different minimum detection diameters $D_{p,\,min}$ the number concentrations appear in the order:

$$N(\text{DMS 500}) \cong N(\text{GRIMM 5.400}) > N(\text{TSI 3010}) > N(\text{TSI 3760A})$$

with N(DMS 500) showing the largest scatter of the studied methods.

Table 12. Average number concentrations measured by the different CPC systems in the raw exhaust gas; dilution factors are corrected. All values are in given as 10^7 cm^3 STP

	TSI 3760A		TSI 3010		GRIMM 5400		DMS 500
	$D_{p,\,min} \cong 14$ nm		$D_{p,\,min} \cong 10$ nm		$D_{p,\,min} \cong 5$ nm		
Condition	#1	#2	#1	#2	#1	#2	
low SN-low OM [#]	0.96	0.81	0.86	0.99	1.22	1.26	
low SN-low OM [§]	1.09	1.32	1.39	1.19	1.60	1.62	2.17
low SN-high OM [#]	2.79	2.16	2.62	2.91	3.61	3.54	3.40
low SN-high OM [§]	1.40	1.8	2.07	1.7	2.58	2.48	
low SN-low OM [$]	N/A	N/A	N/A	N/A	N/A	N/A	
high SN-low OM [#]	1.86	1.64	1.79	1.89	2.14	2.26	1.92

[#] TSI 3760A #2 and TSI 3010 #1 connected to TD
[§] TSI 3760A #1 and TSI 3010 #2 connected to TD
[$] during this run, the CPC sample line did not work properly

Table 13. Results of linear regression analysis of two identical CPC of type GRIMM 5.400 operated in parallel for all investigated rig conditions.

Date	Condition	Slope	Ratio	r
30/03/2009	*low SN-low OM*	1.049 ± 0.001	1.070 ± 0.108	0.993
31/03/2009	*low SN-high OM*	0.978 ± 0.001	0.979 ± 0.038	0.987
01/04/2009	*high SN-low OM*	1.011 ± 0.002	1.039 ± 0.146	0.944

Figure 26 and Table 13 compile the results of the parallel operation of two identical CPC instruments of type GRIMM 5.400. Because the other CPC models were not operated under similar conditions during the trials the direct comparison was performed for laboratory air. Results are shown in Figure 27. This intercomparison yields the value of the instrument response *f(CPC)* to sampled aerosol with a detection efficiency relative to a reference instrument with

$$f(CPC) = N(CPC\#2) / N(CPC\#1)$$

The value of *f(CPC)* varies from 0.0 to 1.0 depending on the instrument. For a set of ideal CPC the relative detection efficiency is 1.0.

Combining the resulting values from the laboratory air test with the results from the GRIMM5.400 correlation analysis (Table 13) yields an evaluation of CPC instruments for the measurement of particle number concentrations:

Model TSI 3760A	$N(CPC\#2) / N(CPC\#1) = 0.925 \pm 0.077$, $r = 0.998$
Model TSI 3010A	$N(CPC\#2) / N(CPC\#1) = 1.044 \pm 0.087$, $r = 0.995$
GRIMM 5.400	$N(CPC\#2) / N(CPC\#1) = 1.013 \pm 0.036$, $r \geq 0.944$

Testing the Hot Dilutor removal efficiency

The determination of the removal efficiency of the deployed DEKATI hot diluter was based on the simultaneous operation of two identical CPC instruments with one being connected to a thermodenuder operated at 350 °C and the other one sampling cold exhaust gas without thermal treatment. Knowing the relative detection efficiencies *f(CPC)* for the two CPC model pairs permits to calculate the transmission efficiency *f(TD)* of the thermodenuder connected to the instrument. This value describes which fraction of the sampled aerosol is transmitted through the heated thermodenuder. For an ideal non-volatile aerosol the transmission efficiency is 1.0.

Assuming that the DEKATI hot diluter removes all volatile matter from the sample, the transmission efficiency of the thermodenuder is expected to equal 1.0 because all particulate matter downstream the hot diluter should be non-volatile. If the DEKATI system does not remove all volatile matter, the thermodenuder transmission efficiency is < 1.0, i.e., the removal efficiency of the DEKATI system is characterised by *f(TD)*.

Switching the thermodenuder (TD) for the same aerosol from one instrument to the other allows determining *f(TD)*:

with TD connected to CPC#1	$f(TD) = [N(CPC\#1) / N(CPC\#2)] \ / f(CPC)$
with TD connected to CPC#2:	$f(TD) = [N(CPC\#2) / N(CPC\#1)] \times f(CPC))$

Table 14 compiles the respective average values and standard deviations of each instrument pair. Please note which of the instruments was connected to the TD. Obviously, the hot dilutor which is expected to remove all volatile particulate matter operates at an average efficiently of 77% to 88%. Differences in the values are related to the different flow rates of the CPC. Model TSI 3010 operates on a flow rate of 1.0 litre per minute while model TSI 3760A operates on 1.5 litres per minutes, resulting in a shorter residence time of the aerosol in the thermodenuder.

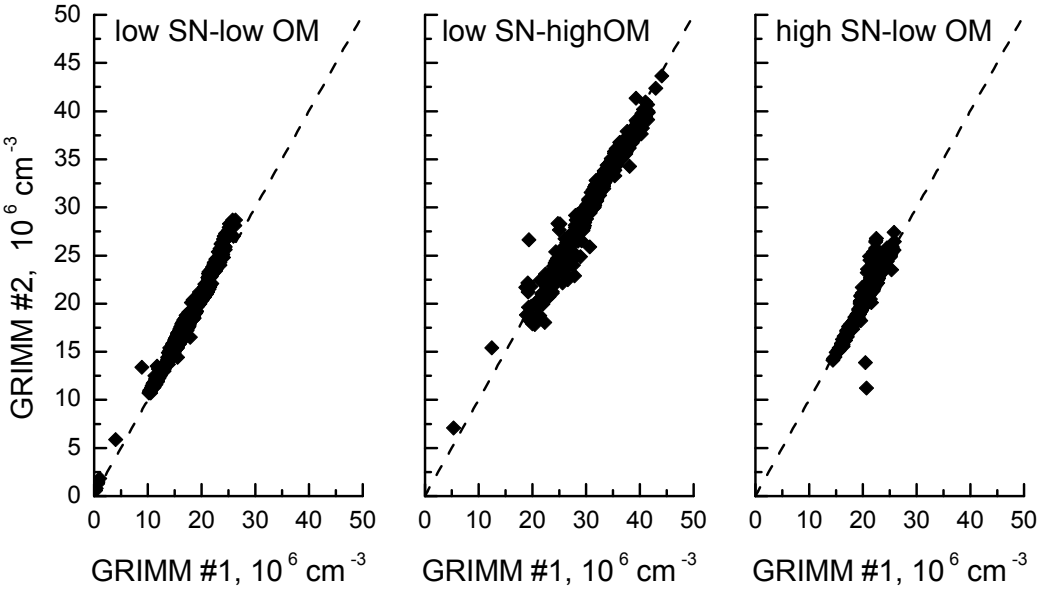

Figure 26. Correlation of two identical CPC instruments of type GRIMM 5.400 for all investigated rig conditions.

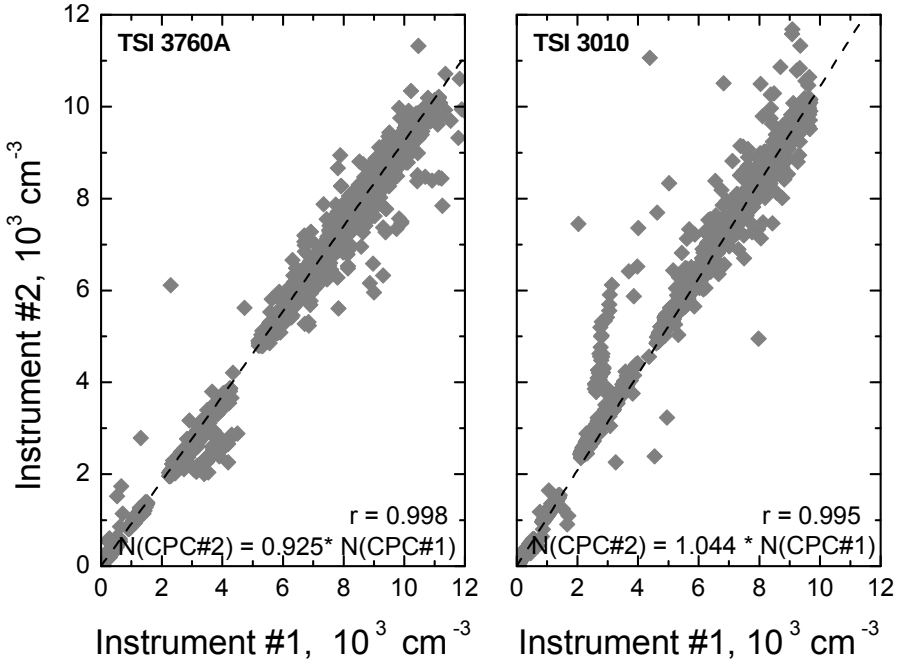

Figure 27. Comparison of TSI CPC models without the thermodenuder being connected to one of the instruments.

Table 14. Ratios of CPC number concentrations measured in the raw exhaust gas; thermodenuder removal efficiencies are calculated as described in the text.

Date	Condition	TSI 3760A CPC#2/CPC#1	TSI 3010 CPC#2/CPC#1	GRIMM 5400 CPC#2/CPC#1	TD removal 3760A	TD removal 3010
30/03/2009	*low SN-low OM* [#]	0.837	1.130	1.038	0.77	0.85
30/03/2009	*low SN-low OM* [§]	1.212	0.853	1.011	0.76	0.89
31/03/2009	*low SN-high OM* [#]	0.774	1.110	0.979	0.72	0.86
31/03/2009	*low SN-high OM* [§]	1.289	0.823	0.961	0.72	0.86
01/04/2009	*low SN-low OM* [$]	0.883	1.053	1.055	0.82	0.91

[#] TSI 3760A #2 and TSI 3010 #1 connected to TD
[§] TSI 3760A #1 and TSI 3010 #2 connected to TD
[$] during this run, the CPC sample line did not work properly

The removal of particles in the thermodenuder which is associated to additional particle losses in the system is unacceptable and would require further investigation. The applied TD system was calibrated with entirely non-volatile particles in earlier laboratory studies. A repetition of these calibration studies seems valuable for testing the removal efficiency of the DEKATI Hot Diluter systems. However, these studies are beyond the scope of SAMPLE.

4.4 Particle size measurement

The data analysis of the Differential Mobility Spectrometer is summarised in Table 15. Compiled are the count median diameter (CMD) and the geometric standard deviation (GSD) for two modes of the size distribution. The CMD is chosen such that 50% of the particles by number are smaller than the CMD and 50% are larger in size. These properties are defined on the basis of a bi-modal log-normal size distribution as [*Hinds*, 1999]

$$\frac{dN}{d\log D_p}(D_p) = \sum_{i=1}^{2} \frac{N_i}{\sqrt{2\pi}\,\log(GSD_i)} \exp\left[-\frac{1}{2}\frac{(\log(D_p)-\log(CMD_i))^2}{\log(GSD_i)^2}\right]$$

DMPS data are not available because of instrument malfunction during the trials.

Table 15. Results of the particle size sensitive instruments; DMS was operated with models of serial numbers M44 and M45.

Condition	DMS #	DMS 500 Mode 1 CMD, µm	DMS 500 Mode 1 GSD	DMS 500 Mode 2 CMD, µm	DMS 500 Mode 2 GSD
low SN-low OM	M45 Line 2	15.1	1.54	50	1.43
low SN-low OM	M45 Line 1	15.3	1.54	54.1	1.42
low SN-high OM	M45 Line 2	14.3	1.55	45	1.31
low SN-high OM	M45 Line 1	15.2	1.55	46.2	1.3
low SN-high OM	M44 Line 1	13.5	1.55	45.5	1.31
low SN-low OM [$]	M44 Line 1	16.3	1.51	53.1	1.39
high SN-low OM	M44 Line 2	17.4	1.5	58.5	1.45
high SN-low OM	M44 Line 1	17.8	1.49	58.1	1.46

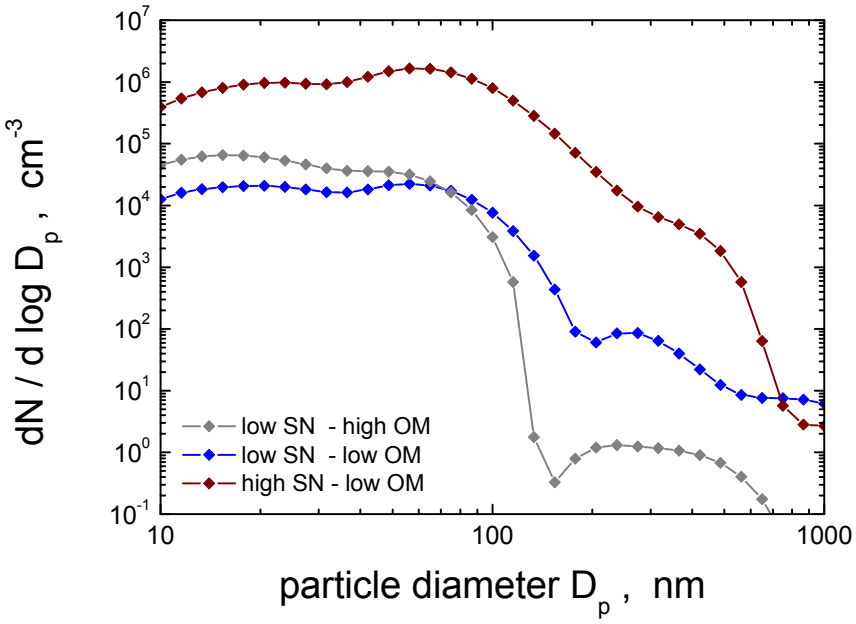

Figure 28. Particle size spectra for all investigated condition measured with a DMS 500; the fraction of particles larger than 10 nm in diameter is > 90% for all investigated conditions.

Table 16. Size distribution measurements for Condition1 and Condition 2 using two DMS 500 instruments in the hot diluted line (line 2).

Condition	DMS 500 1st Mode CMD (nm)	GSD	2nd Mode CMD	GSD	Instrument Serial No.
low SN - low OM	15.8	1.54	53.5	1.40	M44
low SN - low OM	15.7	1.53	51.6	1.39	M44
low SN - low OM	15.8	1.54	50.0	1.41	M45
low SN - high OM	15.1	1.53	46.6	1.30	M44
low SN - high OM	14.1	1.54	46.9	1.32	M44

Summarising, the exhaust aerosol always occurred in a bi-modal size distribution with mode 1 being centred in the diameter range from 13.5 to 17.8 nm and mode 2 being centred in the range from 45.5 to 58.5 nm. Examples for each condition are plotted in Figure 28.

The count median diameters of the modes depend on operation conditions: particles are largest for high smoke conditions and they are smallest for low smoke – low OM conditions. The reproducibility of particle size measurements is shown in Table 16. Performing measurements in the same sampling line with two types of the DMS 500 instruments yields relative deviations of measured CMD values of < 4%.

5 Conclusions

Mass-based methods:

1. Total mass from the gravimetry method (TM_{GRAV}) exceeds all other mass measurements.
2. Total mass determined from the sum of the major chemical constituents (TM_{SUM}) balances the gravimetric mass TM_{GRAV}. TM_{SUM} includes elemental carbon, organic matter (= organic carbon plus an estimate for oxygen and hydrogen contents of organic matter), and an estimate of sulphate from the fuel sulphur content using the First Order Approximation Version 3 (FOA 3). No major particulate matter constituent is missed in the chemical analysis.
3. In general, total non-volatile carbon from the 2-Step Combustion method agrees well with total non-volatile mass data calculated from the SN equation within FOA 3 (±10%) as long as the organic carbon content is small. However, as this non-volatile part of FOA 3 does not account all of the organic matter, it can underestimate total carbon mass by approx. 40% where particulate matter contains a high organic matter fraction.
4. The non-volatile part of FOA 3 has an even greater underestimation of gravimetrical mass (19 to 53%), depending on the organic carbon fraction. Neither the oxygen and hydrogen contributions to organic matter fraction, nor sulphate, is recovered by the non-volatile part of FOA 3.
5. Black carbon from MAAP, elemental carbon from 2-Step Combustion and non-volatile carbon from Thermogravimetry agree well for particulate matter with low organic matter content. For particulate matter of high organic matter content, Thermogravimetry reports a fraction of non-volatile organic carbon compounds which is neither measured by optical methods (because it absorbs no light) nor by 2-Step Combustion (because it classifies all carbon above a volatilisation temperature of 340°C as elemental carbon). The non-volatile organic carbon fraction can contribute approx. 15% to total carbon.
6. Black carbon from MAAP and elemental carbon from 2-Step Combustion report particulate matter fractions contributing 35 to 70% to total mass from Gravimetry. This ratio is a measure for the underestimation of total mass if light-absorbing black carbon or elemental carbon is used as a proxy for non-volatile particulate mass.
7. MAAP as an on-line instrument measuring light absorbing carbon (black carbon) proved successful and well applicable to exhaust studies as long as the sample gas prior to the measurement is diluted. The application of high carbon loadings requires instrument modifications by the manufacturer to allow operation at lower flow rates.
8. The laser-induced incandescence technique which is capable of measuring black carbon from either undiluted or diluted exhausts in real time detected the presence of super-micron particles (sampling artefacts see 'Sampling line effects'). The existence of these large particles meant that the BC mass measurement could not be directly compared with other methods. However, statistical inclusion of the super-micron detection incidences did provide good agreement with other methodologies measuring total BC mass (see specific LII report in the Appendix A).

9. Indirect methods for measuring mass concentrations such as differential mobility spectrometers (or other size distribution instruments) appear to be of limited applicability for gas turbine particulate exhaust because they suffer from sampling limitations - inability to distinguish non-volatile/volatile composition and from the need for a priori assumptions of particle effective density and shape. In addition, their size cut-off limits the measurement of the sample line shedding phenomenon.
10. Experience from the DMS, LII and microscopy measurements point towards the application of an upper cut-off diameter for sampling in order to prevent measurement of mechanically generated super-µm particles. The consequences of such a size restrictor on sampling performance and maintenance have to be carefully considered. It should be noted that automotive regulated particulate measurements include an upper cut-off for health impact reasons, but this is why the particle shedding phenomenon has not previously been detected as a sampling artefact in combustion particle studies.

Number-based methods:

1. Condensation particle counter based instruments are highly robust tools for the measurement of aerosol number concentrations, characterised by maximum deviations of 7.5% and correlation coefficients $r > 0.94$. Dilution of sample gas prior to the measurement is required.
2. Absolute number concentrations given by different condensation particle counter models require careful consideration because the absolute values are highly sensitive to the minimum detection diameter, defined for 50% detection efficiency. Number concentration data can differ significantly between instruments with different 50% detection efficiency diameters.
3. The definition of a standard method requires an agreement on the 50% detection efficiency diameter of the applied instrument. Measured non-volatile particle size distributions indicate a bi-modal size distribution with the smaller mode centred at 15 – 16 nm (Table 15). Modelling results for the hot sample line indicate a volatile particle mode below 10 nm in diameter (Appendix C, ONERA report, Figure 14). From these results, a 50% detection efficiency diameter of 10 nm appears appropriate.
4. Indirect methods for the measurement of particle number concentrations as Differential Mobility Spectrometry should not be considered as a condensation particle counter. Accepting indirect methods as a standard procedure requires additional intercomparison efforts.

Particle size-based methods:

1. Differential mobility spectroscopy yields relative deviations of measured count median diameters of < 4%.
2. Differential mobility spectrometry appears to be a well reproducible method for measuring particle size distributions in aircraft engine exhaust.
3. The intercomparison between different instruments using differential mobility spectrometry was not performed within SAMPLE due to the failure of one instrument. The intercomparison of average particle sizes determined with different methods is an open issue for future method evaluation studies.

Sampling line effects:

1. Particle nucleation is clearly correlated to the sample thermodynamic changes (especially temperature).
2. Particles even form in the hot diluted line, in spite of a 1:100 overall dilution with dry air.
3. As indicated from sample line model results (see specific sample line model study in the Appendix), entirely volatile particles remain small in diameter (below 10 nm). Measurements document, that more than 90% of non-volatile combustion particles are larger than 10 nm in diameter.
4. Soot particles are affected in terms of weak particle growth which is dominated by condensation of volatile material. The increase in the particle count median diameter is less than 5 nm. Thus, particle coagulation is not a major process, but particle growth.
5. Large (super-micron) black carbon particles were detected by several instruments as a function of particle shedding. These mechanically generated particles are a secondary source of soot particles that have deposited on surfaces due to thermophoretic motion and diffusion, and then re-entrained into the sample flow due to flow turbulence. This process will reach some sort of equilibrium but with uncertain shedding frequency. In order to only measure the gas turbine combustion particulates an upper cut-off size would be required to remove these shedding artefacts.

6 Recommendations

Based on the above conclusions, the main recommendations from the SAMPLE study are:

1. Considering the decreasing smoke level of modern aircraft engines, gravimetry as the reference method for total non-volatile PM mass measurement is limited by filter exposure time. Sample exposure times of 40 min (Table 8) and more are not practical for engine testing.
2. Carbon sensitive methods like 2-Step Combustion (off-line, filter exposure time < 15 min) or light absorption photometry (on-line, 1 Hz data resolution) offer modern and highly sensitive alternatives to gravimetry for measuring non-volatile particulate matter.
3. Considering the effect of large mechanically generated particles (shedding), an upper size cut-off limit should be applied. Gas turbine combustion produces soot particles <1um, therefore a 1 micron cut-off seems reasonable. However further research is required to assess this issue.
4. Precise instruments for particle number measurements are available. An agreement on the 50% detection efficiency diameter of the applied instruments is required. Based on current experience, a value of 10 nm appears appropriate.
5. Particle size distribution measurement by electrical mobility spectrometers offers a promising way forward. Intercomparison of different instruments and the definition of respective operation conditions are potential remaining issues for further research.

6. Removal of volatile and semi-volatile matter by a hot dilution system followed by a sampling line of sufficient length ensures complete removal of volatile compounds. Details in terms of residence time, i.e., line length and volumetric flow rate have yet to be specified and require further research.
7. Sample dilution is required for suppressing particle coagulation and enabling the application of current particle counting methods, on-line mass-based methods and particle sizing methods. Based on current experience, specifications for sample dilution have to be developed within further research.

7 References

Agrawal, H., et al. (2008), In-use gaseous and particulate matter emissions from a modern ocean going container vessel, *Atmospheric Environment*, *42*(21), 5504-5510.

Aiken, A. C., et al. (2008), O/C and OM/OC Ratios of Primary, Secondary, and Ambient Organic Aerosols with High-Resolution Time-of-Flight Aerosol Mass Spectrometry, *Environ. Sci. Technol.*, *42*(12), 4478-4485.

Baron, P. A., and K. Willeke (2001), *Aerosol measurement: Principles, techniques and applications*, 2nd ed., John Wiley and Sons, New York.

Burtscher, H., et al. (2001), Separation of volatile and non-volatile aerosol fractions by thermodesorption: Instrumental development and applications, *J. Aerosol Sci.*, *32*(4), 427-442.

CAEP (2007), Particulate Matter Characterisation, *CAEP Information Paper*, CAEP/7-IP/6.

CAEP (2008), FOA Guidance Manual for Use By MODTF, *CAEP Working Paper*, CAEP8-WG3-WP09.

Hinds, W. C. (1999), *Aerosol Technology: Properties, Behaviour and Measurement of Airborne Particles.*, 483 pp., John Wiley & Sons, Inc., New York.

Petzold, A., and F. Schröder (1998), Jet engine exhaust aerosol characterisation, *Aerosol Sci. Technol.*, *28*, 62-76.

Petzold, A., and M. Schönlinner (2004), Multi-angle absorption photometry - A new method for the measurement of aerosol light absorption and atmospheric black carbon, *J. Aerosol Sci.*, *35*(4), 421-441.

Petzold, A., et al. (2005a), Particle emissions from aircraft engines – a survey of the European project PartEmis, *Meteorologische Zeitschrift*, *14*, 465-476.

Petzold, A., et al. (2005b), Evaluation of multiangle absorption photometry for measuring aerosol light absorption, *Aerosol Sci. Technol.*, *39*, 40-51.

SAE (1997), ARP 1179: Aircraft gas turbine smoke measurement, *SAE Aerospace Recommended Practice*.

SAE (2004), AIR 5892: Nonvolatile Exhaust Particle Measurement Techniques, *SAE Aerospace Information Report*.

SAE (2009), AIR 6037: Aircraft Exhaust Nonvolatile Particle Matter Measurement Method Development, *SAE Aerospace Information Report*.

Schmid, H., et al. (2001), Results of the carbon conference international aerosol carbon round robin test stage I, *Atmos. Environ.*, *35*, 2111-2121.

Snelling, D. R., et al. (2005), A calibration-independent LII technique for soot measurement by detecting absolute light intensity, *Applied Optics*, *44*, 6773-6785.

Symonds, J. P. R., et al. (2007), Diesel soot mass calculation in real-time with a differential mobility spectrometer, *Journal of Aerosol Science*, *38*(1), 52-68.

Wilson, C. W., et al. (2004), Measurement and prediction of emissions of aerosols and gaseous precursors from gas turbine engines (PartEmis): an overview, *Aerospace Science and Technology*, *8*, 131–143.

This page is intentionally blank.

8 Appendices

A –QinetiQ Fuel Analyses

B – Atrium LII SAMPLE Report

C – ECATS - ONERA Sampling Line Modelling Report

D - ECATS – ONERA Electron Microscopy Report

E – SAMPLE - Calibration Source Study

This page is intentionally blank.

Fuel analysis

FAO: Mike Miller
QinetiQ GTT,

Report Summary			
Report No.	F200903188	**Material**	AVTUR F-35
Overall Status	n/a	**Specification**	DEF STAN 91-91/6
Received From	QinetiQ GTT	**Senders Ref.**	Email Mike Miller
Date Received	24/FEB/2009	**QinetiQ Ref.**	PROJ/12/7/9
Sample Description		**System Information**	
1 x 1 Litre glass bottle.		2009003188 - GTRC fuel sample.	
Reason For Test			
For hydrogen, sulphur, carbon content & calculated calorific value.			
Comments			
Please see results overleaf.			

Sample Results				
Sample Number	**Status**	**Test**	**Results**	**Method**
2009003188	n/a	Calculated Specific Energy	43.33 MJ/kg	IP 355
		Density at 15 °C	796.1 kg/m3	IP 365 (FLM 42)
		Hydrogen	13.93 % Mass	IP 338 (FLM 50) ASTM
		Sulphur By XRF	0.03 % Mass	FLM183
		Carbon content (by deduction)	86.04 % Mass	

From: Fuels & Lubricants Centre
Cody Technology Park,
Building A7, Room 1035,
Farnborough, Hampshire.
GU14 0LX

Tel : 01252 39 7421
Fax : 01252 39 4503
Email: jaamero@QinetiQ.com

Report By: J.A.Amero

Name: J Amero

Authorised By: S Holbrake

Date: 24/FEB/2009

This page is intentionally blank.

Artium Technologies Inc.
150 West Iowa Avenue, Unit 202
Sunnyvale, CA 94086

Study on Sampling and Measurement of Aircraft Particulate Emissions (SAMPLE) Report

William D. Bachalo and Gregory J. Smallwood*

5-15-09

Laser-Induced Incandescence

Introduction:

We were pleased be able to participate in this very important program of instrument evaluations for gas turbine engine particulate emissions monitoring. Particulate matter (PM) emissions are known to be hazardous to both human health and the earth's atmosphere. As gas turbine engines are continuously developed to produce lower particulate emissions, methodologies that worked at the higher particulate emissions have become impractical. For example, filter-based methods that are used to produce an SAE smoke number have been applied with the justification coming from visibility criteria of aircraft plumes. This relatively crude approach does not provide direct information on particulate mass nor does it distinguish between particle sizes and is known to miss capturing all of the solid particles, especially the smaller particles. With the goal of identifying and applying modern methods for measuring particular matter, the purpose of the current program is specified as "to test and evaluate techniques and methods for PM measurements in the exhaust of aircraft engines at engine exit plane conditions". The goal of the tests was to "provide the community with necessary information on instrument applicability and method characteristics under real-world conditions corresponding to engine certification measurements". Tests were conducted using the simulated combustor known as the PARTEMIS TAY Combustor which is connected to the Hot End Simulator (HES) located at Port Talbot, Wales. This facility is designed to simulate gas turbine combustor sections of aircraft engines and to produce particulate with "physicochemical" properties comparable to particulates emitted from real aircraft gas turbines.

Our concern and approach focuses on nonvolatile PM emissions measurements which falls in line with the test program goals associated with nonvolatile particulate sampling. Under these test criteria outlined in the DLR proposal, are methodologies and standards for instrument

* National Research Council Canada, 1200 Montreal Road, Building M-9, Ottawa, ON, Canada K1A 0R6

calibration associated with PM measurements. Furthermore, development of sampling systems required for transporting exhaust particulate emissions to the measurement instruments while minimizing sample line effects on the particle concentrations and properties are part of the evaluations program. One candidate method, Laser-induced incandescence (LII) has the unique advantage of being able to sample the direct exhaust from combustion systems. LII only detects and measures elemental carbon (EC) particles and is not affected adversely by the presence of condensed material or other particulate matter. As such, it may be considered as a means of determining the presence of other particulate matter by way of comparison to methods that measure all of the PM simultaneously. In addition, large agglomerate particles in the sample exhaust which may be considered to be artifacts of the sampling process may be detected. As will be noted in the following sections, these very problems with large agglomerates appear to exist in sampling systems and it is my opinion that the existence of these large agglomerates will impact the measurement results produced not only by LII, but by all the various instrument types.

In the following sections, we will provide a description of the LII method, the specific set up and sampling configuration used at the Port Talbot facility, and will summarize results acquired. Measurement examples will be given to support our observations and conclusions. Where possible, comparative results will be presented and the differences explained or at least discussed. Difficulties associated with the instrument during the testing will also be described along with the tests used after the experiments to evaluate and confirm the possible effects of these instrument problems on the results reported.

Laser-Induced Incandescence (LII 200) Instrument

A detailed description of the LII 200 instrument may be found in the appendices along with references that provide even greater detail on the measurement principles. The LII 200 instrument has been developed over the past decade to provide an easy-to-use, low maintenance method for measuring nonvolatile particulate, primarily, elemental carbon or soot. The method has undergone extensive development and evaluations over this period and these efforts have proven the instrument to be a reliable means for measuring the soot volume fraction (svf) from direct engine exhausts or the conditioned exhaust from dilution tunnels. The instrument has a very high dynamic range and excellent sensitivity to low soot concentrations down to as low as the fraction of a microgram per meter cubed. By incorporating a combination of special optical components and software driven detector gain control, the instrument can cover a dynamic range of over a factor of 10^6 in soot concentration. These optical and electronics components can respond in a fraction of a second.

Examples of the LII performance when measuring gaseous diffusion flame generated soot are shown in the following three figures. Soot was generated using a well-known CAST burner which can produce stable concentrations of soot over a relatively wide range. Comparisons to

other methods show remarkable linearity of the method over a very wide range of soot concentrations.

CAST Burner soot source

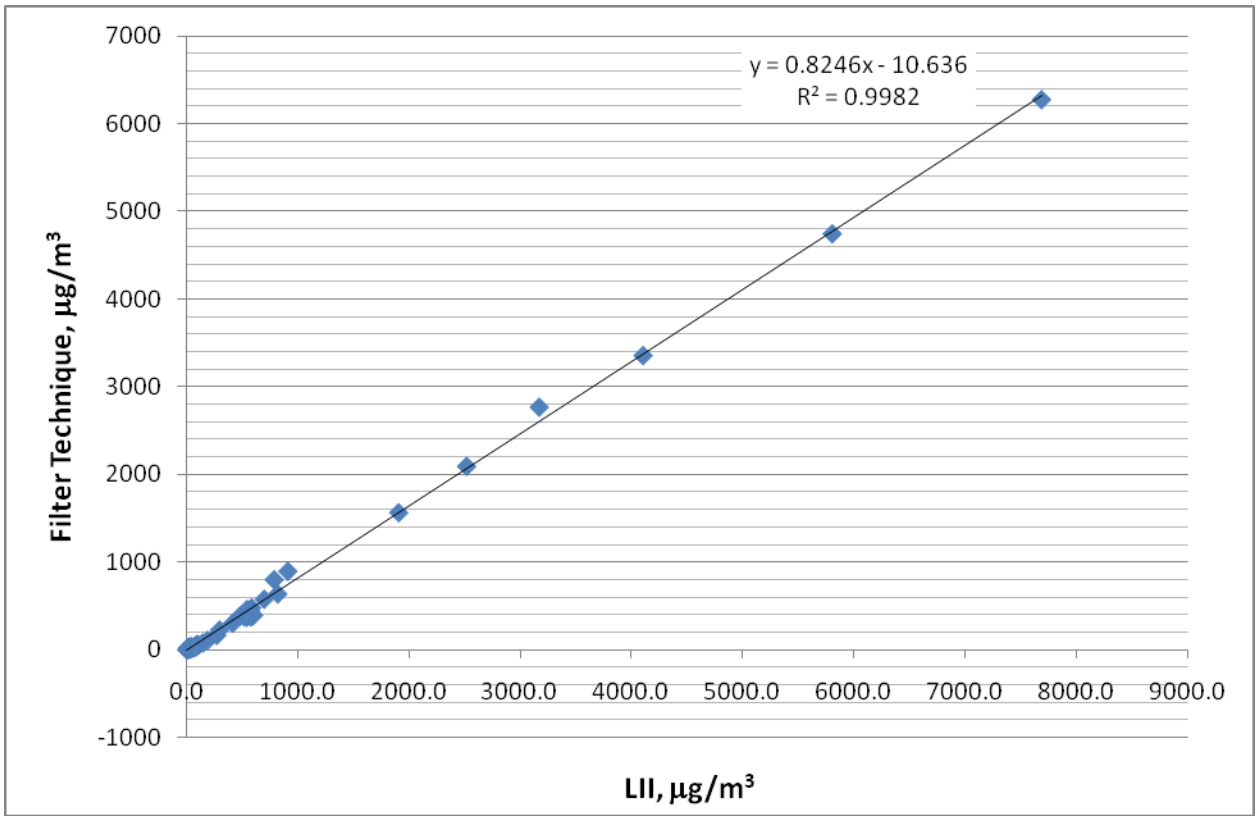

NASA Glenn Research Center tests conducted in December 2009 prior to measuring gas turbine particulate emissions with comparisons to a MAAP instrument.

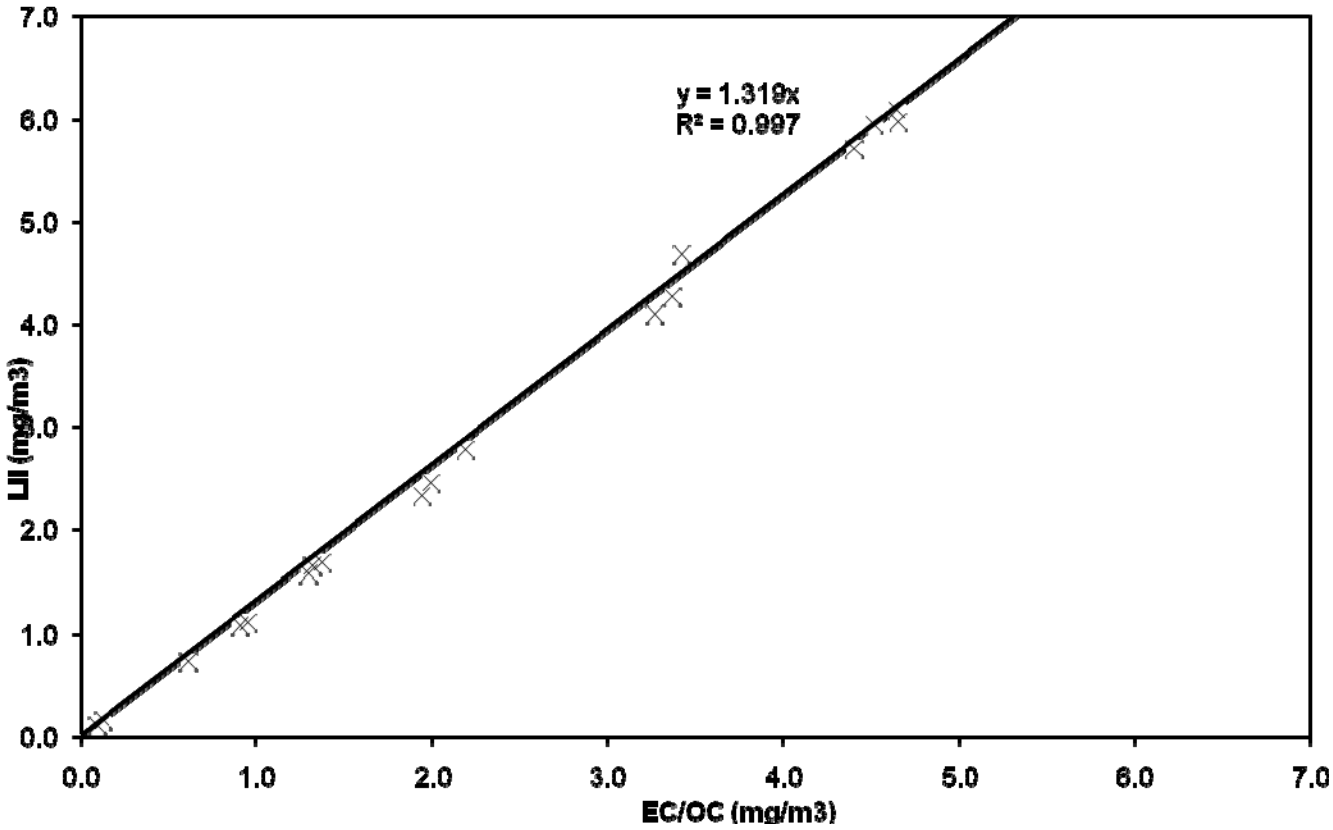

Cummins sponsored tests at Southwest Research Institute with comparisons to the Sunset Instruments EC/OC instrument.

Procedure:

LII Setup:

The **LII 200** instrument was thoroughly evaluated and calibrated before being transported to Wales for the SAMPLE measurement campaign. Calibration was accomplished with a traceable light source consisting of an integrating sphere, a halogen lamp, and a calibrated spectrometer. With this approach, the spectral content of the calibration lamp is measured directly during the calibration process. Calibration was conducted over the entire range of photomultiplier tube voltage settings and for each neutral density filter in the system. Calibration was repeated several times to ensure consistency and high precision. This approach has been evaluated by comparing soot concentration measurements from a gaseous diffusion flame to gravimetric techniques. Some of the results are shown above which verifies the calibration procedure and the theoretical analysis required for reducing the LII incandescence signals to soot volume fraction.

During transportation of the instrument to Wales, a possible static electric shock or other phenomena damaged one of our ADC converters in the LII instrument. This resulted in dropped bits in the LII signal that may have had an effect on the measured soot temperature determined

using two color pyrometry. Incorrect measurement of the soot temperature would result in an error predicting the soot volume fraction. Observations of the measured soot temperature indicated that the soot temperatures reached levels of 4500 K which is much higher than expected (4000 K). This error in temperature measurement will produce an under-prediction in the measured soot volume fraction.

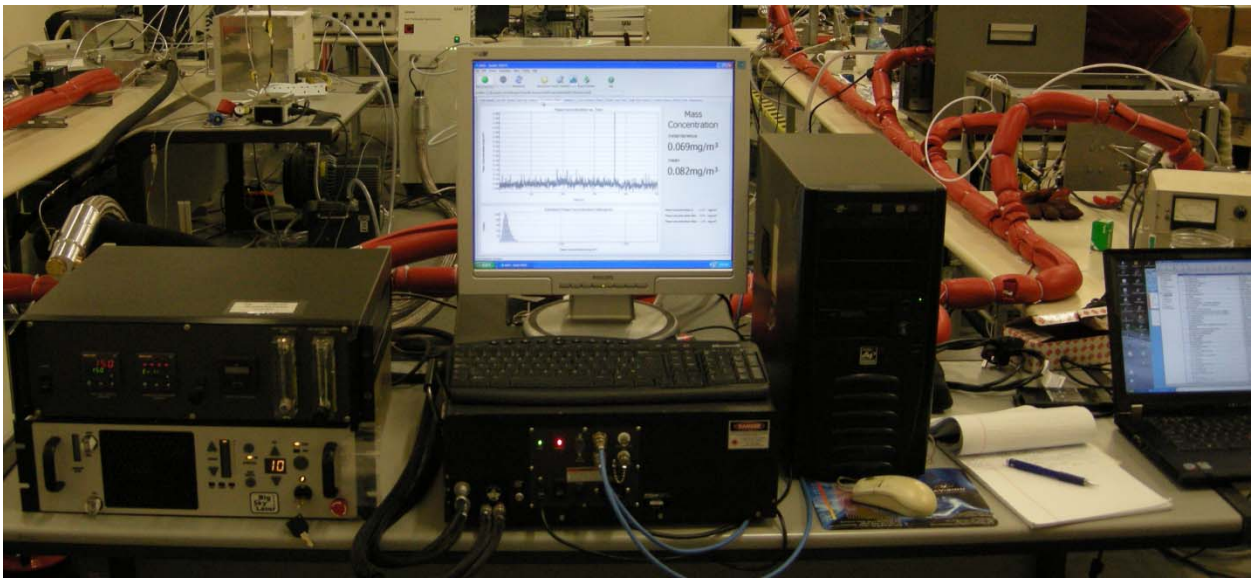

LII 200 instrument set up for the SAMPLE Tests at Port Talbot on the PARTEMIS TAY Combustor

Rear of the LII 200Instrument with the heated gas sampling lines and connections shown.

Sampling System:

The LII 200 instrument was installed directly above the simulated gas turbine combustor. Two sample lines were available which connected to the LII sampling cell via a T connector. Valves were provided so that either sample line could be selected. The length of the sample line from the combustor to the LII sample cell was estimated to be 4m long. Prior to the actual testing, the sampling system was burned in by operating the combustor with soot-laden flow through the sample lines for several hours to ensure equilibrium was reached (particle adhesion to the walls equaled particles re-entrained from the walls and surfaces). Several basic tests were conducted to evaluate the sampling system. LII measurements were made with the sample valves closed showing no measurable sample and then with the valves open to verify that the sample was being drawn through the LII sampling cell. During the test, we also measured the samples after passing through the dilution systems and obtain measurements consistent with the dilution ratio.

Questions have been raised regarding our sampling approach so this issue was addressed. We changed out the air amplifier approach used for pulling a sample and installed a new air driven vacuum pump to mitigate any potential problems associated with reliably drawing the sample

through the sample cell. The new vacuum pump provided very good suction which insured that a continuous gas sample was being collected even if the sample line pressure dropped well below ambient.

All connections on the sampling system were checked and determined to be airtight. The test cell windows were cleaned even though they only had slight contamination. We connected the sampling cell to the heated hose, checked suction, and determined that the sampling system was working properly.

Concern also has been expressed regarding window purge air and whether it may possibly be diluting the sample flow in the test cell. During steady-state sampling, window purge air was disconnected during the run and reconnected and the process repeated several times while observing the soot volume fraction values recorded by the LII instrument. There was no detectable difference in the measurements with the purge air on or off, indicating that the low flow of window purge air is not affecting the measured concentration of soot.

Air flow to the air driven vacuum pump was also changed to determine if the amount of vacuum generated would affect the measured soot volume fraction. These tests showed that as long as the sample was being pulled through the sample cell (which was true for all vacuum pump flows tested), there was no measurable difference in the soot volume fraction measured by the LII instrument, and thus sample flow rate is not affecting the measured concentration of soot.

Warm-up Tests March 30, 2009

Our first day of testing consisted of "burning in" the sample lines in an effort to ensure that the soot adhesion to the walls and re-entrainment had reached some sort of equilibrium. Tests were conducted on all of the instrumentation providing an opportunity to debug the systems and ensure proper operation. Since the LII 200 is very easy to set up, this offered an opportunity to acquire samples under the various operating conditions and to thoroughly evaluate the sampling conditions. Some time was spent optimizing instrument setup parameters and evaluating the sampling system. For example, sampling was switched from one sample line to the other to confirm the values measured were approximately the same from either sample line. Data were also acquired while the MAAP instrument was running to determine if sample flow drawn by that instrument would overwhelm our sampling system. LII samples continuously while the MAAP instrument samples periodically. No differences in the LII measurements were detected when the MAAP instrument was drawing a sample.

The following data table shows the results from the initial warm-up tests. An obvious problem was recognized immediately. The LII measurement svf (soot volume fraction) values were as much a factor of 3 lower than the measurements observed by the MAAP and smoke meter. All functions of the LII 200 were rechecked several times and observations of the raw signals were made to ensure that there were no faults. At this point, the problem of dropped bits on the ADC sampler for one LII channel was observed as shown in the figure below. However, it was very

unlikely that these dropped bits were affecting the measurements to any significant degree. At worst, the dropped bits may have caused a 10 to 20% error, but not a factor of 3. Several e-mail discussions were conducted with our engineers at Artium and with Greg Smallwood at NRC Canada during this phase of the tests. Possible answers to the problem were investigated but none could explain the large difference in measured svf.

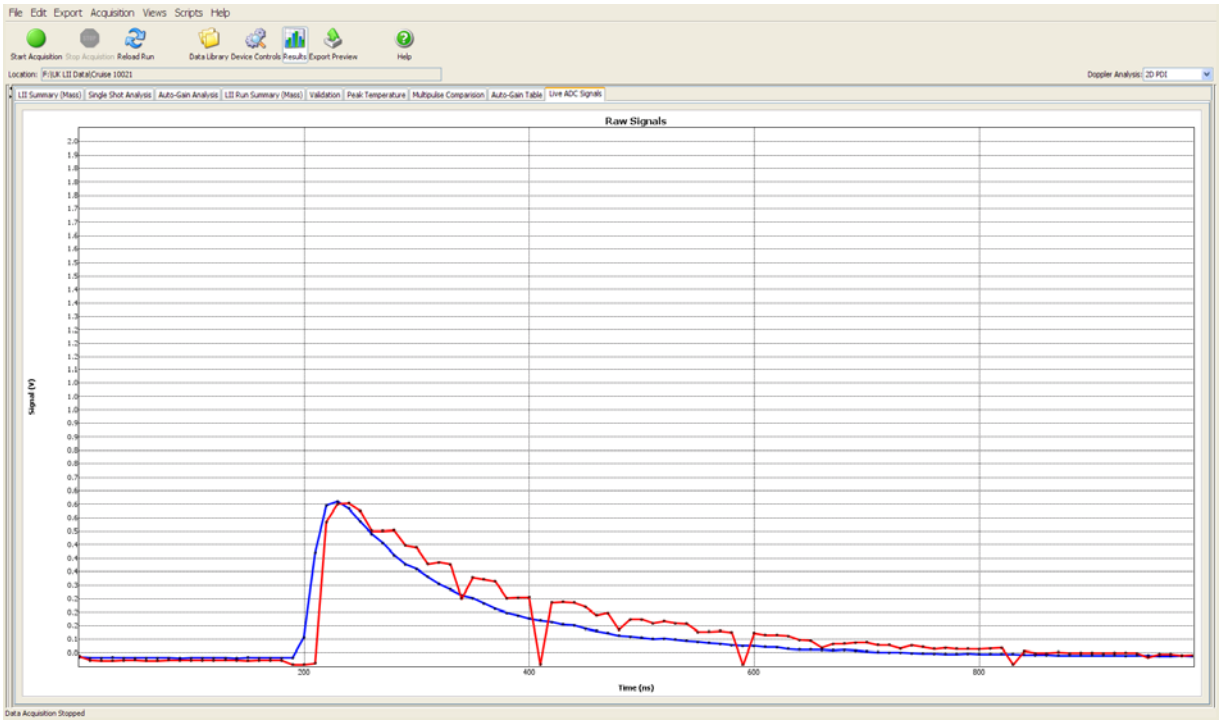

Sampled LII signals showing dropped bits on the ADC for the red trace.

However, I noted that there were large spikes (large excursions in the soot volume fraction readings) reported on the svf versus time plots with values as much as an order of magnitude greater than the baseline steady-state measurements. It is very unlikely that such extremely high gradients could be sustained in a turbulent pipe flow which exists in the sampling line and sampling cell. Either these large spikes were due to some failure of the LII instrument or to some other phenomenon in the particulate sampling. The LII instrument has the advantage that it records every raw signal and allows observation of the signals in great detail. Individual signals responsible for these large spikes were identified and observed in the LII data recording system. Signal amplitude was very high for these large values which would be consistent with locally (within the LII sample volume) very high concentrations of soot. An example of the svf versus time records is shown in the following figures.

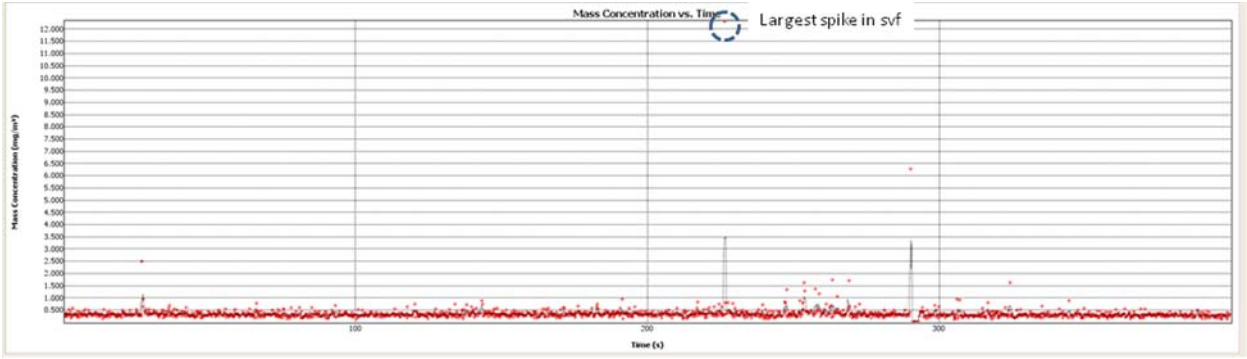

Svf versus time plot showing spikes in the svf values which cannot be accounted for as large concentrations of soot aggregates in the sample volume. In a turbulent flow, such high concentration gradients cannot exist for long.

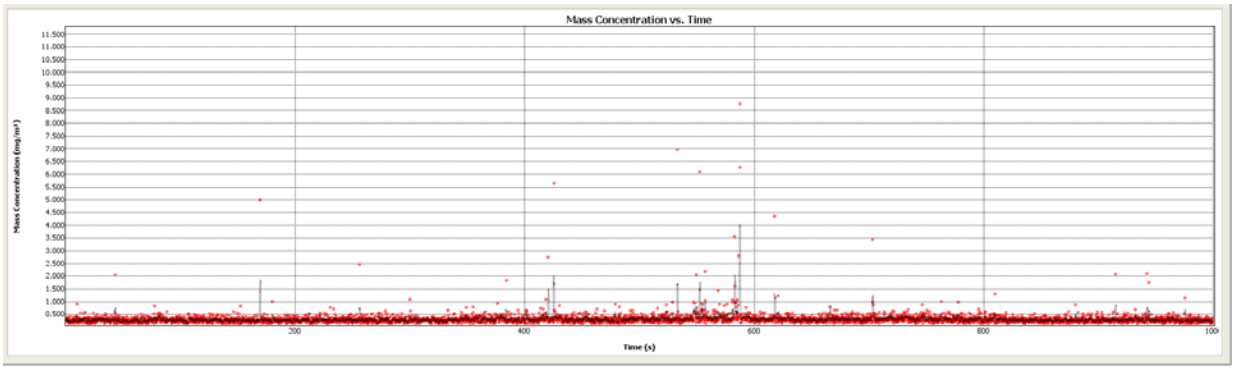

Svf versus time for the warm-up test at Cruise conditions (Cruise 0006) of the PARTEMIS TAY Combustor showing an increasing number of spikes in svf values over the earlier conditions. My hypothesis is that these spikes are due to large particles in the flow that have been shed from the combustor surfaces and sampling lines.

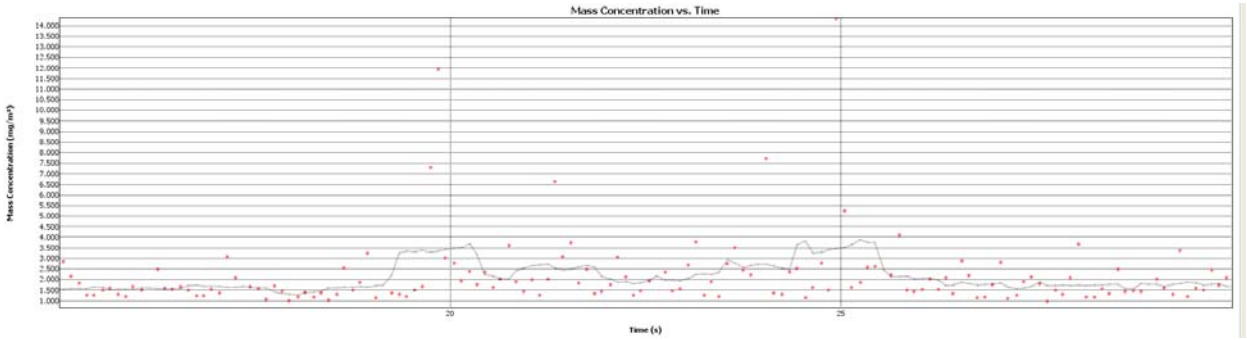

Expanded section of the svf versus time plot for the CruiseRich 0010 condition showing bursts of large signals presumably produced by shedding of large particles from the combustor and sampling line surfaces.

UK SAMPLE Test for EASA 3/29 to 4/1/09

30-Mar-09

Dilution = 170

No.	Computer Clock , 1 hour behind data clock	Run ID Sequence	LII SVF	MAAP 1 SVF	MAAP 2 SVF	Ratio 1	Ratio 2	Smoke #	Smoke #	Notes	LII Temp	PPS
	AM	Practice	mg/m3	mg/m3	mg/m3				mg/m3	3/30 SVF 0.31		nm
			0.34	**1.1**						1.2 Expect ~1/2 OC		
			0.35									

Gravimetric 1.9 mg/m3

Summary data from the first day warm-p tests showing the differences between the LII results and the MAAP and smoke meter data.

As a reference, the figure below was acquired from a real gas turbine engine exhaust. Although the mean svf value is much higher, there are no isolated spikes as seen in the results from the current test. The LII instrument will not generate “outlier” signals on its own. These signals are generally associated with some phenomena in the sample flow. Since the sample flow is well-mixed on the scale of the sample volume size, one must assume that these spikes are due to agglomerates of soot particles that are stuck together, presumably shed from the combustor surfaces and sample lines.

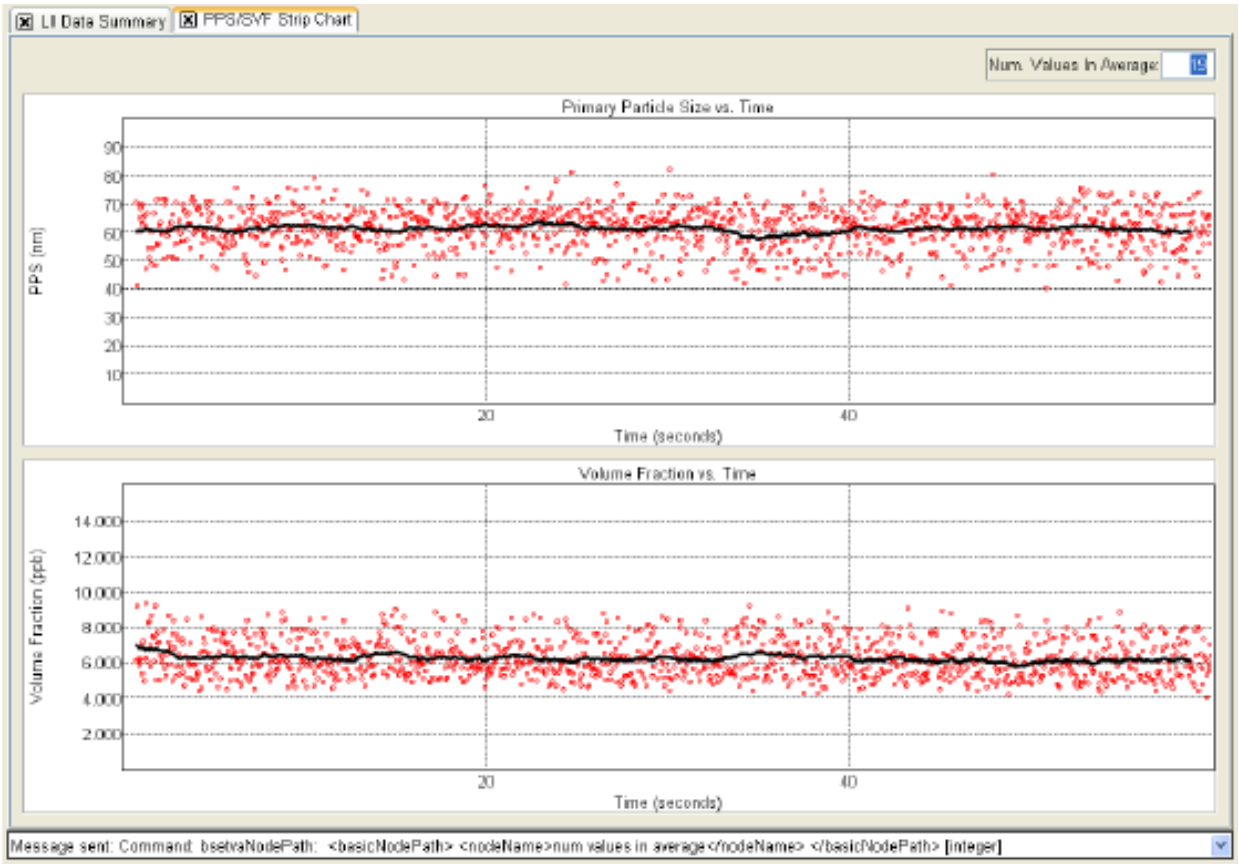

Real gas turbine LII svf data obtained from a working gas turbine engine. Although the average soot volume fraction results are much higher, it is noteworthy that the data is well-behaved with no single value excursions as seen in the results for the current simulated combustor tests.

I have spent significant time thinking about why we were consistently low on svf with the LII instrument for these tests. We carefully calibrated the instrument before I left for the UK and I was confident that the instrument was set up properly. There was the issue with the failed ADC on one of the channels. However, when I returned home we set up a stable soot concentration and measured it with the faulty sampling card and then swapped sampling cards for one that we knew was good. The results were essentially the same so I do not believe the faulty bit in the ADC caused any significant error. Something else was causing these discrepancies. Recalling that LII data agrees with the MAAP and EC/OC instruments when using the CAST burner to generate soot, one must suspect the soot sampling and morphology as the possible sources of these discrepancies.

Fortunately, I was able to acquire a filter from the smoke meter and saved it for later observations under an optical microscope. Particles on the order of 10 µm in approximate diameter were clearly visible on the soot filter. It is highly probable that the large spikes were caused by single large particles passing the LII sample volume during laser firing. I do not believe that the large particles were a result of contamination on the filter from the ambient air.

These large particles were actually collected during the sampling process. After returning to our laboratory, I ran another experiment wherein I simply removed the short piece of sampling pipe I had on the sample cell and blew a puff of air through it with a filter at the other end. I collected particles of similar morphology and size as seen on the smoke meter filter. I realize that the sizing instruments contradict this possibility but how would one explain the presence of a large particles on the filter?

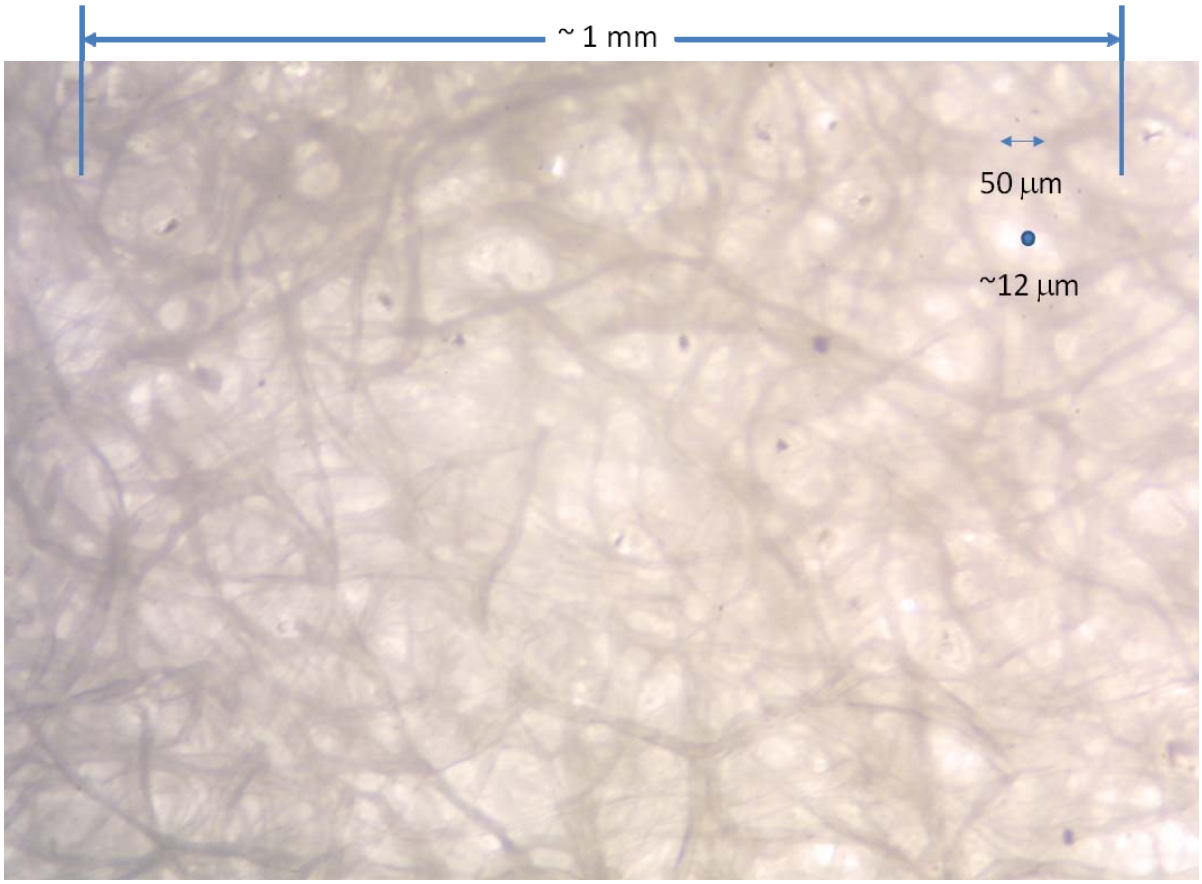

Cardiff tests 31 3 09 to 1 4 09
W.D. Bachalo

Optical microscope images of the soot filter obtained from the smoke meter showing large particles on the filter. Given the area of the filter and the area of observation and particle count, the total number of large particles on the filter is estimated to be approximately 20,000.

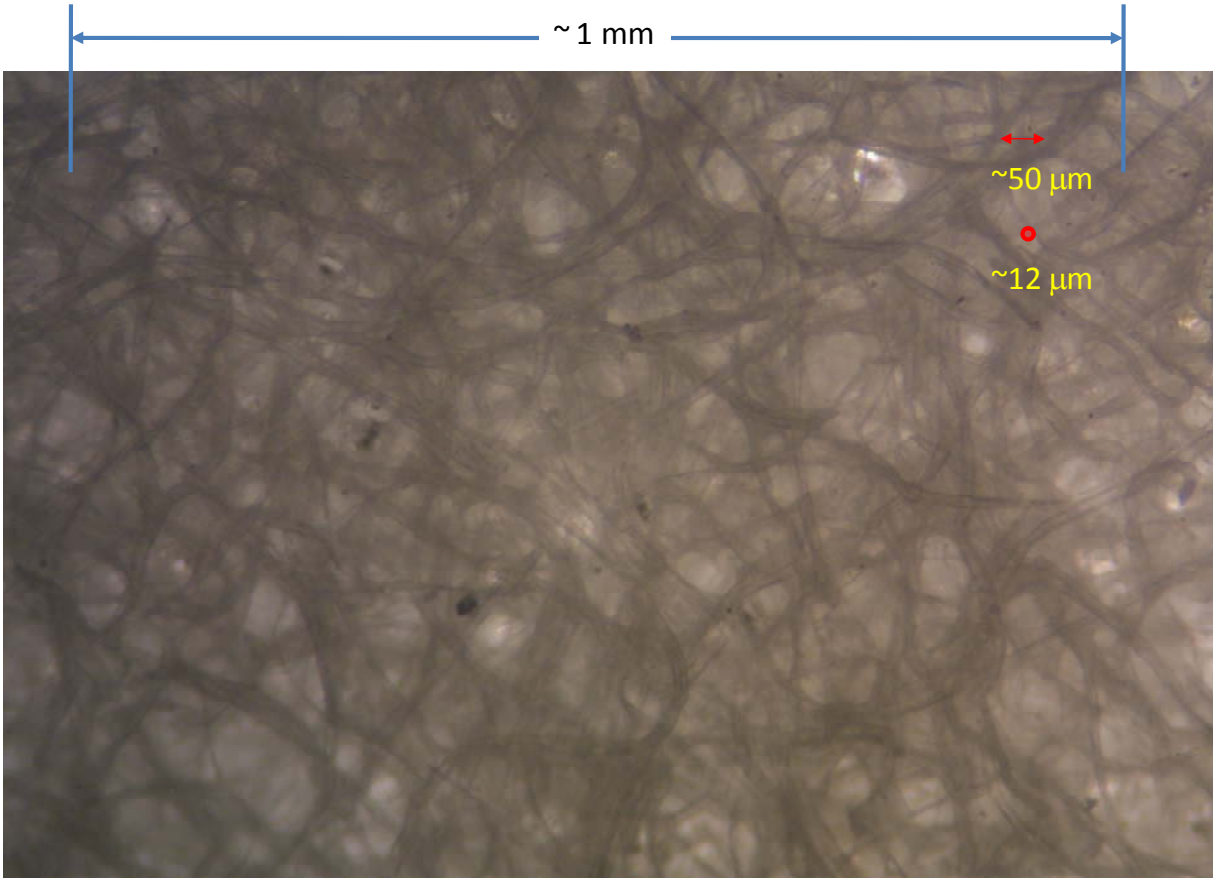

Cardiff Tests 31-3-09 to 1-4-09
W.D. Bachalo

Another optical microscope image of a different area of the soot filter obtained from the smoke meter showing large particles on the filter. Given the area the filter and the area of observation and particle count, the total number of large particles on the filter is estimated to be approximately 20,000.

Supporting my hypothesis, Richard, (facility manager, GTRC, Cardiff University) informed me that they observed Soot build-up on the nozzle of the burner to about 25 mm long when they had dismantled the rig in the past. Inevitably this soot must be breaking off and entering the sample lines. With the noise and vibration of the burner, it is very likely that this process reaches some sort of equilibrium.

Agglomerate*: aka "large particle", closely packed collection of soot aggregates, condensed material, accumulated on combustor and sampling line surfaces and re-entrained into the sample flow appearing as large quasi-spherical particles.*

LII Sampling Statistics

As a means for supporting my hypothesis, the following observations and analysis are provided. We can assume that the gravimetric filters collect most, if not all larger particles in the gas

stream drawn into the sampling tube (and through the cyclone separator, if one is in place). It also is important to recognize that the LII instrument is sampling the gas stream passing through the sampling cell by instantaneously measuring the collection of regular soot particles that reside within the sample volume at that instant. The sampling frequency is essentially the laser pulse rate which may be set to a range of values from 1 to 20 Hz. In the present case, it was set at 5 Hz. The LII sample volume was approximately 8 mm^3.

When dealing with normal soot particles which are submicron aggregates of nanometer-sized primary particles, these particles can be assumed to be homogeneously mixed (on the size scale of the LII sample volume) in the gas phase with a large number of soot particles existing in the LII sample volume at any instant. When the LII laser fires, this collection of particles is heated to incandescence temperature and produces a signal from the ensemble particles in the sample volume. Changes in the relative numbers of soot particles in the sample volume as the sample flow passes through it manifests as changes in signal amplitude, which is related to the concentration of particles in the sample volume at that instant.

What happens when there are large particles in the flow at relatively low concentration? One or more of these large particles may or may not be present in the sample volume for each measurement during the laser shot? I have concluded that large particles are present in the flow field since I have observed them on the filters using an optical microscope. (Since this first discovery, we have observed numerous other soot laden filters and found many large particles on most of them). These large particles will vary in concentration depending on the soot volume fraction and other conditions (vibrations of the engine, gas flow velocity in the sample lines, etc.) of the measurement environment. Particles may be assumed to be Poisson distributed within the flow and will be randomly detected. In fact, my observations and discussion in the following sections indicate that the particles are not randomly distributed but tend to appear in bursts in some cases. At low concentrations, a low probability of detection exists. As the concentration increases, the probability of detecting these particles with each laser shot will increase. This process may be predicted using Poisson statistics given as

$$P(1) = VNe^{-(VN)}$$

where P(1) is the probability of 1 large particle residing in the sample volume, V is the size of the LII sample volume (8 mm^3), and N is the concentration of large particles (not the normal soot aggregates).

1 = P(0) + P(1) + P(2) + P(3) + …

which states that the sum of the probabilities of 0, 1, 2, 3 and so on number of particles in the sample volume must add up to 1.

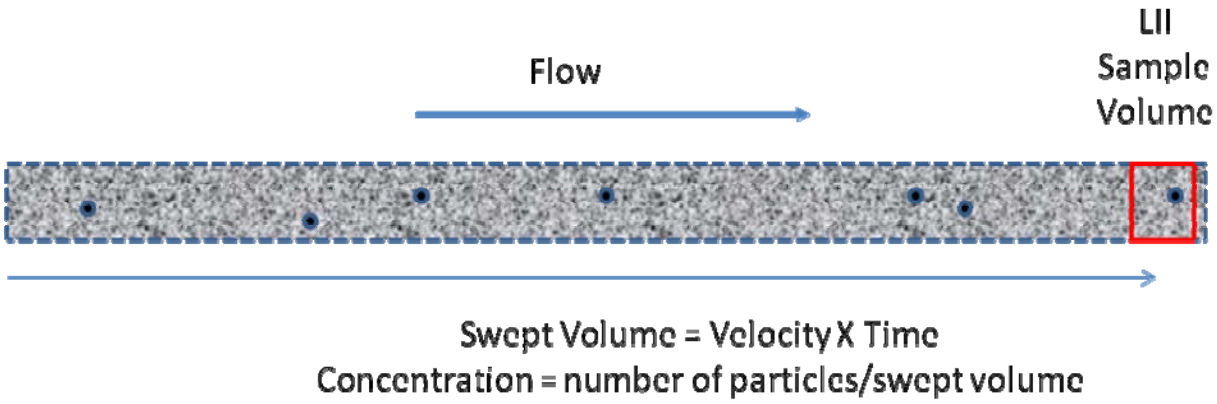

A schematic diagram is provided to illustrate the random arrivals of the large particles to the LII sample volume simulated in red. The background is intended to simulate the homogeneously dispersed normal soot particles which are very small and have a very high number concentration with many particles continuously passing the LII sample volume during the laser firings.

It is instructive to look at some examples to get an idea of what will happen when there are a few large particles present. We can look at the problem from two directions, one in which we have a concentration difference between measurements which we want to attribute to large particles. The other is to observe the rate of spikes in the LII time record and estimate the apparent number density of the large particles. These order of magnitude estimations can be used to provide information as to whether the observed results, namely differences in mass concentration measured by LII and the svf spike rate are consistent with the observed measurement differences. The approach below has been developed on an Excel spreadsheet so that rapid order of magnitude estimations can be conducted. As an example:

Consider the figure above which was acquired with a sample rate of 5 Hz. For 1000 seconds, 5,000 samples were recorded. If we consider the values well above the average svf value as being caused by large particles, approximately 30 such samples or “spikes” are observed. From the filter image shown below, the average large particle size is approximately 10 μm (this is just a rough estimate). The LII results and gravimetric were approximately 0.35 and 1.9 mg/m^3 respectively, with a difference of 1.5 mg/m^3. MAAP gave a value of 1.1 mg/m^3 which may be a

better comparison to LII since gravimetric also includes SOF. Thus, we can use a difference of 0.75. Applying these values to the Poisson analysis, we have the following results:

Given Concentration Measurements, Figure Out Spike Rate

What mass concentration difference is there between two measurements?	**0.75**	mg/m**3
What size particle do you think represents the "big" particles?	**10.00**	μm
What density do you want to use for soot?	**1.90**	g/cc
How large is your LII probe volume?	**8.00**	mm**3
Sample time in Seconds	**100.00**	
The mass of each large particle is:	**9.95E-10**	g
The expected number of large particles per probe volume is:	**6.03E-03**	
The fraction of pulses with no large particles is:	**9.9E-01**	
The fraction of pulses with at least one large particle is:	**6.0E-03**	
The ratio of pulses without a spike to those with a spike is:	**1.7E+02**	

Given Spike Rate, Figure Out Number Density of Large Particles

What is your spike rate in (spike pulses) / (all pulses)?	**8.00E-02**	
How large is your LII probe volume?	**8.00**	mm**3
The number density of large particles is:	1.04E+01	particles/cc
The average volume per single particle is:	5.24E-07	mm**3
Volume Sampled (LII PV times number of shots)	8.00E+02	mm**3

Based on our count of spikes in the svf time record of 34 in 5000, the ratio of spikes to total number of measurements is 0.7 in 100. The Poisson analysis using the given svf difference and the estimated large particle size of 10 μm gives a probability of 1 particle in 170 or 0.6 in 100

shots. I have conducted this simple estimation on many runs and found reasonable agreement. Although not definitive proof, the results support my hypothesis.

We want to emphasize that for such large particles, the LII signal cannot be expected to be proportional to the svf. LII theory is built the assumption that soot primary particles are in a range of tens of nanometers which when heated act as volume emitters of incandescence. Large particles will behave as surface emitters which will require some additional theoretical development, if there is any relate incandescence from such large particles to the volume of soot in the particle. I must also emphasize that the svf spikes do contribute to the LII cumulative svf measurement but the contribution is not expected to be proportional to the actual volume or mass of the large particles. Further work is required to determine if there is some theory that could be used to relate these large signals to the mass of the large particles.

An approach that might be used to deal with this problem is to perform a rough estimate of the volumetric mean size of large particles observed on the filters by the optical microscope. A rough count of these particles can also be made. Given the flow rate to the filter and the number of particles counted, an estimate of the large particle concentration in the sample line can be obtained. This result can be compared to the estimated number based upon the count of large spikes in the LII time record and the concentration estimated using the Poisson analysis.

It was stated earlier that the large particles are not properly measured by the LII instrument because the LII theory expects small spherical particles on the order of 10 to 100 nm in diameter in loose aggregates that may have an approximate size range of from 0.05 to 1 μm in equivalent diameter. The large particles observed in the soot filters have diameters as large as 50 μm and appear to be tightly packed agglomerates of soot. These particles, when heated, will emit incandescence as surface emitters rather than volume emitters as is the case for nanometer sized primary soot particles. Nonetheless, large particles will produce very large incandescence signals due to their very large size, relative to the soot particles.

The appropriate solution to this problem is to eliminate large particles from the sample since the regulation assumes that particles larger than 2.5 μm are not present in the sample. If the large particles are to be measured, a basic light scattering system could be developed to size and count the large particles to achieve an estimate of the mass associated with these particles.

Why does the presence of large particles lead to LII under-predicting values at low svf

Large particles are randomly distributed within the flow and at low soot volume fraction. These large particles will not be present in the probe volume for each LII laser shot. In addition, the incandescence signals cannot be expected to be proportional to their mass. As stated above, the probability of having a particle in the sample volume during the firing of the laser depends upon the concentration of particles in the flow and the size of the LII sample volume. As a Poisson process, the presence of a particle in the sample volume is predictable based on the particle concentration and sample volume size. For low concentrations of large particles, the probability

of a large particle present in the sample volume during laser firing is relatively small. Filters will collect all particles including all of the large particles present in the flow.

Results and Discussion:

In this section, results will be provided for selected runs along with summary results showing comparisons of the LII 200 data with the MAAP and smoke meter data. Plots of svf versus time will be provided to show the spikes in the data. As discussed earlier, spikes are attributed to the presence of large agglomerate soot particles in the flow which are collected on the filters and only randomly sampled by the LII instrument. The Poisson analysis will be provided for each case to show that the presence of these particles can produce differences seen in the measurements. Sample data obtained on March 31 and April 1 are provided. A brief description of the conditions for these tests will also be provided with the data.

March 31 Test Series

Tests conducted on the second day were labeled “Smoke” and were a continuation of the shakedown experiments. Nonetheless, this gave an opportunity to continue evaluation of the LII instrument and sampling arrangement provided. The following plots of svf versus time are provided to show that individual isolated large signals are present. These signals are as high as 10 times the average svf values. The vertical scale is automatically set to the highest signal for that particular run. In the case shown immediately below, the largest reading is 1.1 mg/m^3 which is over 10 times the mean value of 0.093 mg/m^3. Please note that the vertical scales on these plots are different for each run because of the auto scaling feature.

Smoke Conditions

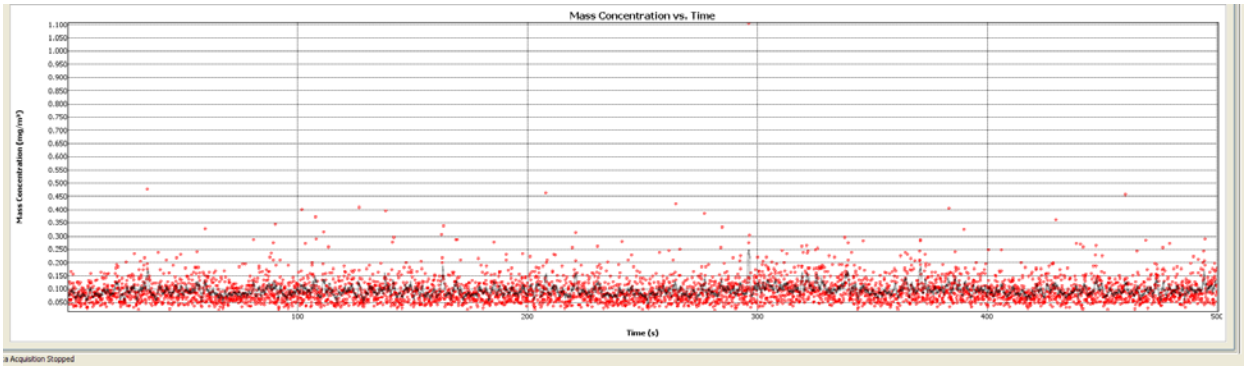

Smoke 50024

Typical plots of svf versus time showing the presence of large svf values which are believed to be due to the presence of large agglomerate soot particles which have been shed from the combustor and sampling line surfaces.

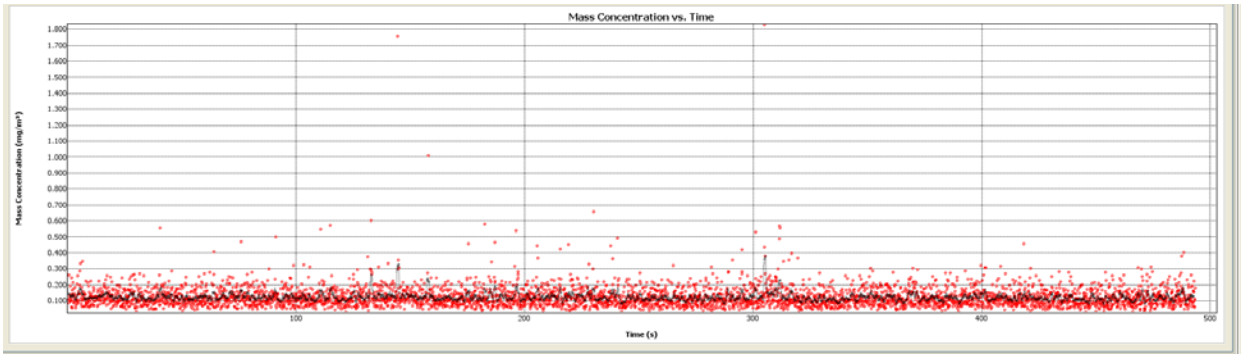

Smoke 50028

Svf versus time plot for a run of approximately 480 seconds with a sampling frequency of 5 Hz producing 2400 measurements. Individual readings as high as 1.8 mg/m^3 are shown as isolated values. However, at approximately 300 seconds, there appears to be a grouping of large values in the neighborhood of the single large reading. This suggests that the large particles may come in bursts on some occasions with a parent and sibling particles.

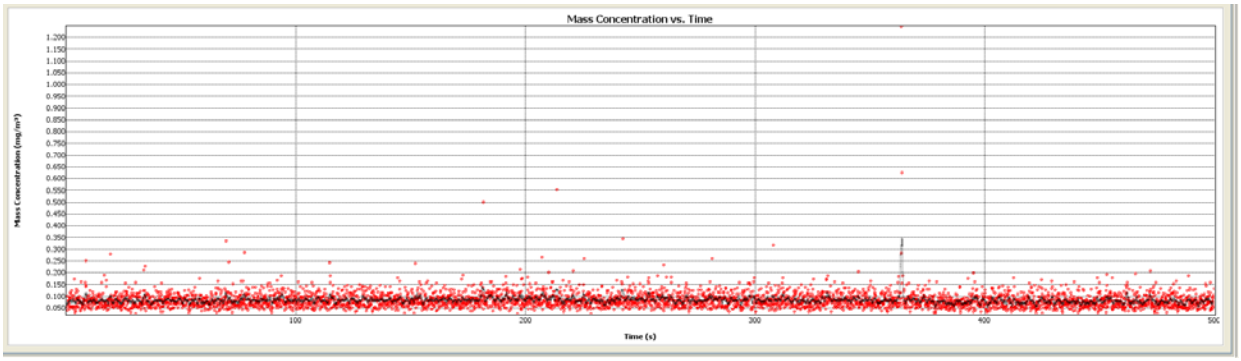

Smoke 50035

In this example, at approximately 350 seconds there appears to be a consistent spike with two particles rising to form a peak. This suggests that the local svf is high due to a change in soot concentration which would be due to more than a single particle.

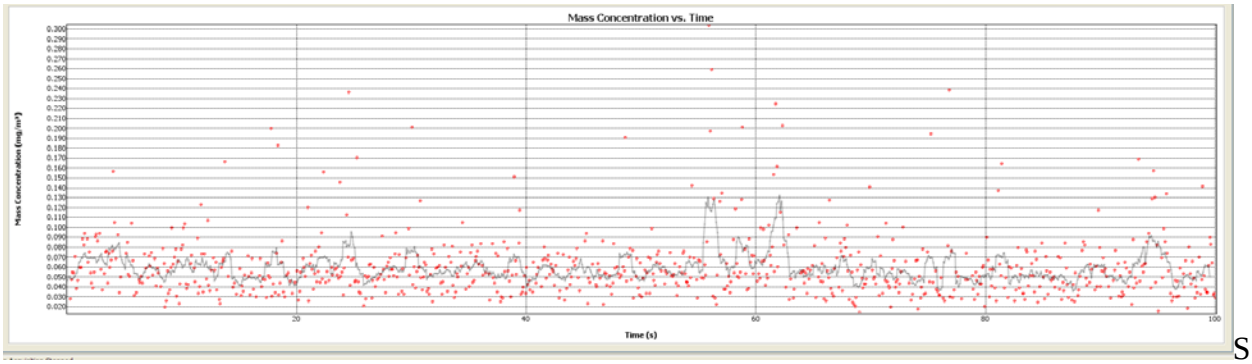

Smoke 50053

Although the above plot of svf versus time appears to have a lot of scattered data, the maximum reading is only 0.3 mg/m^3. There are no very large individual readings in this sample. Note the timescale stops at 100 seconds which is 500 readings.

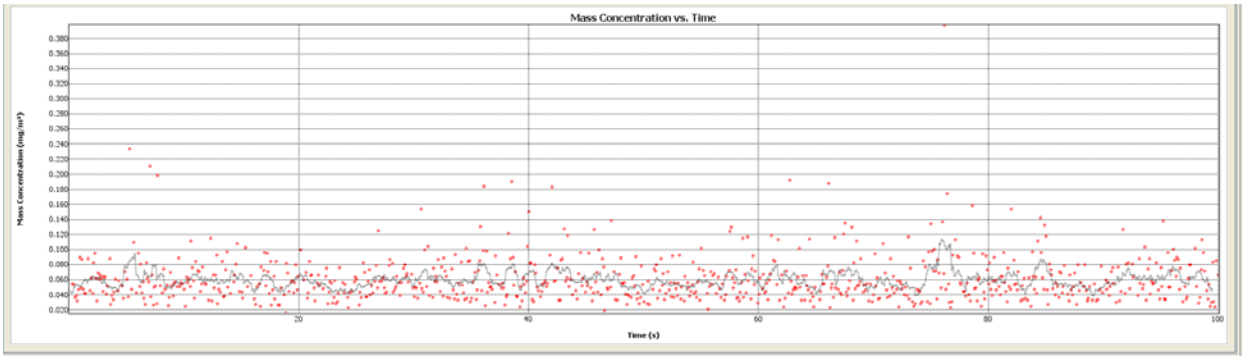

Smoke 50054

In this case, the maximum value is only 0.4 but is clearly due to an isolated single particle rather than a systematic increase in the soot concentration. It is unlikely that such local large gradients and soot concentration could persist in a turbulent pipe flow.

In this series of tests, it is clear that in most cases the large readings of svf may be attributed to a single isolated event which must have been generated by a single large particle passing the sample volume. Flow in the sampling line is typically turbulent, especially when passing through tee connections and bends in the pipe. Under such turbulent conditions, such large spikes in the svf could not be sustained. In some cases, there appeared to be a systematic rise in the svf which would then be due to an increasing concentration of the aggregates within the LII sampling volume during these sequences of measurements. It is also possible that the large particles break off with daughter particles leaving at the same time.

No.	1 hour behind data clock	Sequence	LII SVF	MAAP 1 SVF	MAAP 2 SVF	Ratio 1	Ratio 2	Smoke #	Smoke #	Notes	LII Temp
	31-Mar-09	Smoke 50012	0.061					6	0.4		4450
		50013	0.044							Laser Rate	
			0.09							10 Hz	
		Smoke 50016	0.086							20 Hz	4500
	Max laser power	50017	0.9	**0.55**		6					
		50024	0.093								4500
	10:00		0.057	**0.69**		12.1			0.4		
	10:19		0.055	**0.736**		13.4					
	10:31		0.054	**0.561**		10.4					
		50035	0.082	**0.825**		10.0					
	10:36		0.056	**0.624**		11.1					
	10:47	50052	0.055	**0.517**		9.4					
	10:57	50053	0.059	**0.144**		2.4					
	11:05	50054	0.059	**0.34**		5.8					
	Average		**0.060**	**0.554625**		9.3					

Summary data for the LII measurements for this particular run are provided in the table above. These results show some variations in the LII measurements which are due to the fact that the combustor was sometimes under adjustment while making LII measurements. When the combustor was stable, it appears that the LII was measuring values at approximately 0.060 mg/m^3. At the same time, if I have the dilution right, MAAP instrument was measuring approximately 0.55 mg/m^3. At first sight, this difference of approximately a factor of 10 was very disturbing. The MAAP instrument, smoke meter, and gravimetric appeared to be in reasonable agreement. After observing a few smoke meter filters, it was apparent that the particle samples were not exactly homogeneous small particles uniformly distributed on the filters. As shown earlier, one of the filters was observed carefully under an optical microscope and was shown to have large particles present which cannot be measured reliably with LII. As a rough approximation, we can use the Poisson analysis to determine if the numbers spikes in the svf versus time data from the LII record could provide some explanation for these large differences.

As an example, the figure labeled Smoke 50035 has approximately 20 readings above an upper level of 0.2 mg/m^3 out of 500s * 5/s = 2500. With our estimation of a 10 μm mean volume diameter of large particles observed on the filter, and the difference in svf between the MAAP instrument and LII of 0.74 (0.825-0.082), we can use the Poisson statistics to estimate the ratio of measured large spikes (large particles) to the total number of samples. The results is:

Given Concentration Measurements, Figure Out Spike Rate

What mass concentration difference is there between two measurements?	**0.74**	mg/m**3
What size particle do you think represents the "big" particles?	**10.00**	μm
What density do you want to use for soot?	**1.90**	g/cc
How large is your LII probe volume?	**8.00**	mm**3
Sample time in Seconds	**100.00**	
The mass of each large particle is:	**9.95E-10**	g
The expected number of large particles per probe volume is:	**5.95E-03**	
The fraction of pulses with no large particles is:	**9.9E-01**	
The fraction of pulses with at least one large particle is:	**5.9E-03**	
The ratio of pulses without a spike to those with a spike is:	**1.7E+02**	

That is, 1/170 spikes would be needed for the svf difference of 0.74. The approximate count of 20 spikes in 2500 is 2/250 or 1/125 which is in reasonable agreement since the sample is not large for the number of expected spikes and the large particles are all assumed to be 10 μm diameter. There is probably some proportionality in the height of the spike to the size of the particle but this is, as yet, unknown. One can assume that smaller spikes represent smaller particles so that would affect the results. In this preliminary evaluation, the statistical analysis is only provided to determine if there is a reasonable probability that the large spikes could help explain the difference in the measurements.

April 1 Test Series

On this day, three series of tests were run, Cruise, Cruise Rich, and then a long Cruise condition was run while a gravimetric sample was acquired. During this series, the Cruise test was repeated and each condition held constant for sufficient time for the slower instruments to acquire sufficient PM for careful evaluation.

Cruise 1 Conditions

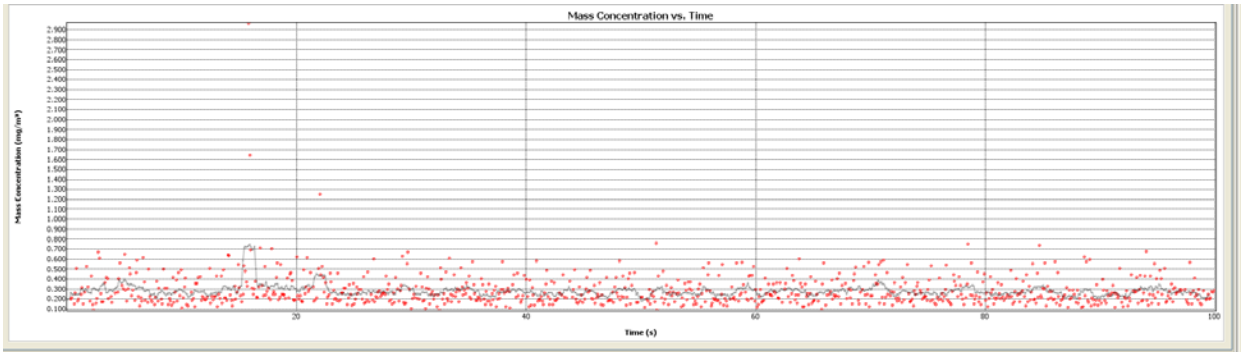

Cruise1 10014

At this condition, the svf versus time looked much quieter with fewer spikes but it would change from sample to sample. Obviously, if it is large particles that are creating the spikes in the svf values, they are coming off the surfaces at random intervals possibly driven by vibrations, changes in a sampling flow and other factors.

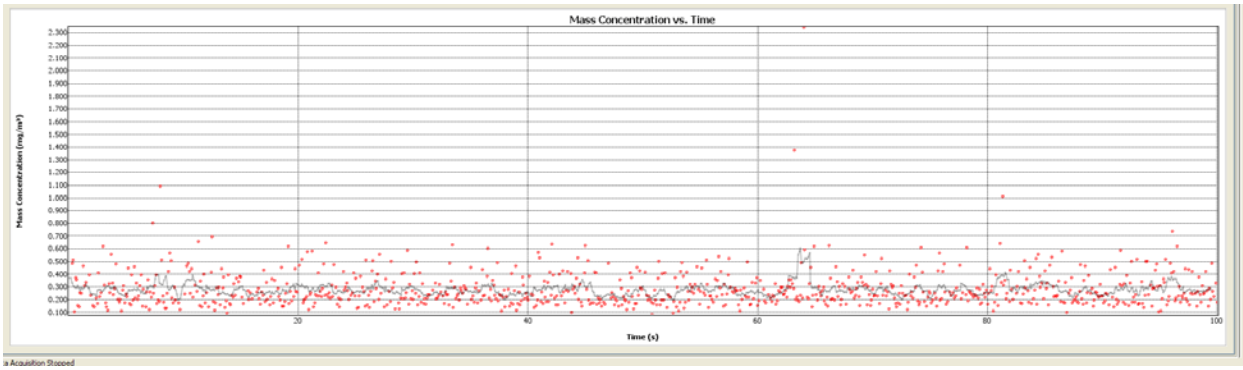

Cruise1 10015

It is difficult to determine the level at which one could assume the signals are due to large particles or to simple excursions in the soot aggregate concentration. For example, in this plot one might consider readings above 0.6 to 0.7 as being due to large particles.

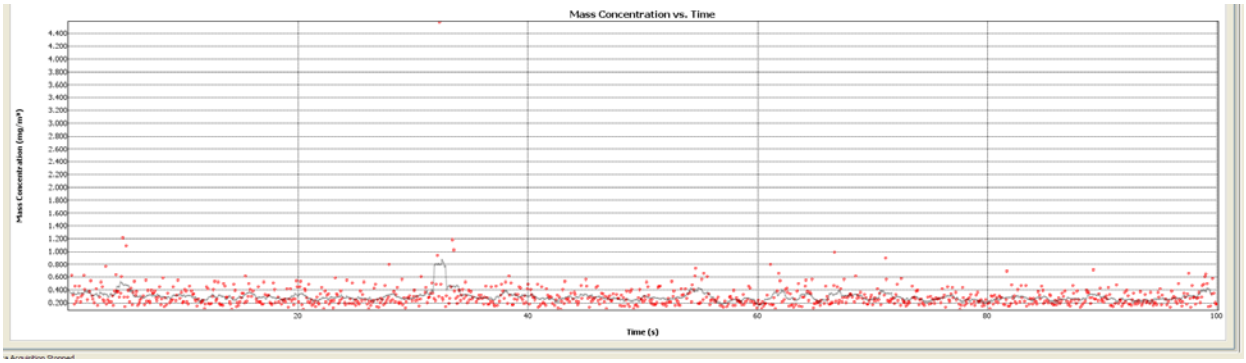

Cruise1 10017

In this record, there is only one very large excursion to approximately 4.53 mg/m^3 with the remainder of the readings remaining somewhat well behaved with a few readings above 0.8.

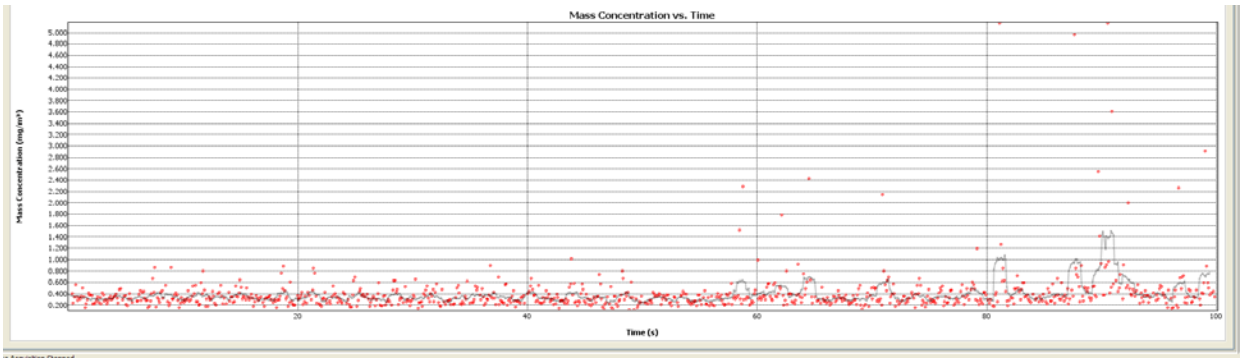

Cruise1 10018

In this case, there appears to be a burst of large particles towards the end of the record. Note that if the problem was due to some failure in the LII instrument, one would not expect the readings to occur in broad groupings as we are seeing. Furthermore, some records show little or no traces of these large readings.

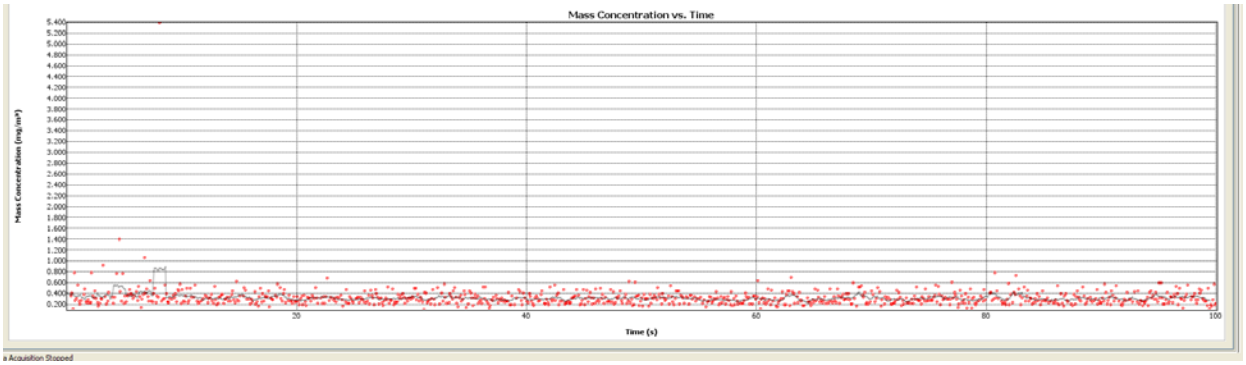

Cruise1 10021

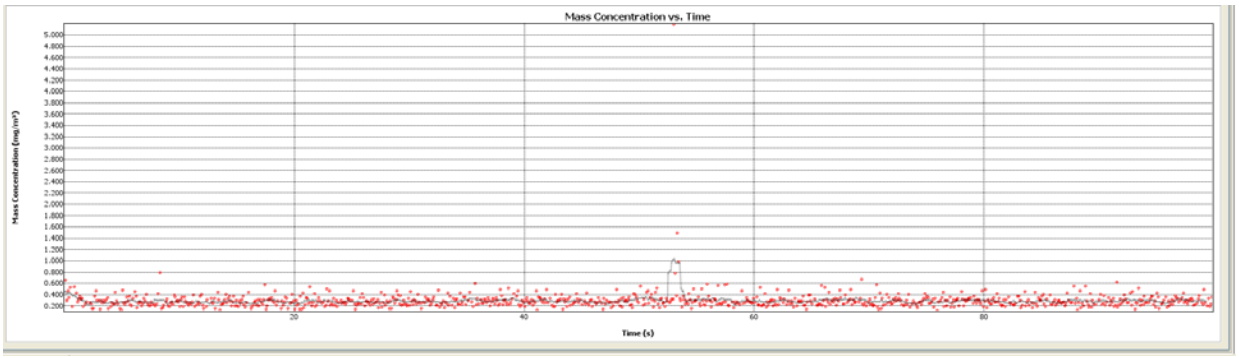

Cruise1 10022

In this record, there is only one large excursion which appears to have three readings in a neighborhood that are rising as well. This case raises a question regarding the single large particle hypothesis since a single particle would not reside in the sample volume for more than one shot. A possible explanation is that the large particle has daughter particles associated with it which broke off together and haven't yet dispersed. It is also interesting to note that the other readings are relatively well behaved with no other large excursions in svf value.

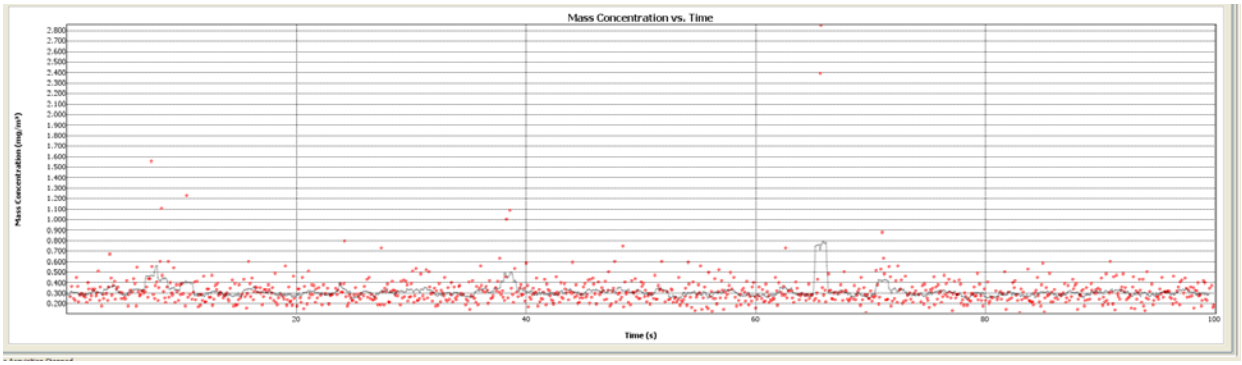

Cruise1 10023

A summary of the results for this sequence of tests is shown in the table below. In this case, both MAAP instruments were read and recorded as was the smoke meter. It is interesting to note that there's a significant difference between the two MAAP instruments. This may have been due to values of the dilution ratios provided to me which may or may not be accurate.

	1-Apr-09				Dilution =	Dilution =						
	Computer Clock ,	**Run ID**			**135**	**33**						
No.	**1 hour behind data clock**	**Sequence**	**LII SVF**	**MAAP 1 SVF**	**MAAP 2 SVF**	**Ratio 1**	**Ratio 2**	**Smoke #**	**Smoke #**	**Notes**		**LII Temp**
	AM	Cruise 1	mg/m3	mg/m3	mg/m3				mg/m3	3/30 SVF 0.31		
1	2:54	10	0.307	1.84	0.94	5.99	3.05	10.83	1.31	Filter	48.5	
2	3:00	11	0.283	1.52	0.64	5.37	2.26	11	1.33			
3	3:06	12	0.281	1.4	0.77	4.98	2.73	10	1.19			
4	3:12	13	0.254	1.27	0.87	5.00	3.43	8	0.90			

5	3:18	14	0.28	1.31	0.91	4.68	3.26	12	1.49		
6	3:24	15	0.277	1.32	0.94	4.77	3.38	10	1.19		
7	3:30	16	0.274	1.36	0.95	4.96	3.47	11	1.33		
8	3:38	17	0.292	1.31	0.95	4.49	3.25	9.1	1.06		
9	3:44:00 AM	18	0.39	1.53	1.00	3.92	2.56	12.9	1.62		
10	3:50	19	0.321	1.67	1.08	5.20	3.36	12.7	1.59		4500
11	3:56	21	0.318	1.74	0.84	5.47	2.64	11	1.33		4600
12	4:02	22	0.29	1.4	0.89	4.83	3.08	10	1.19		4600
13	4:11	23	0.315							Ratio	
Averages			**0.299**	**1.4725**	**0.90**	**4.97**	**3.04**		**1.29**	**4.32**	

It is interesting to note that the differences between the LII instrument and the MAAP instruments and gravimetric were now approximately a factor of three to four. Once again, we can apply the simple Poisson statistical analysis to determine if the numbers of spikes in the record would account for the differences in the measurements. For example, the figure identified as Cruise1 10018 has approximately 30 spikes above 0.8 mg/m^3 out of 500 readings or about 0.6/100. The difference in svf values is approximately 1.2 (LII = 0.39, MAAP = 1.5, Smoke Meter = 1.6). Using this value in the Poisson analysis yields the following results:

Given Concentration Measurements, Figure Out Spike Rate

What mass concentration difference is there between two measurements?	**1.20**	mg/m**3
What size particle do you think represents the "big" particles?	**10.00**	μm
What density do you want to use for soot?	**1.90**	g/cc
How large is your LII probe volume?	**8.00**	mm**3
Sample time in Seconds	**100.00**	
The mass of each large particle is:	**9.95E-10**	g
The expected number of large particles per probe volume is:	**9.65E-03**	
The fraction of pulses with no large particles is:	**9.9E-01**	
The fraction of pulses with at least one large particle is:	**9.6E-03**	
The ratio of pulses without a spike to those with a spike is:	**1.0E+02**	

The analysis indicates that it would require about 1/100 spikes for the total number of signals to produce the difference in the svf values. There are significant differences from one plot to another which is due to the fact that the large particle arrivals are not entirely random and that the sampling system is causing shedding due to some other phenomena such as vibrations, large flow changes with the activation of a MAAP sample, etc. For example, the sample identified as Cruise1 10022 only has about 6 readings above the expected level.

Cruise Rich Test Condition

The Cruise Rich condition is characterized as having high smoke and low OC. The LII instrument reported a mean svf of approximately 1.5 mg/m^3 whereas the MAAP instruments reported 4.3 and 1.9 respectively. The average smoke meter reading was 3.55 mg/m^3.

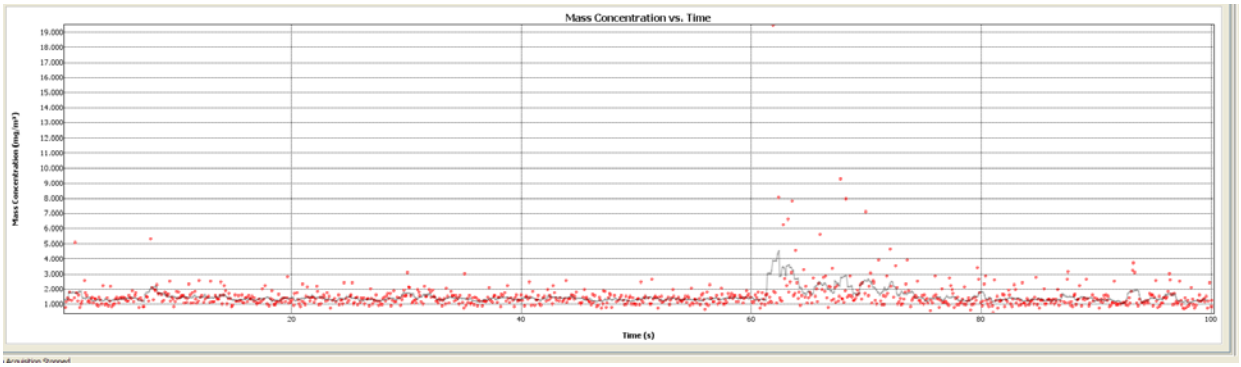

CruiseRich 0000

In this trace, there is clearly a burst of particles starting at approximately 60 seconds. The random large values of svf appear to tail off and continue at a lower level to the end of the trace. Once again, this could be explained by particles shed from the walls due to a vibration event or surge in the flow. If this was due to an actual change in soot concentration, the local readings would not be expected to drop back to the mean level and rise again abruptly.

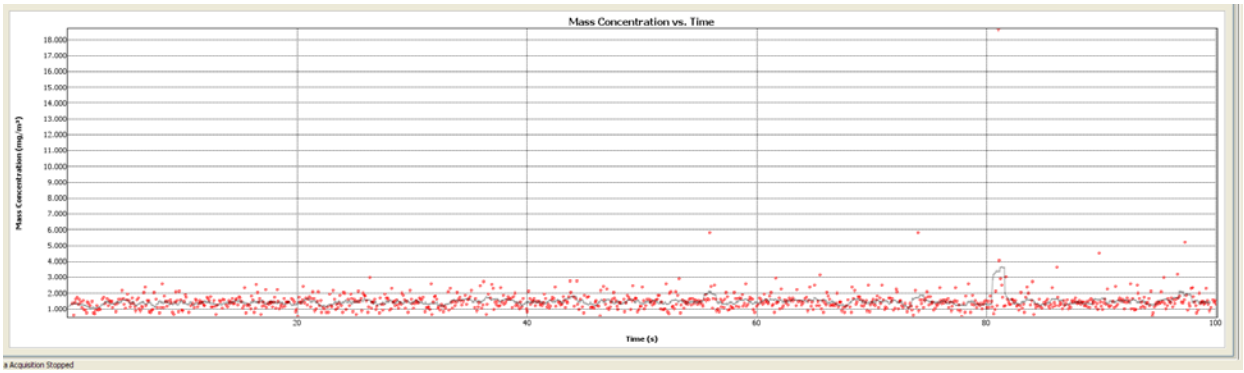

CruiseRich 0002

This trace taken at the same conditions but 12 minutes later shows a relatively quiet behavior with one large excursion to over 10 mg/m3 but with a few other values above the mean value.

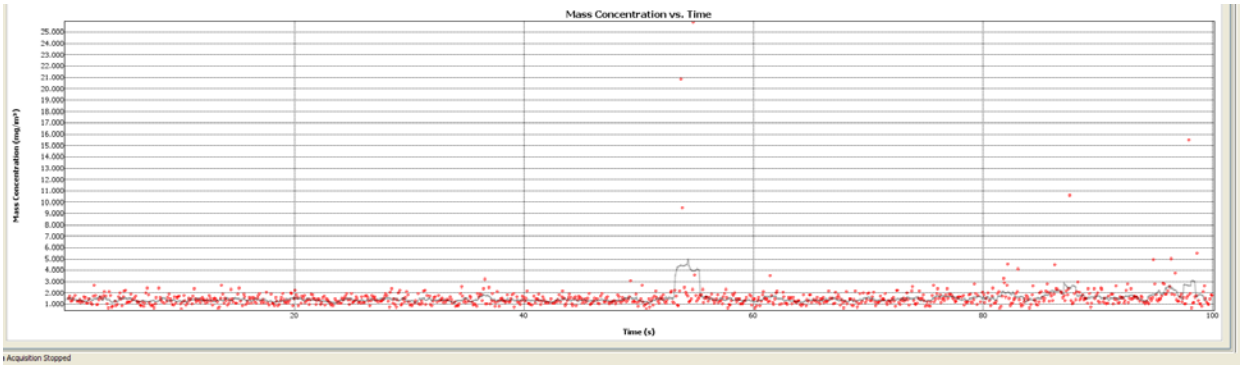

CruiseRich 0004

This trace has an interesting spike in values at approximately 55 seconds. Unlike in the case of isolated large value readings, this spike has a systematic increase over three or four points. This would indicate a sharp rise in soot volume fraction that may not be attributable to a single particle. As stated before, it may also be due to a cluster of particles shed from the surface.

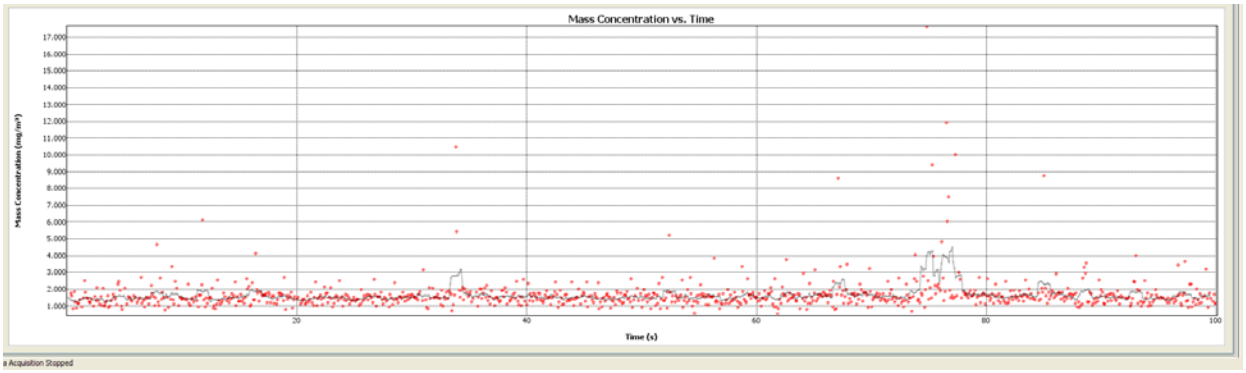

CruiseRich 0007

A similar burst of high svf values is also present in this trace at about 75 seconds. These concentrated high-value measurements suggest that either the soot volume fraction in the normal sense of large numbers of soot aggregates passed through the probe as a cluster or it is a cluster of large agglomerate particles If it was small homogeneously dispersed soot aggregates, the values would not drop to the mean between firings. This behavior is more symptomatic of a cluster of larger particles.

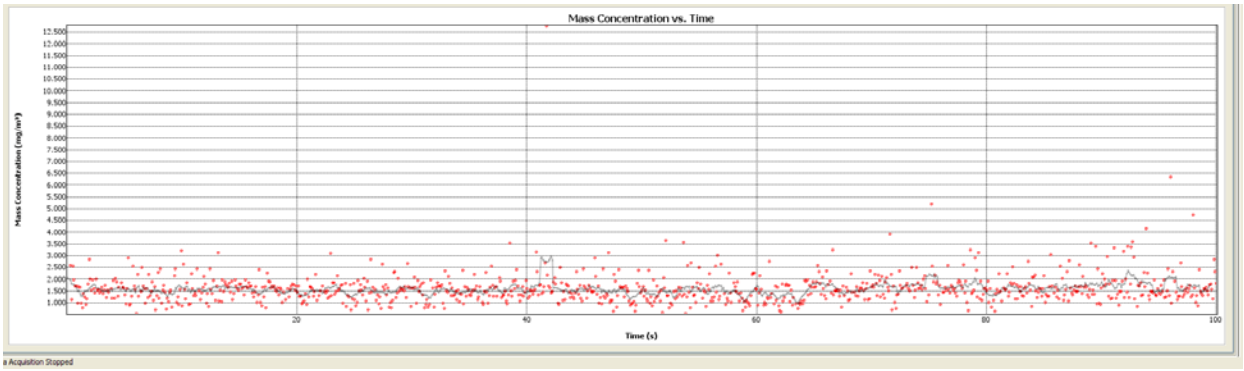

CruiseRich 0008

In this example, there is only one very high-value about 13 mg/m^3 but with other values significantly above the mean value. In this case, these isolated large values can be easily attributed to single large agglomerate particles.

	1-Apr-09	CruiseRich		Dilution =	Dilution =						
	Computer Clock ,	Run ID		135 to 117	33 to 35						
No.	1 hour behind data clock	Sequence	LII SVF	MAAP 1 SVF	MAAP 2 SVF	Ratio 1	Ratio 2	Smoke #	Smoke #	Notes	LII Temp
	AM									Filter 100	
1	6:05	0	1.49	2.78	1.65	1.87	1.11	20	2.79	high	
2	6:13	1	1.44	4.06	2	2.82	1.39	22	3.14	smoke	
3	6:18	2	1.46	4.48	1.98	3.07	1.36	22	3.14	low OC	
4	6:24	3	1.37	3.88	1.75	2.83	1.28	24	3.49		
5	6:30	4	1.54	4.2	1.87	2.73	1.21	24	3.49		
6	6:36	5	1.36	4.84	1.87	3.56	1.38	25	3.67		4482
7	6:44	6	1.74	4.89	1.82	2.81	1.05	26	3.85		
8	6:50	7	1.65	4.57	1.89	2.77	1.15	28	4.22		
9	6:56	8	1.59	5.13	1.99	3.23	1.25	26	3.85		
10	7:02	9	1.89	3.84	1.99	2.03	1.05	26	3.85		4489
11											
	Averages		**1.55**	**4.267**	**1.881**	**2.77**	**1.22**		**3.55**		**2.3**

MAAP1`/MAAP2 = 2.26

This summary data above show that the LII values are closer to the filter-based methods. In fact, the LII results are within 20% of the second MAAP instrument values. Note also that the two MAAP instruments differ by over a factor of two with a smoke meter readings coming in exactly between the two MAAP measurements (4.27 – 3.55 = 0.72, 1.88 + 0.7 = 3.5).

A similar Poisson analysis can be conducted for this case. The difference in the svf measurements between the Average MAAP readings 1.5 mg/m^3. The number of spikes in the data that would be produced by large particles that would be needed to account for this difference and that would be detected by the LII instrument is given as:

Given Concentration Measurements, Figure Out Spike Rate

What mass concentration difference is there between two measurements?	**1.50**	mg/m**3
What size particle do you think represents the "big" particles?	**10.00**	μm
What density do you want to use for soot?	**1.90**	g/cc
How large is your LII probe volume?	**8.00**	mm**3
Sample time in Seconds	**100.00**	
The mass of each large particle is:	**9.95E-10**	g
The expected number of large particles per probe volume is:	**1.21E-02**	
The fraction of pulses with no large particles is:	**9.9E-01**	
The fraction of pulses with at least one large particle is:	**1.2E-02**	
The ratio of pulses without a spike to those with a spike is:	**8.2E+01**	

That is, there would be 1 spike in 82 readings. Looking at figure CruiseRich 0002, there are approximately 6 spikes in 500 or 1.2 in 100. However, some of the other plots show a greater number of spikes. Clearly, there are cases with clusters of particles or large values of soot concentrations. This basic analysis cannot entirely resolve these questions and further work is needed. It would be useful to examine many more smoke meter filters in addition to the MAAP filters.

Collection for Gravimetric Analysis

A similar condition was set for this run but for an extended period of time without any changes to the combustor and sampling systems. The average LII data for this condition was 1.55 mg/m3 with MAAP1 reporting 3.83 and MAAP 2 reporting 1.81.

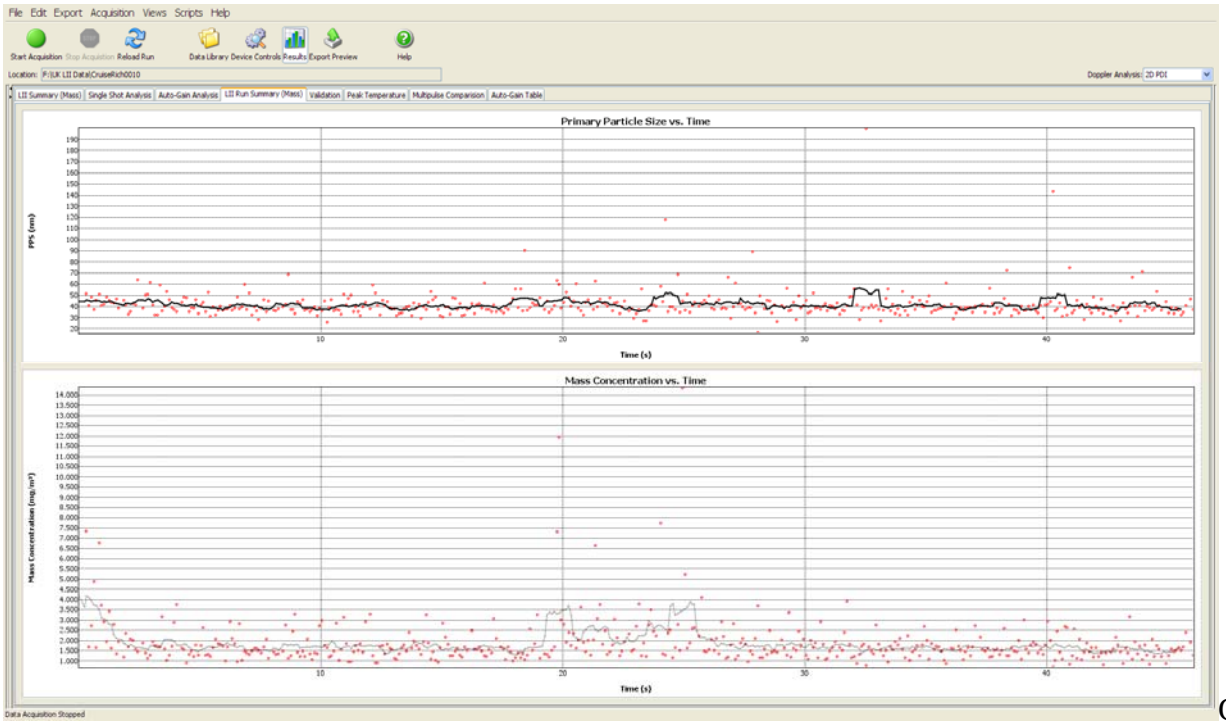

Gravimetric 0010

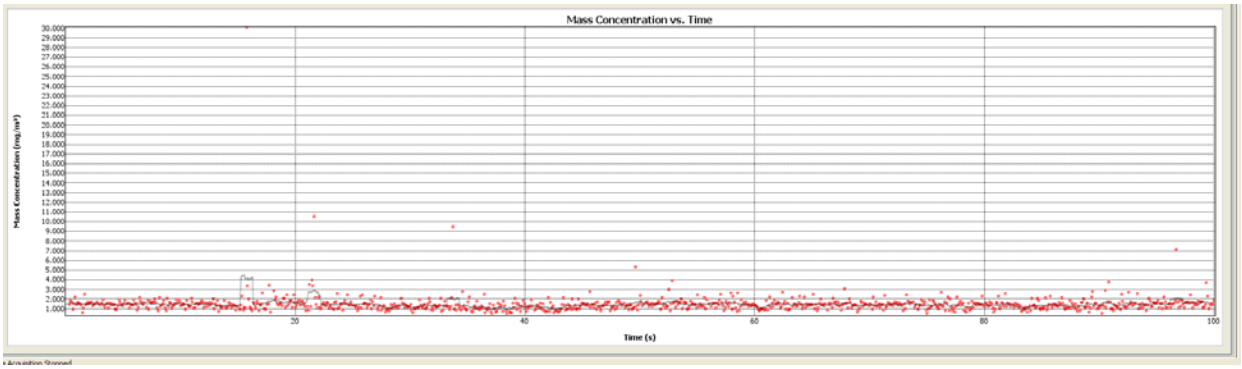

Gravimetric 0012

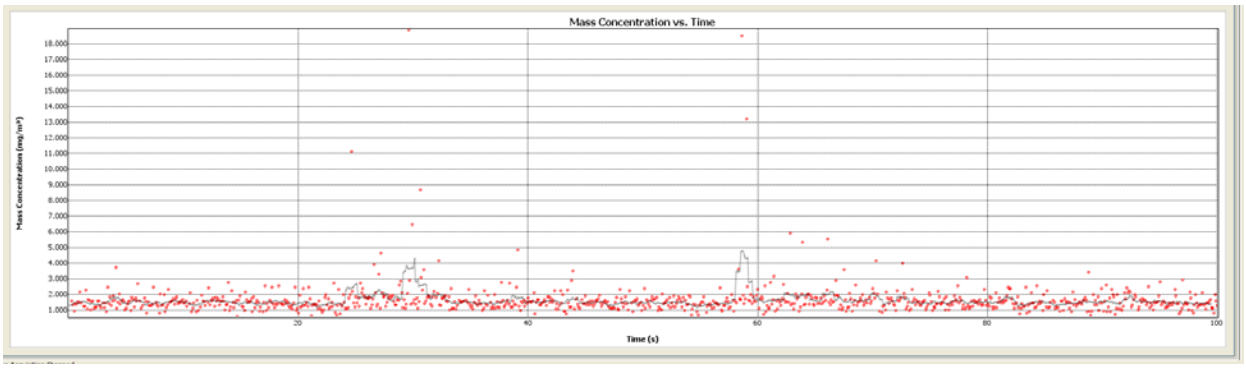

Gravimetric 0014

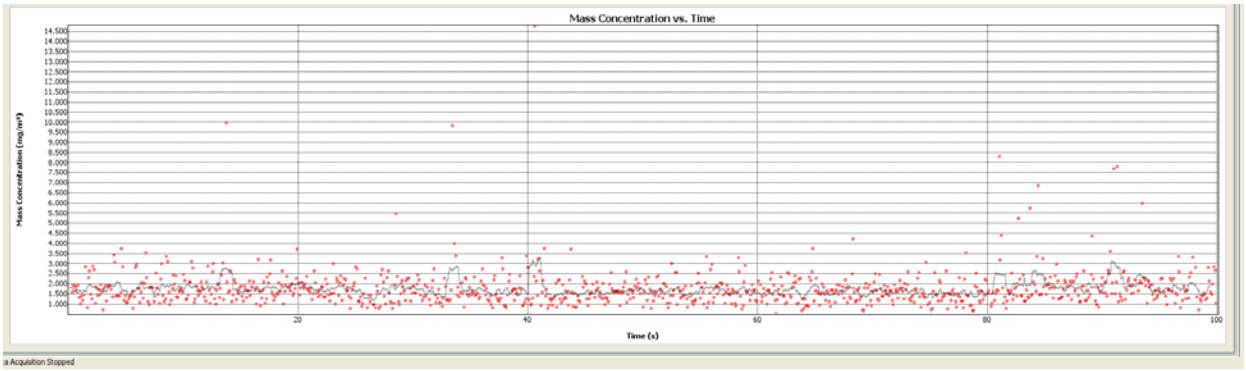

Gravimetric 0020

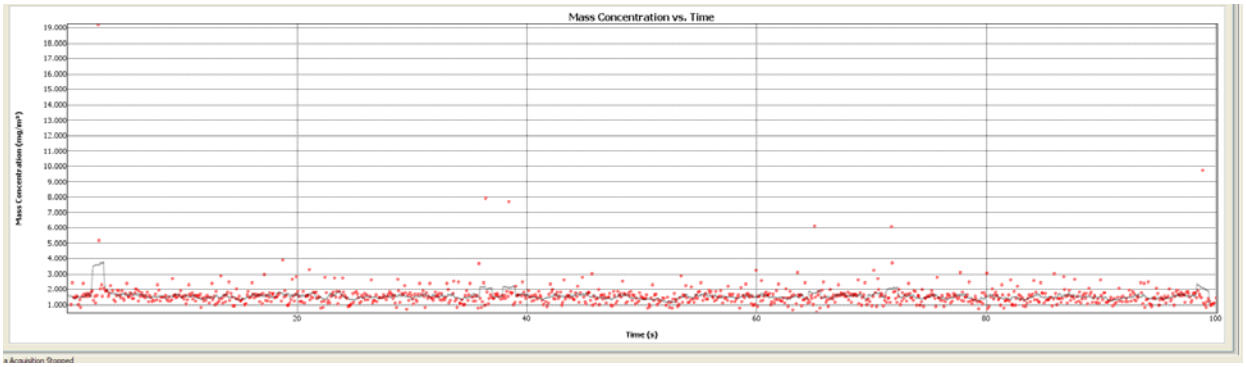

Gravimetric 0022

Same condition for Gravimetric filter Approximately 4:30 UK time

No.	1 hour behind data clock	Sequence	LII SVF	MAAP 1 SVF	MAAP 2 SVF	Ratio 1	Ratio 2	Smoke #	Smoke #	Notes	LII Temp
1	7:33	11	1.3							Filter 48.5	
2	7:35	12	1.46							Filter 48.5	
3	7:37	13	1.56							Filter 48.5	
4	7:40	14	1.6							Filter 48.5	
5	7:48	15	1.52							Filter 48.5	
6	7:50	17	1.63	3.49	1.76					Filter 100	4365
7	7:05	18	1.54							Filter 100	
8	8:04	19	1.72	3.92	1.81					Filter 100	
9	8:19	20	1.74	3.94	1.83						4375
10	8:25	21	1.57	3.97	1.82					Filter 100	
11	8:28	22	1.565							Filter 48.5	
Average			**1.56**	**3.83**	**1.81**						

Some Examples from the World of Diesel Particulate Emissions:

To further support the argumentation that LII does not produce random large excursions in the svf measurements, examples from diesel exhaust measurements will be provided and discussed in this section. Similar disagreement in the diesel measurements were observed when making comparisons between LII and gravimetric results. This was somewhat perplexing, as stated earlier, given the excellent agreement achieved when measuring soot generated by the gaseous diffusion flames. As a result of the initial observation of large particles on the filters, as observed using an optical microscope, additional filters acquired from diesel tests were also examined to determine if large particles were similarly present on the filters.

Diesel Filter Evaluations:

Approximately 50 filters from various tests on diesel engines were obtained and studied under an optical microscope. Most filters revealed the presence of large particles (1 to 50 μm), all with similar morphology and size distributions. I was assured that these filter results were collected after 2.5 μm cyclone separators which are built into the gravimetric sampling systems. For example, filters indicating a weight of approximately 40 μg of soot had a relatively large number of large particles (roughly estimated as 10,000 from a microscope count) as well as many smaller particles trapped within the filter mesh. The lighter loaded filters (10 to 20 μg) had fewer large particles but visible particles were present with small particles (estimated at <1 μm) present in relatively large numbers. The question is; where does this agglomeration of particles occur? Does it happen in the combustor or in the sampling system? Do these particles represent PM emissions from the combustors?

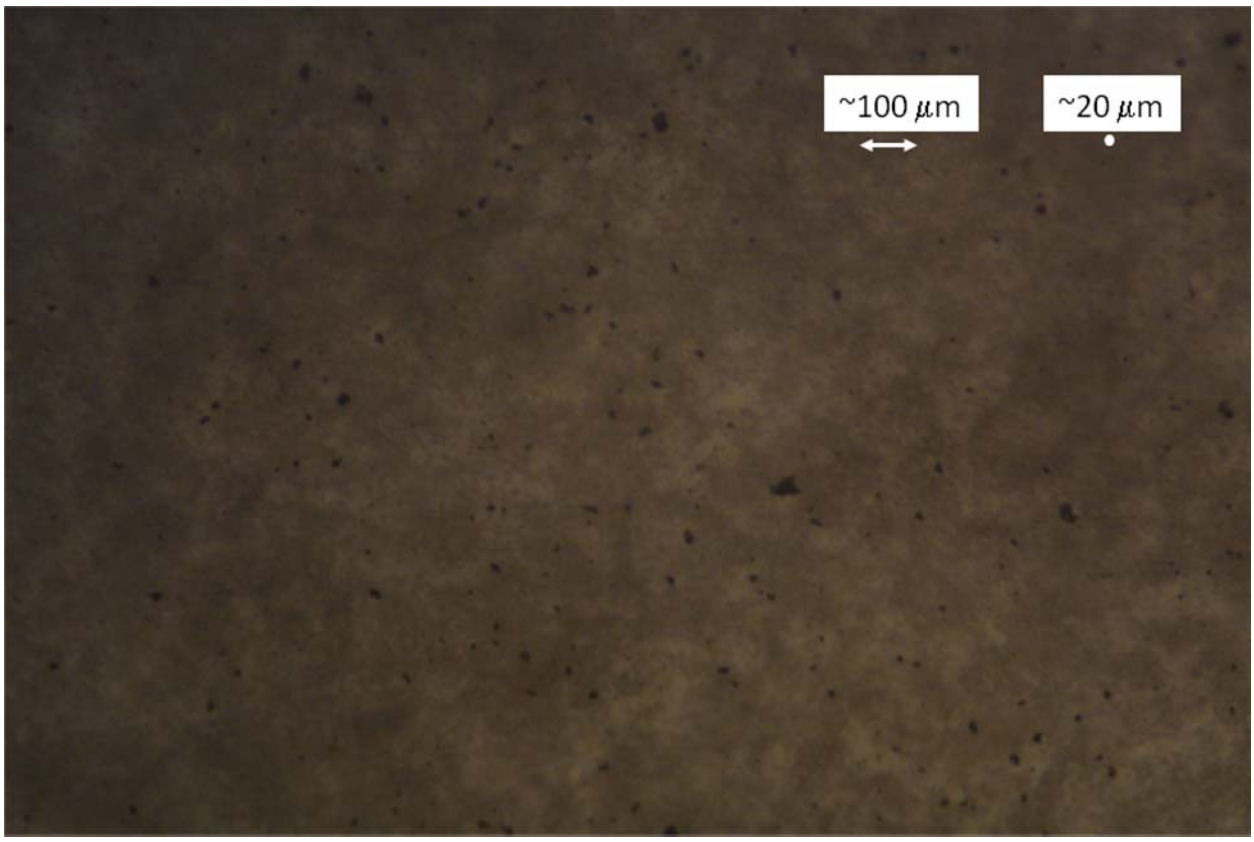

Optical microscope images of soot filters obtained from a diesel exhaust samples. Filter data were obtained downstream of a cyclone separator supposedly able to cut off particles larger than 2.5 μm. The scale shown in the image is approximate and is provided for a rough reference for particle size estimation.

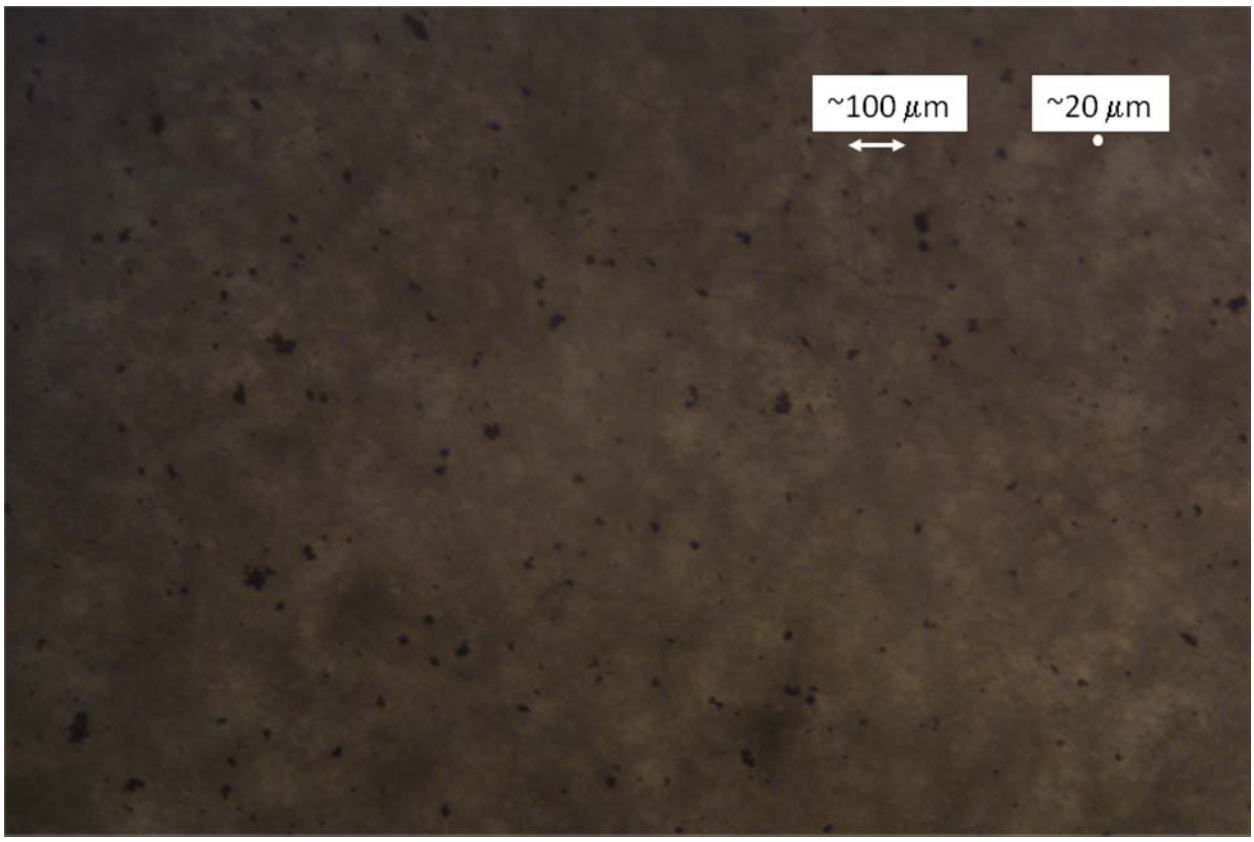

Optical microscope images of soot filters obtained from diesel exhaust samples. Filter data were obtained downstream of a cyclone separator supposedly able to cut off particles larger than 2.5 μm. Note that there are particles as large as 50 μm in these images. The filters were contained in a petri dishes and were not contaminated before or during the microscope observation process.

Clearly, the cyclone separators which are supposed to remove particles larger than 2.5 μm are not completely effective in removing large particles. These data provide irrefutable evidence that the filters are collecting large particles as well as soot aggregates. The LII instrument was not designed to measure such large particles reliably. If these large particles are present, other additional means will be required to characterize them.

EPA FTP Cycle Measurements Showing Data Repeatability

Tests were conducted with the LII instrument from a dilution tunnel to show that large excursions in the LII measurements do not occur at random but are an indication of large particles in the sample. Three cycles were measured to demonstrate repeatability and to evaluate the quantitative results as compared to gravimetric. Typical results for the LII soot volume fraction versus time are shown in the following figure. These results show very low variations for shot to shot measurements. Clearly, this suggests that there were few, if any, large particles in these samples. The large excursions and soot volume fraction were due to the changing engine conditions of this EPA FTP cycle, and not due to individual large particles. A closer examination

of the time record shows that LII readings systematically track the rise and fall of the soot volume fraction with time. That is, individual readings consistently increase and then consistently decrease rather than showing very large changes for individual LII readings.

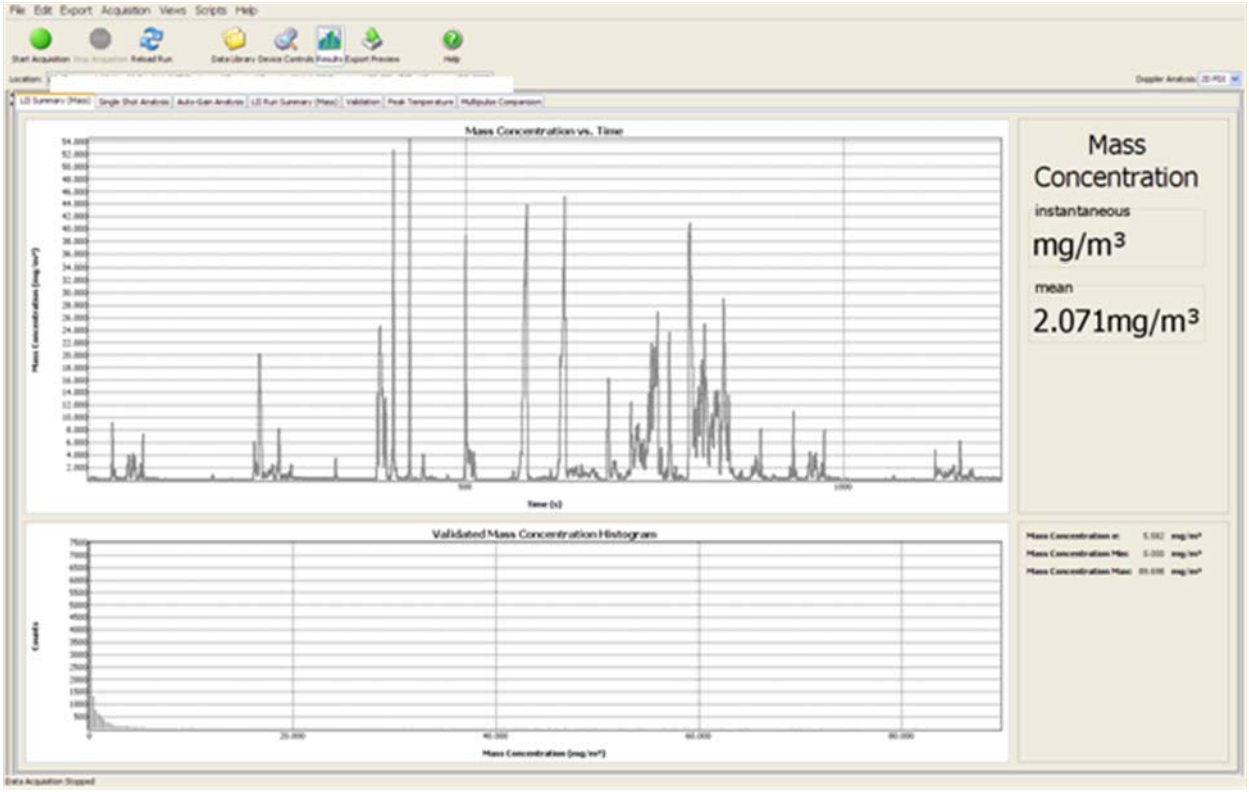

In this test, the sampling was essentially ideal in the sense that there were no isolated large spikes that would indicate the presence of large particles. The CVS and sampling system appeared to be clean and the LII signals were very consistent with low variations from shot to shot except during changes in engine cycles.

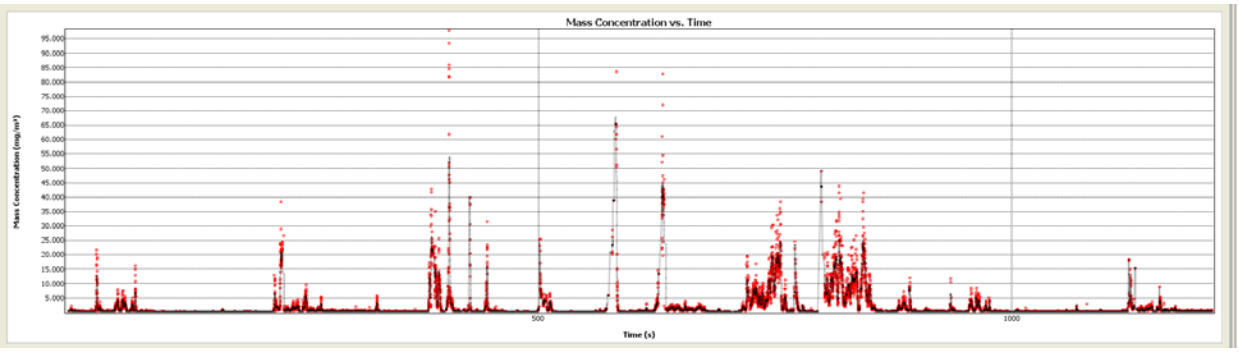

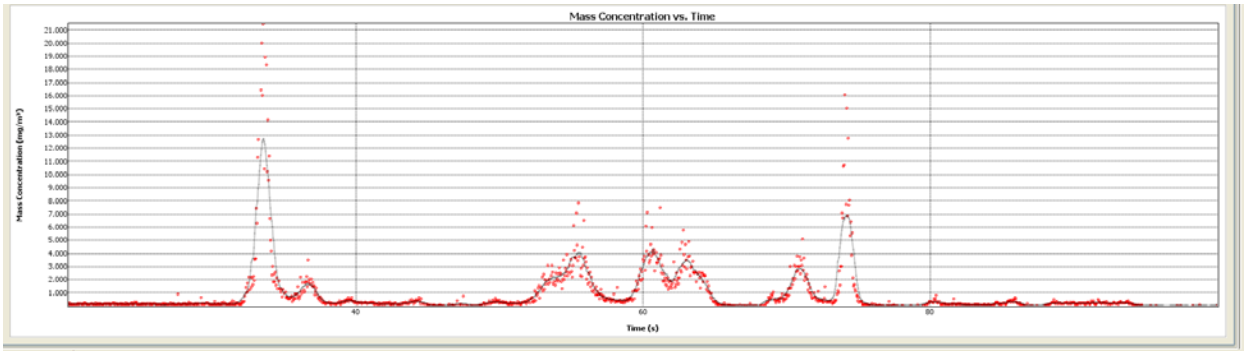

A closer observation of a section of the FTP cycle shows that the LII measurements consistently rise and fall shot to shot indicating that there are no individual spikes in the data. This implies that there are no large particles in the sample and so the results should agree with gravimetric.

The figure below consists of three overlaid FTP runs emphasizing the excellent agreement from run to run. The LII instrument is able to track very fast changes in soot volume fraction, especially when sampling at 20 Hz. The sampling rate is more than adequate for tracking the large excursions in soot volume fraction as engine conditions are changed abruptly.

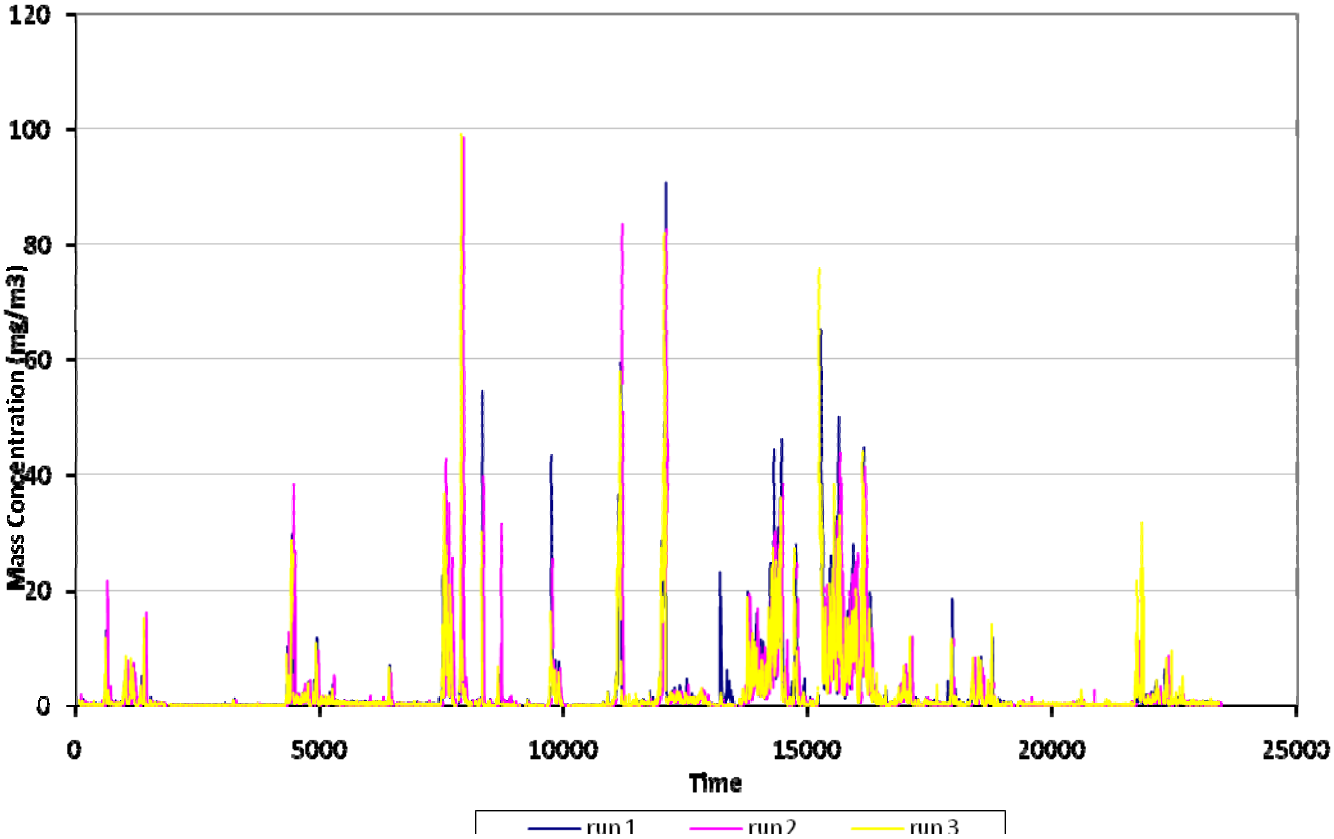

Three repeated FTP cycles are overlaid in this figure showing the excellent agreement from test to test.

Without large particles present, the LII measurements agreed relatively well with the gravimetric results. The gravimetric values were approximately 30% higher than the LII measurements but this was expected since the gravimetric filters collect both the SOF (soluble organic fraction) material as well as the elemental carbon (EC) . We expect that comparison with extracted (EC only) filter data will be much better.

run #	cycle	work (bhp)	cvs flow (scfm)	gravimetric PM (g)	cvs flow (m3/sec)	LII conc. (mg/m3)	LII soot (g)
a438445	FTP	29.99	2117.0	3.045	0.999	38908.109	1.944
a438447	FTP	30.00	2111.4	3.025	0.996	37997.471	1.893

Summary and Conclusions:
Tests were designed to evaluate several instruments for measuring particulate emissions from gas turbine combustors. The LII technique represents a strong candidate for this purpose due to its unique ability to measure only EC from undiluted exhausts in real time and with very low maintenance.

Prior to the testing at Port Talbot, the LII instrument was thoroughly checked out. Tests were conducted on all components including the sampling electronics, the optics, and photodetectors. Thorough calibrations of the instrument were conducted using the integrating sphere approach which is deemed to be more reliable than the incandescent lamp filament method used previously. Retesting of the instrument after these changes indicated that soot volume fraction measured from an inverted laminar diffusion flame agreed very well with gravimetric soot measurements. Unfortunately, in the present tests soot produced by a simulated gas turbine engine combustor and measured by filter-based systems such as MAAP, Smoke Meter, and a gravimetric approach did not agree with the LII results. Questions remained as to why the LII instrument does not produce consistent results when measuring simulated gas turbine particulate? Similar differences were observed when measuring diesel particulate.

In addition to evaluating the LII method when measuring gas turbine soot, an objective of the tests conducted in Wales was to prove or at least further support the hypothesis that the discrepancies we were seeing in the soot volume fraction measurements from gas turbine and diesel exhaust were, in fact, due to the presence of large particles (greater than 1 μm). These large particles are believed to be artifacts of the sample process. Even though there may be cyclone separators in line with some of the filter-based techniques, the cyclones appear to be faulty in terms of removing all particles larger than 2.5 μm. Observations using an optical microscope of a smoke meter filter obtained during the present tests indicated that large particles were present on the filter. Subsequent observations of a random sampling of gravimetric filters obtained for diesel particulate testing also showed conclusive evidence of large particles present on the filters. Concentration of large particles appeared to vary relative to the reported weight of

the filters. Filters from diesel exhaust samples with weights of approximately 40 μg showed a relatively large number of large particles (on the order of 10,000) with sizes as large as 50 μm. My hypothesis regarding the presence of large particles has been supported by these observations using an optical microscope. Analyses have been provided to show how the presence of these large particles can affect the sampling statistics. Thus, measurements with different methods cannot be expected to agree consistently unless the problem of large particles is addressed (eliminated).

Selected figures from the SAMPLE series of tests were presented and discussed. These records of svf versus time clearly showed isolated spikes in the data. Such isolated high values of svf are not consistent with a locally homogeneous distribution of separate soot aggregates. It is much more probable that the large spikes are due to large agglomerates of soot that have been shed from the combustor and sampling line surfaces. These large particles do not represent the normal soot particulate formed in the combustion process but are artifacts of the sampling process.

To demonstrate that these large spikes are not always present in LII data, an EPA FTP cycle measured for a heavy duty diesel engine was shown. The LII results showed consistent behavior which was expected since there were no large particles present in the gas stream (no large spikes in the LII data). Each shot followed a consistent pattern with large excursions in soot volume fraction only occurring with changes in engine cycle. The results from these tests were in good agreement with gravimetric.

From these observations one must conclude that the sampling approach is problematic and must be corrected. That is, large particles are being generated by soot accumulating on surfaces and subsequently re-entrained into the flow. These large particles cannot be measured reliably by the LII method alone. Furthermore, these large particles produce ambiguity to the gravimetric results since it is difficult to predict when the particles were accumulated on the wall and when they were released. In short, my conclusion is that the current gravimetric method is flawed. To obtain reliable measurements, cyclones that perform as specified need to be added to both the gravimetric sampling line and the LII sampling line so that instruments are measuring under the same conditions. Gravimetric filters need to be systematically examined using an optical microscope to determine whether or not large particles are present. These large particles need to be accounted for in the results since they can be a significant contributor to the weight of the collected soot mass. Consistent agreement between LII and other instruments will not be achieved unless the sampling system is operating properly wherein the sample consists of soot aggregates and not large agglomerate particles.

LII is very robust in that it will not detect or measure condensed material or material other than elemental carbon. LII can also measure directly from the engine (or combustor) exhaust which may be a very important requirement since that would limit the amount of agglomeration of soot particulate into large particles (greater than 1 μm). Furthermore, the need for costly dilution systems can be eliminated.

Appendices:

Appendix 1:

9. LASER-INDUCED INCANDESCENCE (EXTRACTIVE)

from Greg Smallwood, E31 Committee SAE AIR TA1, Sep. 2008

Laser-induced incandescence (LII) is performed by measuring the thermal emission (incandescent light) emitted from particles heated by a pulsed laser to temperatures in the 2500 K to 4500 K range (Ref. 2.2.9, 2.2.10). A community of science has developed to advance the LII technique at a large number of organizations around the world, and three international workshops to assess the improvements in the LII technique have been held since 2005 (Ref. 2.2.11). LII is highly selective, responding only to the presence of black carbon, making it decidedly appropriate for measuring the nonvolatile particles produced as a combustion emission. This selectivity is due to the fact that the nonvolatile particles are primarily black carbon. BC absorbs laser radiation over a broad spectral range, and is refractory, so that the nanoparticles survive heating to the temperatures necessary for the incandescence to be detected. At these temperatures, all volatile components that my have been condensed on the BC particles will be promptly evaporated, and most other noncarbonaceous particles will have also evaporated or undergone sublimation. Due to this selectivity, LII cannot be used for the measurement of total particle mass. Black carbon is the primary and most stable constituent of the particle matter emissions in the exhaust of a gas turbine engine (Ref 2.2.7). Analysis of the signals from LII results in the determination of the mass concentration, volume concentration, active surface area, and primary particle diameter of the particle emissions. LII performs these measurements with each laser pulse at a 20-Hz rate, permitting online time resolved data collection and reporting of results in real time.

9.1 Equipment

A variant of LII, autocompensating laser-induced incandescence (AC-LII), has emerged which further enhances the LII technique by recording the temperatures of the irradiated particles during the LII process (Ref. 2.2.9). This new technique automatically compensates for any changes in the experimental conditions, including fluctuations in local ambient temperature, variation in laser fluence, laser beam attenuation by the particulate matter, or desorption of condensed volatile material. The LII 200 instrument produced by Artium Technologies distinguishes itself from other LII instruments by being the only commercially available instrument offering AC-LII.

The LII 200 consists of a self-contained rugged optics enclosure which includes the laser and all components needed for operating the instrument. The optical system consists of a computer-controlled automated laser beam energy detection and adjustment system that maintains the laser light fluence at the sampling volume at

optimum conditions. The system automatically maintains constant laser fluence over a wide range of environmental conditions. The incandescence signal, produced by the particles during and immediately after irradiation by the pulsed laser, is measured normal to the transmitted laser beam from a well-defined measurement volume. The incandescence signal is detected by a pair of detectors employing light interference filters centered at wavelengths of approximately 450 nm and 750 nm. The innovative two-color pyrometry technique permits accurate measurement of BC particle temperature and leads to an auto-compensating approach for BC concentration measurements. Measurement of the BC temperature allows the use of low fluence heating of the particles so that sublimation of BC is insignificant. Besides measuring the volume and mass concentration of BC, the LII signal decay characteristics are also processed to measure the active surface area and infer the primary particle diameter. The LII 200 instrument for measuring these properties of black carbon in real time is shown in Figure 9-A. As with all LII approaches, the LII 200 instrument measures the BC, which is the primary constituent of the nonvolatile particulate matter. The LII 200 does not measure the concentration of total particulate matter.

FIGURE 9-A: Artium Technologies LII 200 Instrument

9.2 Analyzer Routines

9.2.1 System Operation

The LII 200 instrument consists of four major rack mount components. They include the optics enclosure with integrated sample cell, the flow control unit, the laser power supply, and the instrument computer. The entire instrument can be operated from a single circuit, requiring less than 10 A at 120 VAC.

The sample is drawn continuously through the sample cell with a vacuum pump. A pulsed laser light beam is fired, typically at 20 Hz, and is directed to the sample cell with a number of optics

designed to control the laser fluence and to provide beam shaping, as shown in Figure 9-B. Operation of the instrument is completely automated, including control of the laser, and is performed by the AIMS software. Upon interaction of the laser light beam with BC particles in the sample cell, the particles are rapidly heated to temperatures at which detectable thermal emission is produced. This incandescence is emitted uniformly in all directions. The lenses in the detection path collect a portion of this incandescence and direct it to the photodetectors. The intersection of the detection path and the laser light beam define the probe volume for the measurement.

The signal on the photodetectors is converted to a voltage through a transimpedance amplifier and digitized at high resolution and high speed (12-bit, 200 MS/s) for further analysis, as described in section 9.7. This is all performed in real-time, so that the black carbon mass concentration can be measured online at a 20 Hz rate.

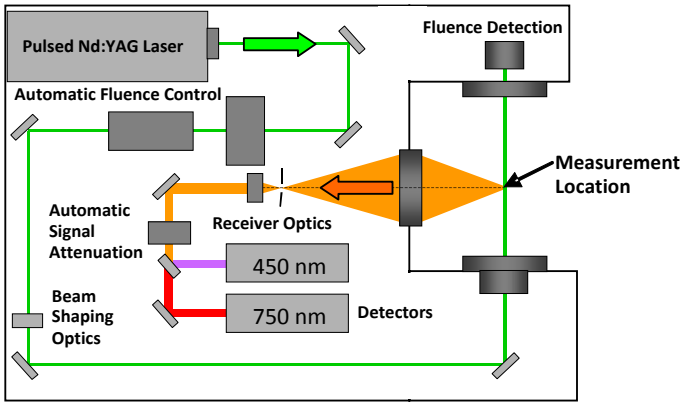

FIGURE 9-B: Schematic of LII 200 instrument optics layout, showing path of laser beam and detected particle incandescence.

9.2.2 Flow Control

A 6 bar compressed air supply is required to provide purge air for the optics case and windows (0.1 SLPM) and to provide motive force to an air eductor vacuum pump for drawing the sample through the instrument. The use of critical orifices ensures balanced flow throughout the instrument. The design of the sample cell is such that the window purge air does not enter the measurement volume, and thus does not alter the concentration of the particles. Redundant controls are in place to ensure that particles cannot flow through the sample cell when the purge air is not active, so that the windows remain clean, even when the instrument is not in use.

A flow audit is unnecessary, as the instrument measures concentration directly, and will do so as long as there is flow present, provided the flow rate is within or not far from the recommended range of 1 – 20 SLPM.

9.2.3 Temperature and Pressure Sensors

There are up to three temperature sensors in the LII 200. The first temperature sensor records the temperature in the sample line just before the sample flow enters the measurement volume. This temperature is used to automatically correct the measured concentration to STP values. The second temperature sensor is used to control the temperature of the sample cell to the set point. The optional third temperature sensor is used to control the temperature of the optional heated sample line to the set point. There is one pressure sensor in the LII 200. The pressure sensor records the pressure in the sample line just before the sample flow enters the measurement volume. This pressure is used to automatically correct the measured concentration to STP values. Any drift in the calibration of the temperature and pressure sensors in the sample line just before the measurement volume would result in a commensurate error in the STP corrected concentration measurement. Audits of the temperature and pressure sensors should be performed at the intervals recommended by their manufacturers.

9.2.4 Sample Cell

The windows in the sample cell must be kept clean. The purge air and flow control systems ensure that the likelihood of window contamination, even at high particle loading, is minimal. The windows are mounted in quick release brackets that allow for rapid removal for inspection and return. Inspection is recommended at monthly intervals or less frequently, as determined through practice. Cleaning of the windows can be performed by qualified instrument operators. The sample cell should be maintained at a temperature of 50°C or greater to minimize the likelihood of water condensation. The LII 200 provides an integrated heater control for maintaining the temperature of the sample cell.

9.3 Calibration Standards

Calibration of the instrument is performed by Artium Technologies using a known NIST-traceable spectral radiance source at a known temperature, which provides calibration factors to associate the measured signals with absolute intensities. This calibration uses the same optical path (windows, lenses, mirrors, filters, photodetectors) as the incandescent light from the particles, so that the measured signal from the incandescent light can be directly related to the absolute intensity of the traceable calibration source with no further steps or assumptions. The conversion of these signals to the mass concentration of black carbon is described in section 9.7. System checks of proper instrument operation are in place and are subject to continuous improvement by Artium Technologies. If a correlation to another particle mass measurement method such as gravimetric is desired, a factor can be entered in the AIMS software to provide this relationship.

9.4 System Layout

The sampling system shall consist of a heated sample line connected to the LII 200 sample cell inlet. The heated sample line shall be set to the same temperature as the heated sample cell,

typically a temperature of 50°C or greater. Refer to the LII 200 instrument manual for further details on the set-up and connection of the sampling system.

9.5 Test Procedure

Refer to the LII 200 instrument manual and the AIMS software manual for details on system operation and control.

Start-up of the instrument is instantaneous, as it is ready for data collection immediately after being turned on. Several parameters can be adjusted as required by the experiment to be performed. These include the data rate (typically in the range 1-20 Hz), the duration (in time, number of laser shots, or indefinite), and selection of the concentration range (via choice of neutral density filter). Once these parameters are set, operation simply requires activation of the green start button for each data collection. Instrument operation is automatically suspended at the end of the specified duration, unless indefinite is selected, in which case activation of the red stop button is required to suspend operation.

9.6 Data Flow

The data files exported at the end of each data collection by the AIMS software supplied with the LII 200 instrument can be either comma-separated values (CSV) or Microsoft Excel format. The instrument can also provide a continuous output of the data via a USB or network connection for collection by the user's data recording system.

9.7 Calculation of Results

The mass concentration of black carbon is calculated based on the temperature determined from two-color pyrometry of the black carbon particles and absolute intensity of the incandescence being emitted by the black carbon particles. This calculation is

$$C_{BC} = \frac{V_{EXP_\lambda}\,\rho}{\eta_\lambda w_b} \frac{\lambda^6\left(e^{\frac{hc}{k\lambda T}}-1\right)}{12\pi c^2 h\, E\left(m_\lambda\right)} = V_{EXP_\lambda}\, K_1\left(e^{\frac{K_2}{T}}-1\right)$$

where:

C_{BC} is the mass concentration of black carbon

V_{EXP} is the LII measured signal (volts)

ρ is the density of black carbon

λ is the wavelength for the detector

η is the calibration factor (relating measured volts to the source spectral radiance)

w_b is the laser sheet width, which determines the depth of the measurement volume

h, c, and k are the Planck constant, velocity of light, and Boltzmann constant, respectively

T is the temperature (K)

$E(m)$ is the absorption function, an optical property of black carbon

K_1 and K_2 are constants, incorporating many of the terms above

Thus, the mass concentration is directly related to the measured signal and the particle temperature. All other parameters are constants. The temperature is determined instantaneously by the well-known method of two-color pyrometry.

As well as the mass concentration, the particle temperature, statistics on the measured quantities, averaging, and many other experimental properties can be reported by the AIMS software, as requested by the user.

2.2.7 *Petzold, A., and Schröder, F.P. (1998). Jet Engine Exhaust Aerosol Characterization,* Aerosol Sci. Technol., 28, 62-76.

2.2.8 Petzold, A., Schloesser, H., Sheridan, P.J., Arnott, W.P., Ogren, J.A., and Virkkula, A. (2005). Evaluation of multi-angle absorption photometry for measuring aerosol light absorption, Aerosol Sci. Technol., 39, 40-51.

2.2.9 Snelling, D. R., Smallwood, G. J., Liu, F., Gülder, Ö. L., and Bachalo, W. D. (2005). A Calibration-Independent LII Technique for Soot Measurement by Detecting Absolute Light Intensity, Applied Optics, 44, 6773-6785.

2.2.10 Schulz, C., Kock, B. F., Hofmann, M., Michelsen, H., Will, S., Bougie, B., Suntz, R., and Smallwood, G. (2006) Laser-Induced Incandescence: Recent Trends and Current Questions, Applied Physics B, 83, 333-354.

2.2.11 http://liiscience.org

2.2.12 Mohr, M. and U. Lehmann (2003). Comparison Study of Particle Measurement Systems for Future Type Approval Application. Research Report No. 202779, EMPA Dubendorf, Bern, Switzerland, May. Available at: http://www.sootgenerator.com/publ.htm

2.2.13 U. S. Environmental Protection Agency (2008). Title 40, U. S. Code of Federal Regulations, Part 86: Control of Emissions from New and In-Use Highway Vehicles, Subpart N: Emission Regulations for New Otto-Cycle and Diesel Heavy-Duty Engines; Gaseous and Particulate Exhaust Test Procedures. Available at: http://ecfr.gpoaccess.gov/cgi/t/text/text-idx?c=ecfr&sid=8055c635b5ea0163d8c9f9421d3311e8&rgn=div6&view=text&node=40:19.0.1.1.1.8&idno=40

Appendix 2:

Some comments from Professor Kittelson, University of Minnesota are provided:

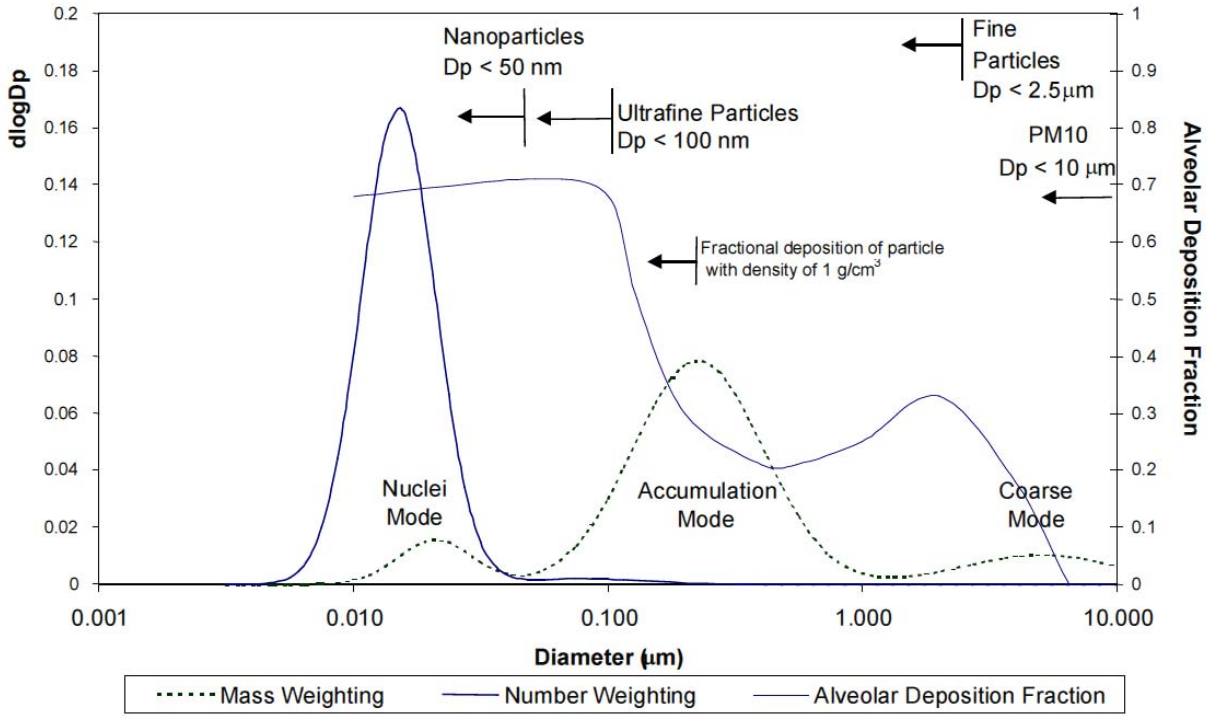

Figure 3. - Typical engine exhaust size distribution both mass and number weightings are shown (Kittelson, 1998a).

This figure was taken from a report by Prof. Kittelson to show the expected particle size distributions for diesel particulate.

Table 3. Particle – Wall Interactions

Mechanism	Impact	Recommendations
Inertial impaction	• Removes small number of the largest particles (represents a larger fraction of the total particulate mass) • Introduces variability through unpredictable reentrainment of deposited mass • Inertial and gravitational losses are quite small for particles in 0.1-1.0 μm range	• Avoid sharp changes in sample line diameter or direction • Isokinetic sampling not as important for submicron particles
Electrostatic deposition	• Electric charge build-up on sample lines attracts charged diesel particulate matter, causing it to deposit on line walls	• Use metal sample lines to avoid electrostatic build-up • Avoid Teflon sample lines, prone to large build-up of electrostatic charge
Thermophoretic deposition	• Large temperature differences between exhaust gas and sample lines causes thermal driving force depositing particles on line walls • Most significant losses occur during transient duty cycles	• Insulate / heat sample lines to avoid large differences in temperature between lines and exhaust gas
Diffusional deposition	• Diffusion for particles in the size range that represents the majority of the mass is negligible (> 0.1 μm) • Diffusion for particles (< 0.03 μm) in the size range that represents the majority of number is also small, but should be considered for the smallest size ranges measured	• Difficult to eliminate diffusional deposition • Use short sampling lines
Gravitational deposition	• Minimal impact on diesel particulate losses • May introduce variability through unpredictable reentrainment of small deposited mass	• Avoid unnecessarily long horizontal sections of sample lines where large particles may settle

Source: Kittelson, D. B., and J.H. Johnson (1991)

From Kittelson, et.al.

exhaust stream. Reentrainment is unpredictable and increases variability in mass measurements because of the increase in the number of coarse (> 1,000 nm) particles. These particles are not necessarily representative of diesel aerosol and make aerosol size distribution measurement more difficult. Another problem related to temperature is the condensation of volatile matter (hydrocarbons and sulfates) on cooler dilution tunnel walls. These volatiles are precursors of new nanoparticles that form when the walls are heated volatizing the material.

- Typically about 85% of the mass of particles emitted by diesel engines was in the submicron diameter range. The submicron size distribution was typically bimodal with "nuclei" and "accumulation" modes at about 0.025 and 0.25 μm volume geometric mean diameters, respectively.

David B. Kittelson, Ph.D., Megan Arnold and
Winthrop F. Watts, Jr., Ph.D.

This page is intentionally blank.

« SAMPLE »

Sampling line modelling

EASA “SAMPLE” project report
EASA.2008.OP.13
21 September 2009

X. Vancassel
D. Delhaye

1 Introduction

Using sampling probes and transport tubes for combustion exhausts measurements requires taking into account that post sampling reactions may alter the collected sample. As a calibration of the line would help defining the penetration factor (or transmission i.e. the ratio between leaving to entering particles in a line), it may not easily estimate how much the exhaust composition has been modified during its transport, from the sampling probe tip to the instruments. This modification of the sample involves chemical reactions occurring after sampling (e.g. further oxidation of sulphur) and microphysical processes affecting primary particles (soot) and gaseous species through new particle formation (nucleation) and other phase transition processes (condensation/evaporation). Therefore, numerical models have been used in order to simulate the relevant physical and chemical processes occurring in the sampling line. The model description and the preliminary results are detailed hereafter.

2 Model Description

The model is mainly based on the work done by Yu *et al*. (1999) and Vancassel *et al*. (2004). It can be considered as a thermodynamic Lagrangian trajectory box model. The box is moved along the sampling line and its thermodynamic properties are adjusted as they evolve during transport. Therefore, temperature and pressure of the sample vary with cooling and heating processes or with any volume expansion due to a change in the diameter of the line for instance. The reference volume is taken at the beginning of the sampling line as the result of the combustion of 1 kg of fuel.

2.1 Combustion exhaust products

The emitted species are mainly selected as a function of their importance for particulate matter composition, for their condensation properties and their thermodynamic properties (e.g. enthalpy of a mixture).

2.1.1 Sulphuric acid

Sulphuric acid is formed by oxidation of the fuel sulphur and the conversion of the resulting sulphur dioxide into SO_3 and H_2SO_4. It is very efficient for new particle formation and easily mixes with water.
The initial concentration of sulphuric acid is obtained from the fuel sulphur content (300 ppm in SAMPLE) and the assumed conversion factor whose value remains uncertain (Schumann *et al.*, 2002). It can reasonably be considered between 0.5 and 5 % or slightly over (see for example Schumann et al. 2002, Katragkou *et al.*, 2003).

2.1.2 Water vapour

The average emission index of water vapour is close to 1.23 kg/kg fuel for cruise conditions. Data from the PartEmis European project were slightly higher at the combustor exit (close to 1.4 kg/kg fuel).

2.1.3 Organic compounds

Organics are assumed to be responsible for volatile particles growth in addition to their potential nucleating properties. The main uncertainty lies in their exact identification and their properties.

Unburnt hydrocarbons may be good candidates but Yu *et al.* (1999) pioneering study identified formaldehyde as a possible choice. The organics initial emission index depends on the engine operating conditions but for cruise conditions it can be estimated close to 40 ppm on average (50 ppm in lean conditions for THC from R. Marsh *et al.*, Sample report)

2.1.4 Chemi-ions

Chemi ions are formed at high temperature in the combustor in huge amount. Mass spectrometer analyses as well as modelling studies estimate that the initial emission index of chemi ions vary between 10^{16} and 5.10^{17} particles /kg fuel. Measurements are very difficult to work out for technical reasons and also because oppositely charged ions tend to recombine very quickly.

2.1.5 Soot particles

Soot are primary aerosol particles formed in the combustor. They are formed of aggregates of primary particles. The shape of their distribution has been considered as lognormal and their initial emission index need to be confirmed by SAMPLE DMS 500 data but probably ranges between 10^{13} and 10^{15} particles per kg fuel.

2.2 Types of particles considered

Different kinds of particles are taken into account in the model. As previously mentioned, soot particles are initialized at the sampling line tip as they are combustion products. Any other particles are formed downstream (see next section for details). The types of aerosol particles are listed below.

- Soot primary particles they are assumed to be initially dry. For the first simulation activation criteria have not been used. Soot particles remain dry or get immediately covered by condensable matter and become hydrophilic.
- Mixed soot (soot covered by volatile material, sulphuric acid, water and organics $(soot)(H_2SO_4)_a(H_2O)_b(OM)_c$) OM= organic matter)
- Volatile particles
- Sulphuric acid clusters and particles (hydrated sulphuric acid $(H_2SO_4)_a(H_2O)_b$)
- Organics clusters and particles $((OM)_a(H_2O)_b)$
- Negatively charged sulphate clusters and particles $((HSO_4^-)_a(H_2O)_b)$
- Positively charged organic clusters and particles $((OM^+)_a(H_2O)_b)$
- Mixed volatile particles (neutral, no charge: $(H_2SO_4)_a(H_2O)_b(OM)_c$)
- Mixed negative volatile particles $((HSO_4^-)_a(H_2O)_b(OM)_c)$
- Mixed positive volatile particles $((OM^+)_a(H_2SO_4)_b(H_2O)_c)$

Where a, b and c are the respective number of molecules of the different compounds composing the particle.

The code has been developed and generalized so that coagulation mixes all the different components and distribute them on the particles. This involves that aerosols are internally mixed and multicomponent i.e. they contain a given fraction of any of the different compounds. This enables any new condensable material to be integrated very easily.
Particles are distributed as a function of their volume in size bins whatever their composition. As a result, two particles of same size and of same type may have different composition e.g.:

Particle 1: H_2SO_4 = 20% H_2O = 30 % OM = 10% Soot = 40%
Particle 2: H_2SO_4 = 15% H_2O = 20 % OM = 25% Soot = 40%

In that case, in a given bin, particles composition respective fractions are averaged. It may cause problems regarding solid cores particles as averaging the soot fraction creates new solid cores that should not exist (solid cores get cut into fractions).

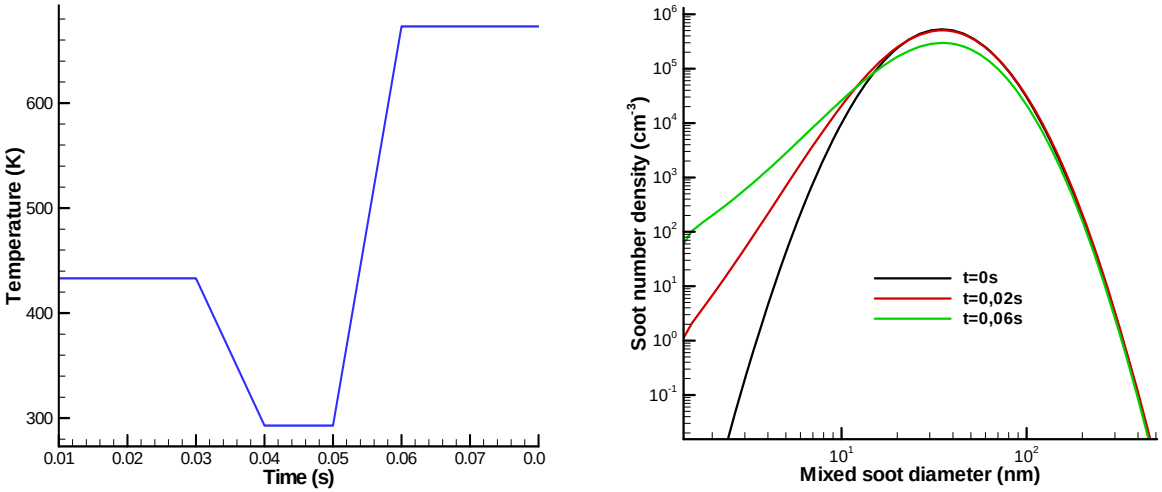

Figure 1: example of temperature variations (left) occurring in a sampling lines and the mixed soot size distribution at 3 different times.

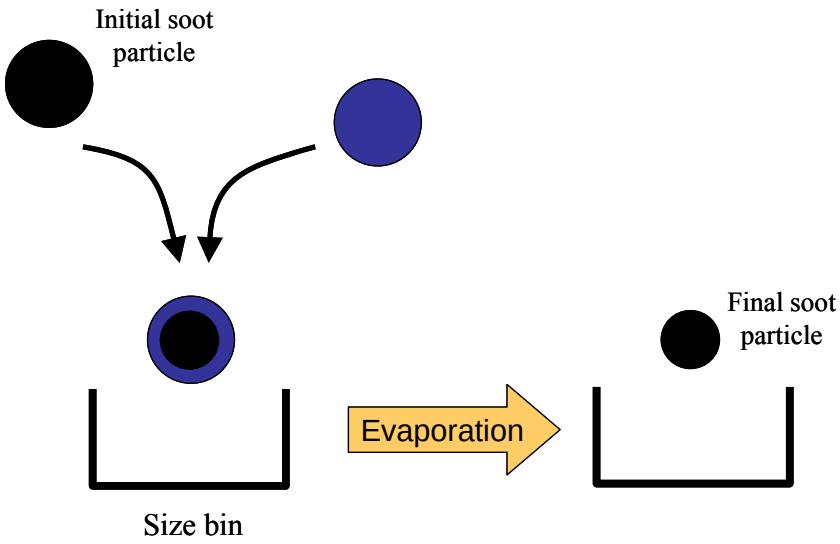

Figure 2: Illustration of the process of averaging between particles of a same size, leading to a non physical change of the soot core (final soot size < initial soot size).

This is clearly visible in figure 1 where the distribution of soot particles is shifted to smaller sizes between t=0s and t=0.06 s. Figure 2 gives a better representation of what happens here.

The initial size of soot solid cores must indeed remain unaffected as this is a physical fact. The code has been modified so that soot particles are distributed as a function of the size of their solid core. They can grow by water or any other condensable gas uptake but in case of sudden evaporation events, the soot cores distribution is preserved (see figure 3).

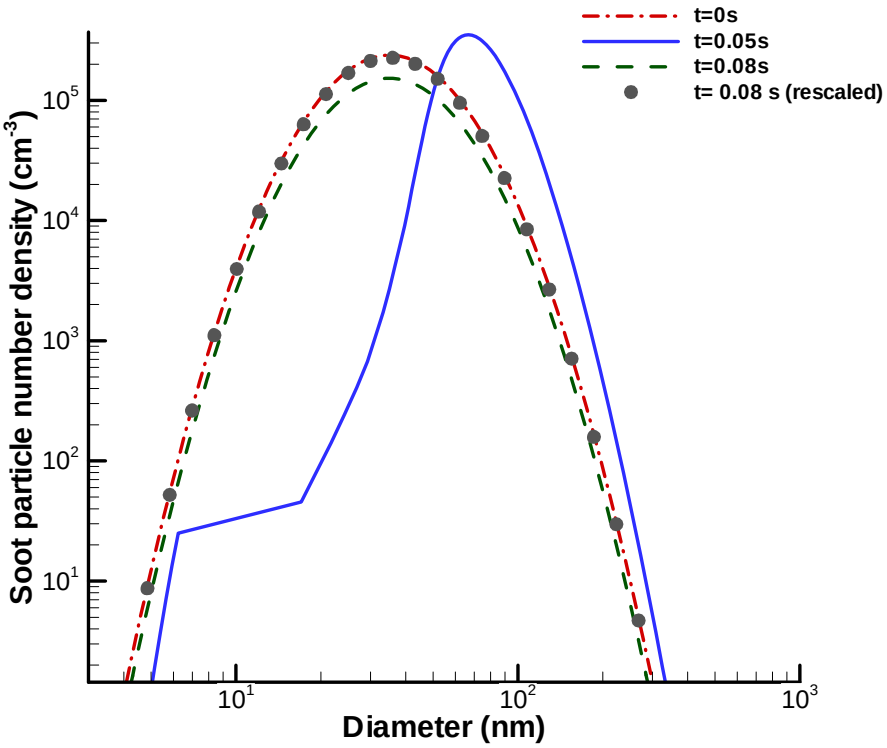

Figure 3: Evolution of the soot particles distribution for various times corresponding to condensation or evaporation phases.

The soot distribution remains nearly unchanged in the first steps of the simulation as the sample temperature remains larger than 400K. When the temperature decreases below 300 K, the particles are moved to larger sizes (peak=80 nm) due to condensation of water. When temperature increases up to 600K, evaporation takes place and contrarily to the first results shown in figure 1 (right), the distribution gets back to its initial state (tip of sampling probe) provided that a correction factor for temperature and pressure change is applied (rescaling). Therefore the necessary modification made in the code is successful.

2.3 Physical processes

2.3.1 Evolution of concentration and composition

Primary particles as well as freshly nucleated particles in the sampling line will undergo various transformations. Their concentration change can be given by:

$$\frac{dN}{dt} = \left(\frac{dN}{dt}\right)_{dilution} + \left(\frac{dN}{dt}\right)_{coagulation} + \left(\frac{dN}{dt}\right)_{nucleation} + \left(\frac{dN}{dt}\right)_{loss}$$

Their composition change mainly depends on coagulation and material exchange between gas phase and condensed phase. As a result, the number of molecules *i* per particle will vary as follows:

$$\frac{di}{dt} = \left(\frac{di}{dt}\right)_{evaporation} + \left(\frac{dN}{dt}\right)_{condensation} + \left(\frac{dN}{dt}\right)_{coagulation}$$

Dilution refers to the change of volume of the sample, triggered by diluters but also to temperature and pressure changes (e.g. when the line is not heated and the sample cools down to ambient temperature). Coagulation stands for collision processes from particles and clusters Brownian motion . Nucleation is treated as kinetically controlled mechanisms between clusters (Yu and Turco, 1998). Loss processes have been determined as a function of the particle size.

2.3.2 Loss processes

As the exhaust sample is transported, particle size distributions get affected by various loss processes. It is likely that some particles are lost in the tube as they come into contact with the walls. In a previous work, Vancassel *et al*. (2004) assumed that volatile particles were affected by turbulent deposition (diffusion) and worked out a size dependent penetration factor using a first order equation. Soot particles were assumed to be lost independently of their size.
For this study, the different types of loss processes have been examined, especially using theoretical or semi empirical laws that can be found in Baron and Willeke (2005).

Gravitational settling

Due to gravity forces, large particles are deposited on the tube. For a turbulent flow (horizontal tube), the transport efficiency is given by:

$$\eta_{grav} = \exp\left(-\frac{4LV_{ts}}{\pi d_p U}\right)$$

$$V_{ts} = \tau g$$

$$\tau = \frac{\rho_p d_p{}^2 C_c}{18\eta}$$

$$C_c = 1 + \left(\frac{2}{0.752 P d_p}\right)\left(6.32 + 2.01\exp(-0.1095 P 0.752 d_p)\right)$$

where V_{ts} is the fall velocity, τ is the relaxation time of the particle, and C_c is the Cunningham correction slip factor. d_p et ρ_p are the diameter and the particle density. U, η, P are the average flow velocity, the kinematic viscosity and the pressure of the flow. Finally, g is the gravity constant.

Assuming that the sample flow rate is constant, the transport efficiency is given as a function of time by:

$$\eta_{grav} = \exp\left(-\frac{4\Delta t V_{ts}}{\pi d_p}\right)$$

η_{grav} vary as a function of the type of particles, through the difference of density. For a vertical tube, the efficiency is equal to 1.

For a laminar flow,

$$\eta_{grav} = 1 - \frac{2}{\pi}\left(2\kappa\sqrt{1-\kappa^{2/3}} - \kappa^{1/3}\sqrt{1-\kappa^{2/3}} + \arcsin(\kappa^{1/3})\right)$$

$$\text{with} \quad \kappa = \frac{3}{4}\frac{L}{d_t}\frac{V_{ts}}{U} = \frac{3}{4}\frac{V_{ts}}{d_t}\Delta t$$

Diffusion

Contrarily to gas molecules or clusters (rebound effect), volatile particles collide to the wall. A concentration gradient exists between the centre and the edge of the transport tube. This is responsible for a diffusion of particles which migrate to the wall, collide and finally get lost.

For a laminar flow:

$$\eta_{diff} = 1 - 5.5\mu^{2/3} + 3.77\mu \quad (\mu < 0.009)$$

$$\eta_{diff} = 0.819\exp(-11.5\mu) + 0.0975\exp(-70.1\mu) \quad (\mu > 0.009)$$

$$\mu = \frac{4DL}{\pi d_t^2 U} = \frac{4D\Delta t}{\pi d_t^2}$$

D et d_t are respectively the particle diffusion coefficient and the tube diameter.

The transmission factor (turbulent) while taking into account loss by diffusion in the boundary layer writes:

$$\eta_{diff} = \exp\left(-\frac{4LV_{dep}}{d_t U}\right) = \exp\left(-\frac{4\Delta t V_{dep}}{d_t}\right)$$

$$V_{dep} = \frac{0.04U}{\mathrm{Re}^{1/4}}\left(\frac{\rho_g D}{\eta}\right)^{2/3}$$

with ρ_g the air density and V_{dep} the deposition velocity.

Inertial deposition

Inertial deposition depends on the flow regime (turbulent or laminar). It is quite efficient when the flow has to deal with changing geometry like an elbow for instance but it is also a function of the particle size

$$\eta_{elbow} = \left(1 + \left(\frac{Stk}{0.171}\right)^{0.452\frac{Stk}{0.171}+2.242}\right)^{-\frac{2}{\pi}\varphi} \quad \text{(laminar flow)}$$

$$\eta_{elbow} = \exp(-2.823Stk.\varphi) \quad \text{(turbulent flow)}$$

φ is the curvature angle of the transport tube (elbow → φ=90°) and Stk is the Stokes number defined as

$$Stk = \frac{\tau U}{d_t}$$

Thermophoretic effect

Temperature gradients in the tube can be responsible for particles migration to cold walls. This is effective for non isolated lines or during dilutions.

For a laminar flow

$$\eta_{thermo} = \exp\left(-\frac{\pi d_t U \Delta t V_{th}}{Q} \right)$$

Q is the volume flow rate and the thermophoretic velocity V_{th} is expressed by :

$$V_{th} = \frac{2C_s U \left[\frac{k_g}{k_p} + C_t Kn \right] C_c}{(1+3C_m Kn)\left[1+2\frac{k_g}{k_p} + 2C_t Kn \right]} \frac{\nabla T}{T}$$

with *Kn* the Knudsen number which is the ratio between the mean free path and the size of the particle.

$$K_n = \frac{2\lambda}{d_p} \qquad C_s = 1.13 \qquad C_m = 1.14 \qquad C_t = 2.63$$

2.3.3 Implementation of loss processes

Taking into account particles loss in the sampling tube is important in order to understand how the collected sample is affected. The aim of the present study was not to implement state of the art numerical techniques to validate the physical processes going on in the line. This would require computationally expensive 3D numerical simulations, dealing with the complex interactions of the fluid and the particles. Therefore we have used parameterized laws for penetration or transmission efficiency calculations and we applied this to a detailed aerosol code, so that particles properties can be followed as the sample is transported along the line.
Some approximations were necessary to take into account the different processes altogether. Although some physical processes are triggered by gradients (concentration or temperature), average flow properties have been used. In particular, the flow has been assumed to be homogeneously mixed and therefore temperature, flow velocity and pressure were the same at the centre or at the edge of the tube.
In figure 4 are depicted the respective contributions of the line loss processes, as a function of the particle size. For this calculation, a 10 m long and 9.78 mm wide tube has been used. The sample temperature was 430K (this is close to the conditions met during SAMPLE for the first part of the “hot line”. The flow was assumed turbulent and the flow rate was 40 $l.min^{-1}$. For expected sizes ranging approximately from 1 nm to 1 µm, turbulent diffusion is the main contributor to particle loss. Gravitational settling as well as inertial losses can be neglected below 1 µm. They become dominant for larger values as particles aerodynamic behaviour and weight effect are significantly modified.

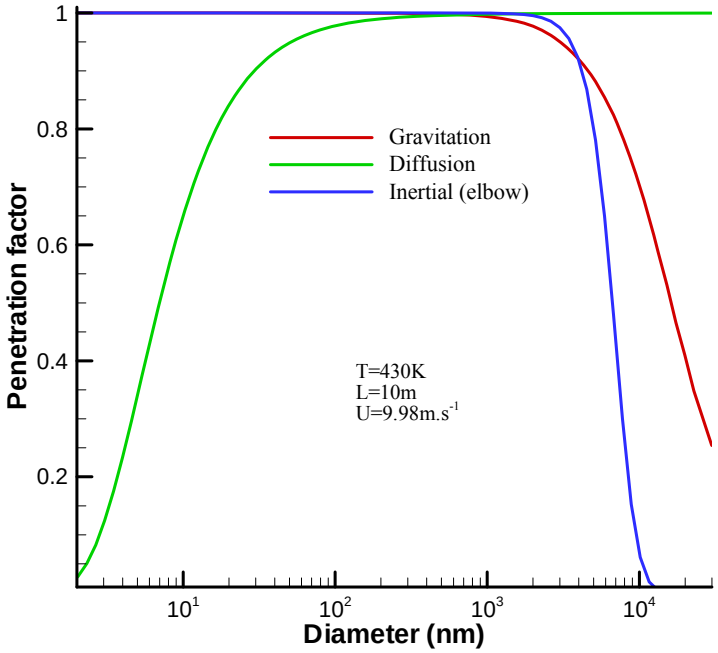

Figure 4: Penetration factor as a function of particle size for three processes

The transmission efficiency is applied each time iteration so that the concentration of the particles are updated to account for line losses. The relationship between the time of residence of the sample in the tube (t) and the line length (l) writes for a constant volume flow rate Q and line diameter d:

$$t = \frac{\pi\left(\frac{d}{2}\right)^2 l}{Q}$$

Once any condensable material on a particle is lost after colliding to the walls, it is assumed to be definitively removed from the system. After each time step, a balance is made to evaluate the amount of condensable matter remaining in gas phase.

$$C_{gas}(t) = C_{total}(t_0) \times f(T, P, dil) - C_{condensed}(t) - \sum_t C_{lost}(t)$$

The equation above shows that the remaining gas in the tube per volume of air C_{gas} is based on the initial concentration $C_{total}(t_0)$ affected by temperature and pressure changes, and by dilution. The number of molecules in aerosol phase is then removed as well as the amount of material lost from t_0 to t.

3 Results

3.1 "AMS line"

The first simulations have been performed using a non diluted part of the line, leading to the Aerosol Mass Spectrometer. This so-called "AMS line" case has been chosen regarding interesting results from the AMS showing the presence of volatile material. The interesting feature of this line is that the last section was not heated and the sample temperature was probably close to ambient. The line has been idealized as illustrated in figure 5. It has been assumed to be composed of different linear sections and elbows but the real line was not that simple as connectors and bended tubes had much more complex geometry. However this line must be seen as a first case and should represent a lower limit for particles loss.

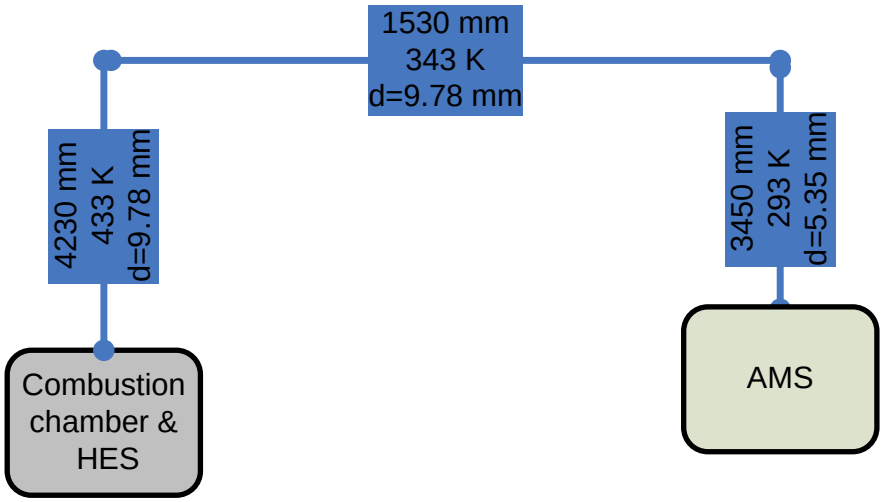

Figure 5: Idealized sampling line from the Hot End Simulator (HES) to the Aerosol Mass Spectrometer (AMS)

The simulation has been initialized with the data available at this time, as processing and analysing data can take quite a long time. Following the fuel analyses, the fuel sulphur content (FSC) has been set to 300 ppm (0.03% in mass). The sulphur conversion factor used was 2.5%, close to experimental results from PartEmis and other related work (Katragkou *et al.*, 2004; Sorokin *et al.*, 2004). The temperature has been assumed to vary instantaneously except for the drop from 343 K to 293 K where a 2 steps cooling has been used.

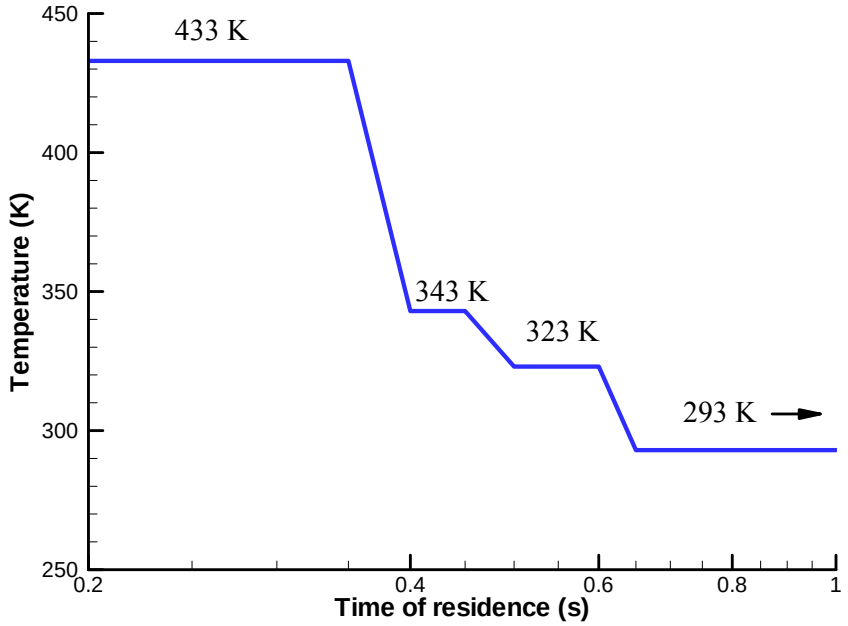

Figure 6: Evolution of the sample temperature in the "AMS line"

Without any dilution and with decreasing temperature, condensable species are likely to form new particles. Volatile particles have been simulated using such temperature drop and monitored at the significant times: 0.35 s, 0.45 s, 0.65 s, and at 5.15 s (end of the line).

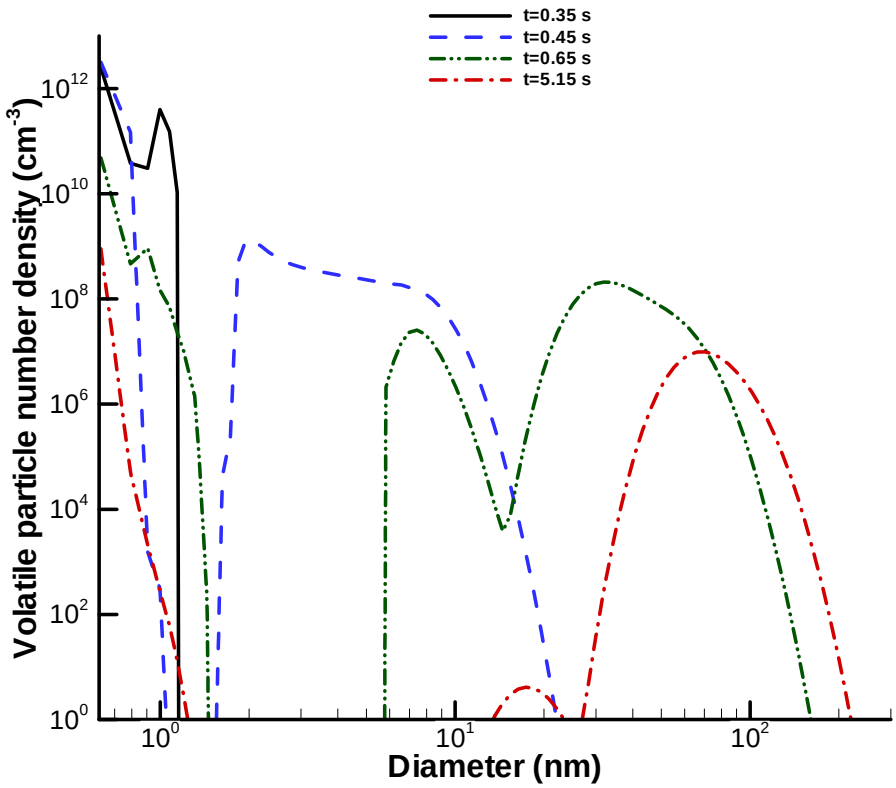

Figure 7: Volatile particles size distribution at 0.35 s, 0.45 s, 0.65 s and 5.15 s.

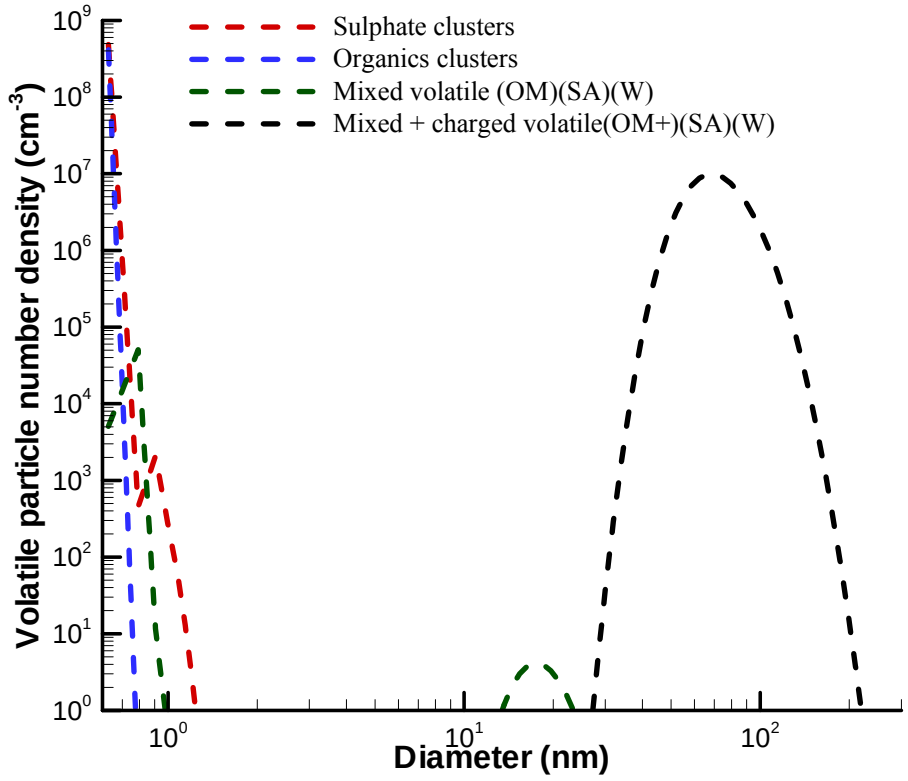

Figure 8: Contribution of the respective types of particles (only most significant plotted) to the total size distribution

Preliminary results must be considered with care as some critical data still need to be adjusted close to experimental results. Soot particles initial concentration need to be precisely determined as they grow by condensable matter uptake (more initial soot particles leads to smaller final sizes after growth).
The first results about volatile particles indicate that particles indeed form in the line and grow with increasing time of residence. Peak values of the size distribution (number density as a function of size) are close to 70 nm and 1.10^7. cm^{-3}. The distribution is initially made of clusters (organics and sulphate) as temperature remains quite high (433 K). With decreasing temperature, particles grow and their distribution exhibits two modes which later merge. The volatile particles are formed of organic matter (OM), sulphuric acid (SA) and water (W) and are positively charged which is mainly due to the method used to treat coagulation between charged particles. Negative and positive ions are initially equally distributed in the plume (assumption made at the nozzle exit) but their recombination processes are treated differently for the 2 charges.

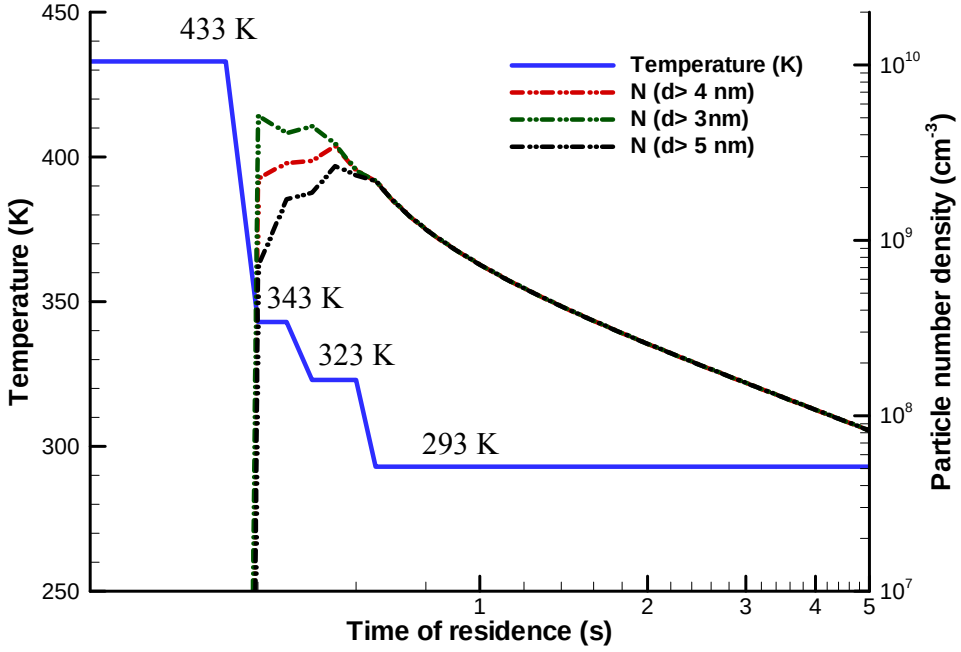

Figure 9: Evolution of the concentration of volatile particles respectively larger than 3, 4 and 5 nm.

Regarding volatile particles concentration plotted in figure 9, the results clearly show that the temperature decrease is responsible for saturation increase and thus for new particle formation. The number of volatile particles larger than 3 nm is maximum when the sample cools down to 343 K and is close to 5.10^9 cm^{-3}. Assuming average sample flow rates, concentrations of about 10^8 cm^{-3} can be expected close to the AMS but these results must be confirmed by additional calculations using more detailed data to fit the experimental conditions. One can also notice that the concentrations of particles larger than 3, 4 and 5 nm are quickly similar as all particles grow and get larger than 5 nm by coagulation.

The particles are affected during transport by sampling line effects, whatever their composition. In figure 10 are plotted the transmission factor for different times in the transport line when diffusion effects only are taken into account. Smaller particles get significantly affected in the first part of the line when the flow rate is rather high (between 0 s and 0.6 s). When the sample is conducted to the AMS through a low flow rate line (1 $l.min^{-1}$), larger particles are more affected but we can assume that this is mainly the effect of the time of residence.

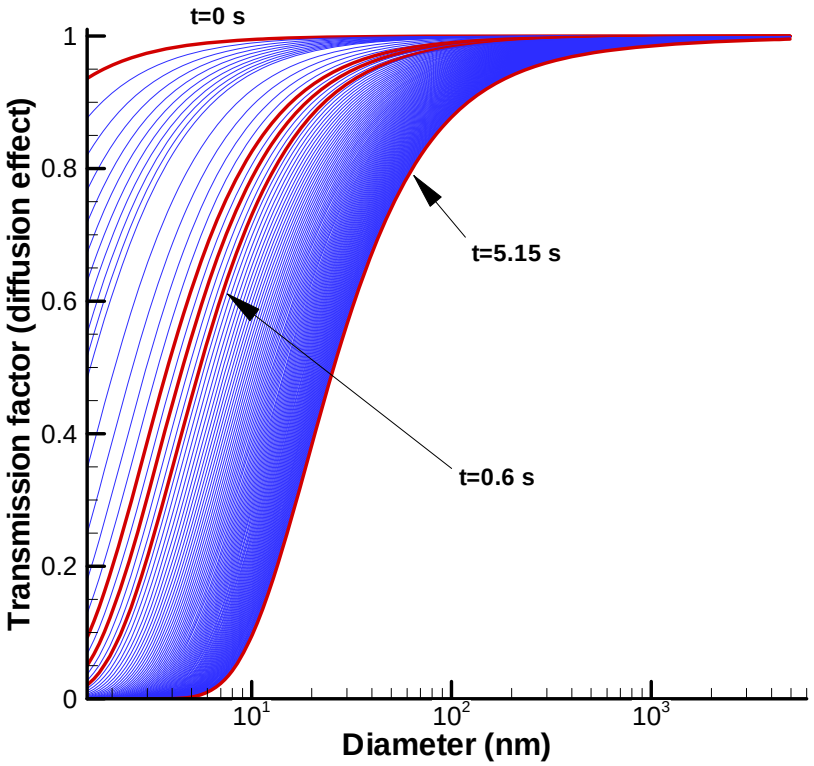

Figure 10: Transmission factor as a function of the particle size for diffusion processes only, at different times after the probe tip. Red curves correspond to temperature or flow rate changes.

3.2 "Hot dilution line"

The "hot dilution line" has been designed to minimize the formation of new particles. A 2 stage dilution comprising a high temperature diluter has been added so that condensable matter evaporates. The line has been modelled following the simple diagram in figure 11.

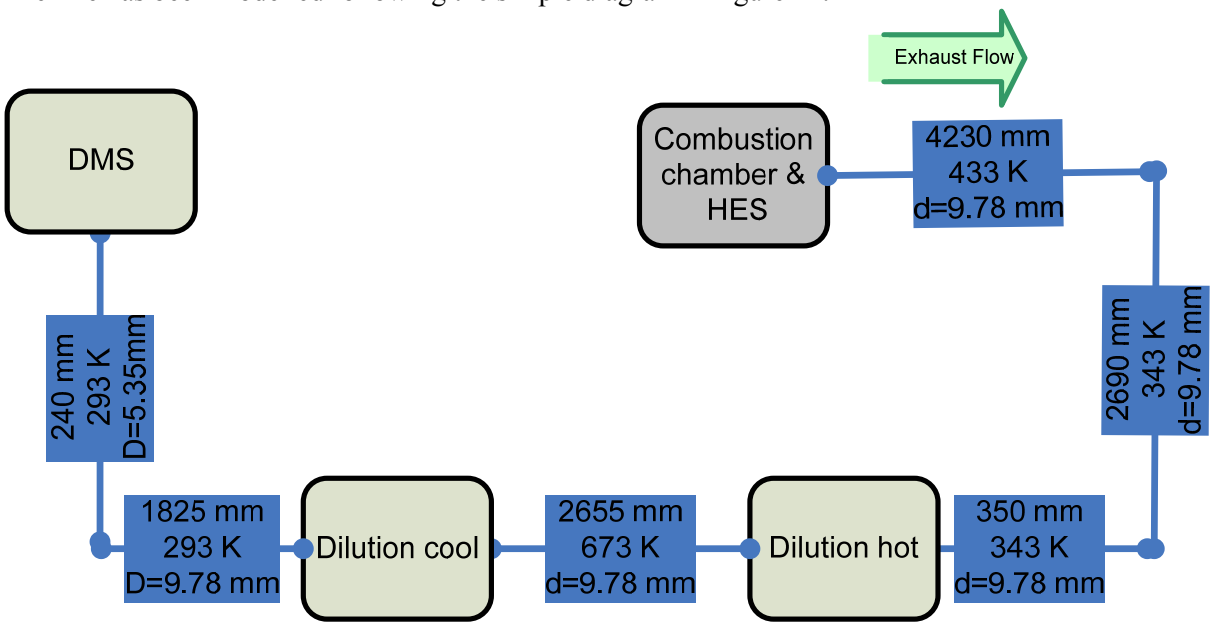

Figure 11: Diagram of the sampling line used for the simulations of the "hot dilution" case

The first calculations have been performed with a low time resolution to speed up the execution of the code and remain a first guess. Dilution ratios have been set to their theoretical values i.e. 1:10 and 1:10.

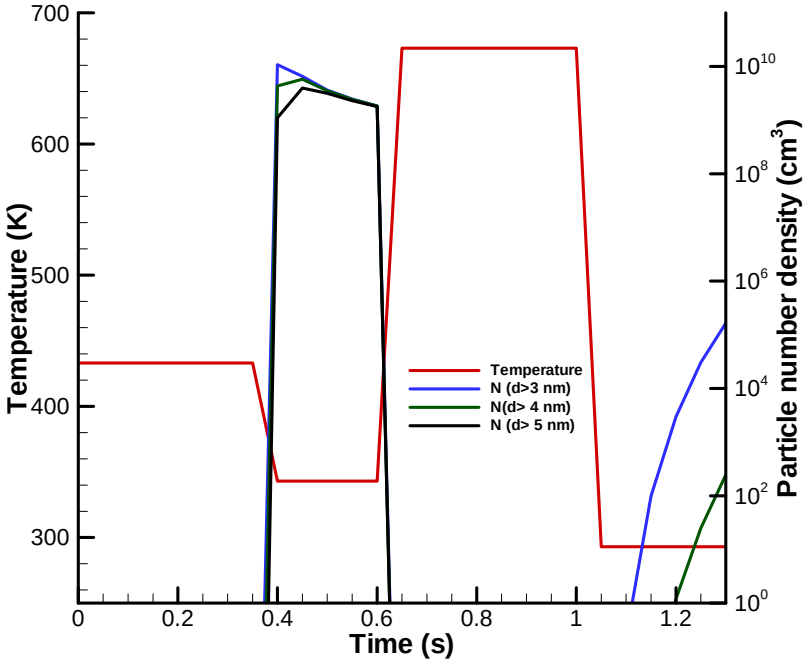

Figure 12: Time evolution of the sample temperature and the particle concentration larger than 3, 4 and 5 nm

The temperature evolution has been simulated assuming instantaneous changes. The sample was cooled down to 343 K and then heated to more than 600 K before being cooled down again to ambient conditions. The effect of the first temperature drop is visible as volatile particles form and reach a maximum value of 10^{10} cm^{-3} very quickly.

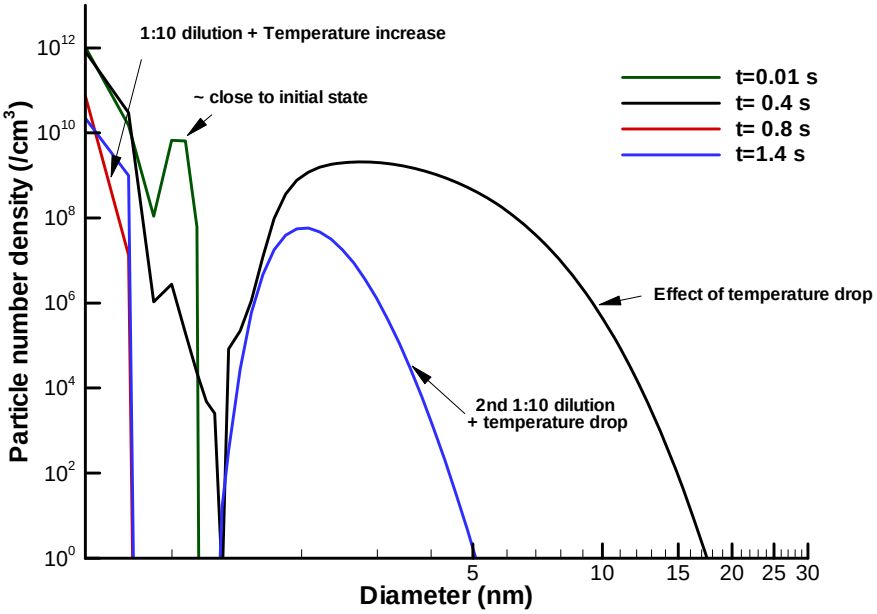

Figure 13: Volatile particles at 4 different regimes in the sampling line

They evaporate immediately as temperature increases but they finally nucleate again when temperature decreases, although the sample is 10 times diluted. This is confirmed by examining the size distribution evolution of volatile particles in figure 13.

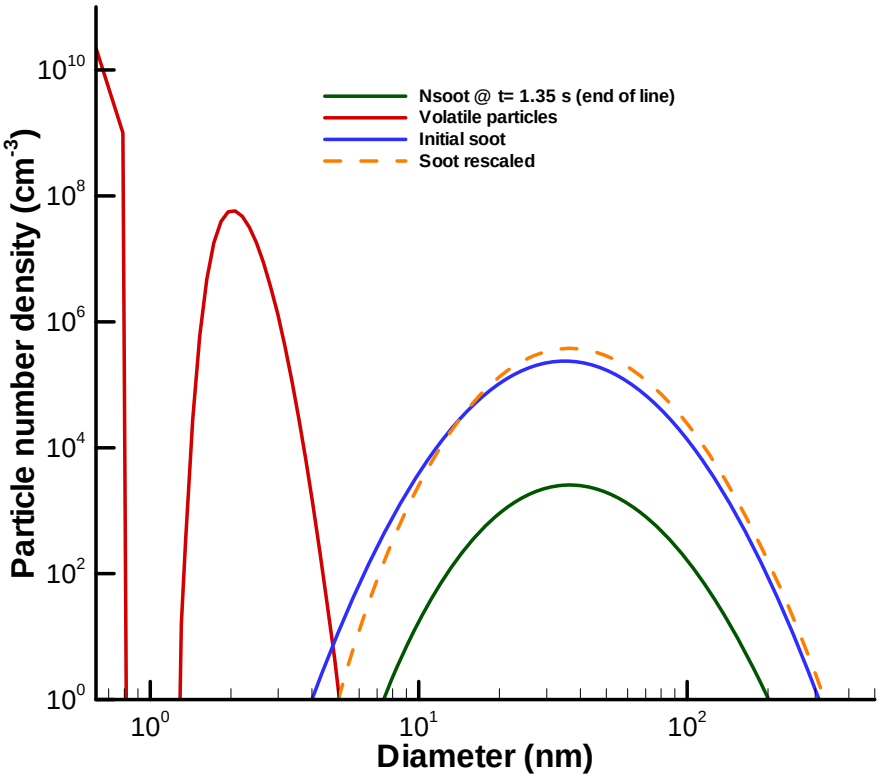

Figure 14: Volatile and soot particles size distribution at the end of the line. “Soot rescaled” means that soot concentrations have been corrected for dilution and temperature effect to allow a comparison with the initial distribution.

Figure 14 shows the number density at the end of the “hot sampling line”. Volatile particles remain quite small as the distribution peaks at about 3 nm. The dilution air has been assumed to be completely dry which a strong assumption to start with but we can suppose that water vapour was present in the diluting air at low concentration though. Soot particles have slightly grown even after the temperature increase up to 600 K but this growth is not very important.

4 Conclusion

A microphysical code has been developed for the SAMPLE study, to take into account multicomponent aerosol involving water vapour, sulphuric acid, organics, soot cores and chemi-ions. Some additional refinements have been found necessary to allow for realistic soot behaviour regarding condensation and evaporation. Finally, a size dependent particle loss module has been implemented to account for post sampling interaction between the particles and the tube. This point is also being improved to establish a hierarchy of the most critical parameters regarding particles loss (time of residence, flow velocity, turbulent or laminar regime etc.).
The first results are encouraging although some improvements are necessary and are still currently under progress. The calculations will especially be carried out a second time with increased resolution to minimize numerical artefacts and draw more robust conclusions. Note that additional calculations are now possible quite easily provided that the line properties are known.
Interesting results have been found for the two different lines studied:

- the model predicted that some particles form in the “AMS” line as there is no dilution and that temperature increases to ambient conditions, leading to an increase of the condensable vapours saturation ratios. These particles are composed of a mixture of sulphuric acid,

organics and water and can be larger than 100 nm. Interestingly, we found positively charged particles.

- Nucleation is clearly correlated to the sample thermodynamic changes (especially temperature).

- Particles even form in the hot diluted line, in spite of a 1:100 overall dilution with dry air. Volatile particles remain small however. Soot particles are also affected and the composition of their coating is available.

Some investigations are currently in progress. The results can be significantly improved using the following:

- The input data will be better adapted to SAMPLE as most of the data are now available. The soot particles initial distribution will be adjusted using an inverse method (from the point of measurement up to the probe tip)

- Particles formation and growth are very sensitive to the condensable matter initially available. The amount of sulphuric acid has been derived from the fuel analysis (300 ppm) and from the best estimate regarding previous studies (sulphur conversion=2.5%). Additional data on the sulphate concentrations would help. This point is also true for the amount of water vapour emitted and injected during dilutions

- Dilution factors need to be refined to fit to the experimental conditions and not only to the theoretical value

- Results need to be evaluated against experiments

Finally, the first part of the sampling line modelling already gives interesting results that will be improved in order to provide important data regarding sampling recommendations and expected behaviour of the particles in the line. The development and the first results can be seen as a successful attempt considering the timescale and are promising.

5 References

Baron P. A., K. Willeke, Aerosol Measurement. Principles, Techniques and Applications. Wiley Interscience, 2nd edition, 2005.

Katragkou, E., S. Wilhelm, F. Arnold, and C. Wilson, First gaseous Sulfur (VI) measurements in the simulated internal flow of an aircraft gas turbine engine during project PartEmis, *Geophys. Res. Lett.*, 31, L02117, doi:10.1029/2003GL018231, 2004.

Schumann U., F. Arnold, R. Busen, J. Curtius, B. Kärcher, A. Kiendler, A. Petzold, H. Schlager, F. Schröder, K.-H. Wohlfrom, Influence of sulphur on the composition on aircraft exhaust plumes: The experiments SULFUR 1-7, *J. Geophys. Res.*, 107, 10.1029/2001JD000813, 2002

Sorokin A., E. Katragkou, F. Arnold, R. Busen, U. Schumann, Gaseous SO_3 and H_2SO_4 in the exhaust of an aircraft gas turbine engine: measurements by CIMS and implications for fuel sulfur conversion to sulfur (VI) and conversion of SO_3 to H_2SO_4, *Atmos. Environ.*, 38, 449-456, 2004.

Vancassel X., A. Sorokin, P. Mirabel, A. Petzold, C. Wilson, Volatile particles formation during PartEmis: a modelling study, *Atmos. Chem. Phys.*, 4, 439-447, 2004

Yu F., R.P. Turco, The formation and evolution of aerosols in stratospheric aircraft plumes: Numerical simulations and comparisons with observations, *J. Geophys. Res.*, 103, 25915-25934, 1998.

Yu F., R. P. Turco, B; Kärcher, The possible role of organics in the formation and evolution of ultrafine particles, *J. Geophys. Res.*, 104, 4079-4087, 1999

SAMPLE campaign from 23 march 2009 to 02 april 2009, Port-Talbot UK
Transmission electron microscopy primary results technical report

By Delhaye David, ONERA, david.delhaye@onera.fr
With Ferry Daniel, CINaM, ferry@cinam.univ-mrs.fr

1 – Experiment

The aim of the work describe in this report was the characterization of the emission of a stable aircraft combustor. Experiments were carried out with the device used during the project "Partemis" [Wilson 2004]. The rig was fueled with JP-10 (0.03% Mass of Sulphur). Description of the rig and test conditions can be find in EASA report EASA.2008.OP.13.

Samples collection was performed with a 2 stages mini-impactor (figures 1 and 2) in which transmission electron microscopy (TEM) grids (300 meshes, carbon film, nickel grid) have been placed as impactor stage support [Kandler 2009].

Sampling was performed on a no-diluted line at two points from engine exit: 6.06 m and 10.05 m. Time of sampling ranged from 0.5 min to 5 min. Sampling flow inside the mini-impactors was around 6.150 L/min depending of rig conditions.

Figure 1 Two stages mini-impactor (left panel: holder; middle panel: nozzles and supports of TEM grids, right panel: experimental set-up)

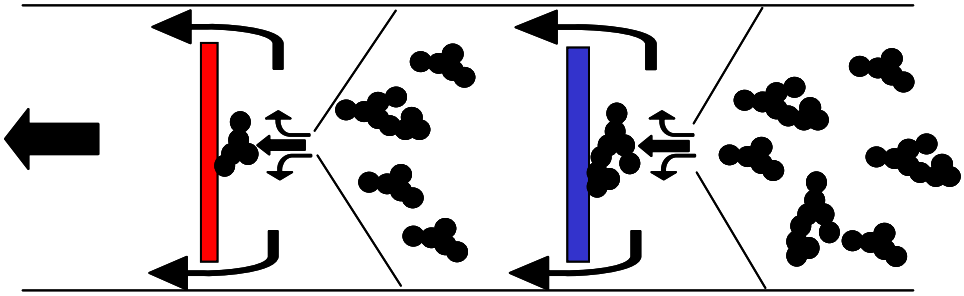

Figure 2 Principal of the mini-impactor, the biggest particles inside the flow are collected on the upper stage while the smallest one are fixed on the lower stage. The combination of the two stage allow removing of all soot particles.

2 – Analyses

Samples were analysed with a JEOL JEM-3010 microscope having a resolution of 1.6Å at 300 kV. The size distribution of primary particles was determined by measuring diameters of these latter via the free software ImageJ (figure 3).

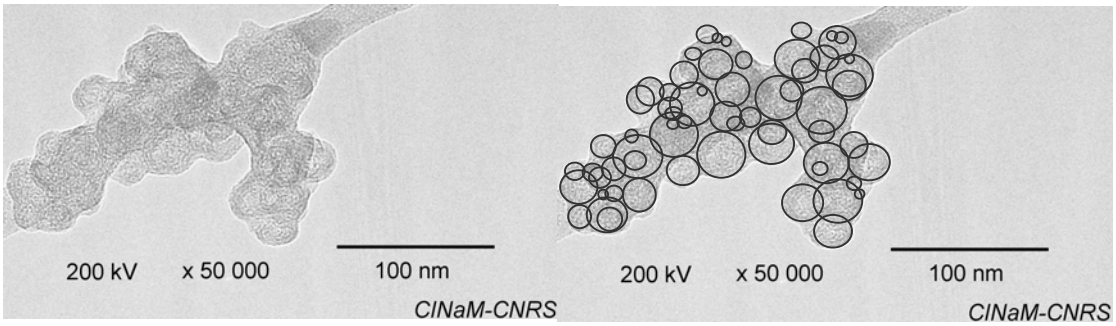

Figure 3 Agglomerate made of carbonaceous particle collected in the engine's exhaust as exemple of the data exploitation process. The left panel shows the original TEM picture and the right panel points out primary particles that constitute the agglomerate.

Then, the fractal dimension of the soot aggregates was established using Neer *et al.* [Neer 2006] equation that linked the projected area A of an aggregate to the mean projected area $\overline{A}_p$ of a primary particle with a mean diameter $\overline{d}_p$:

$$N = k_a\left(\frac{A}{\overline{A}_p}\right)^{\alpha} = k_a\left(\frac{4.A}{\pi.\overline{d}_p^{2}}\right)^{\alpha} \qquad (1)$$

where coefficients k_a and α have admitted values of 1.155 and 1.095 respectively. However, Meakin *et al.* [Meakin 1989] have also shown that when $N \le 10000$, coefficients α and k_a vary versus the number of the primary particles that compose of the aggregate. The equation that links projected areas A, $\overline{A}_p$, and the number of primary particles can be reformulated as:

$$\frac{A}{A_p} = 0.4784 \cdot N + 0.5218 \cdot N^{0.7689} \qquad (2)$$

Equations (1) and (2) allow us to determine more « reliable » values of k_a and α.

Using a common quasi-fractality assumption for soot aggregates, the projected fractal dimension of aggregates $D_{f,2D}$ is established by using the equation [ref]:

$$N = k_L\left(\frac{L}{\overline{d}_p}\right)^{D_{f,2D}} \qquad (3)$$

With L the aggregate maximal projected length, N the number of primary particles that the aggregates is made, and k_L a prefractal correlation constant.

We then determine the 3D fractal dimension $D_{f,3D}$ from $D_{f,2D}$ by applying the following equation, established in [Baron 2001]:

$$D_{f,3D} = D_{f,2D} \cdot \alpha \qquad (4)$$

with α the coefficient previously determined by combining of equation 1 and 2

3 – Results

Microscopy study is a time consuming study that why in this report only the low smoke number – low organic matter engine condition results are reported. The other engine conditions samples are under investigation.

A - Soot primary particle size distribution

TEM pictures reveal that samples are mainly made of soot. All soot aggregates are made of spherical primary particles (figure 4). All the primary particles have a turbostratic structure: $\overline{d_{002}} = 3.5 \pm 0.3$ Å.

Figures 5 represents soot primary particle size distributions established from 11 384 diameters measurements for the low smoke number – low organic matter condition. This size distribution exhibits a well defined log-normal behavior with small mean diameter values, much lower than 10 nm. Parameters of the distributions are reported in table 1.

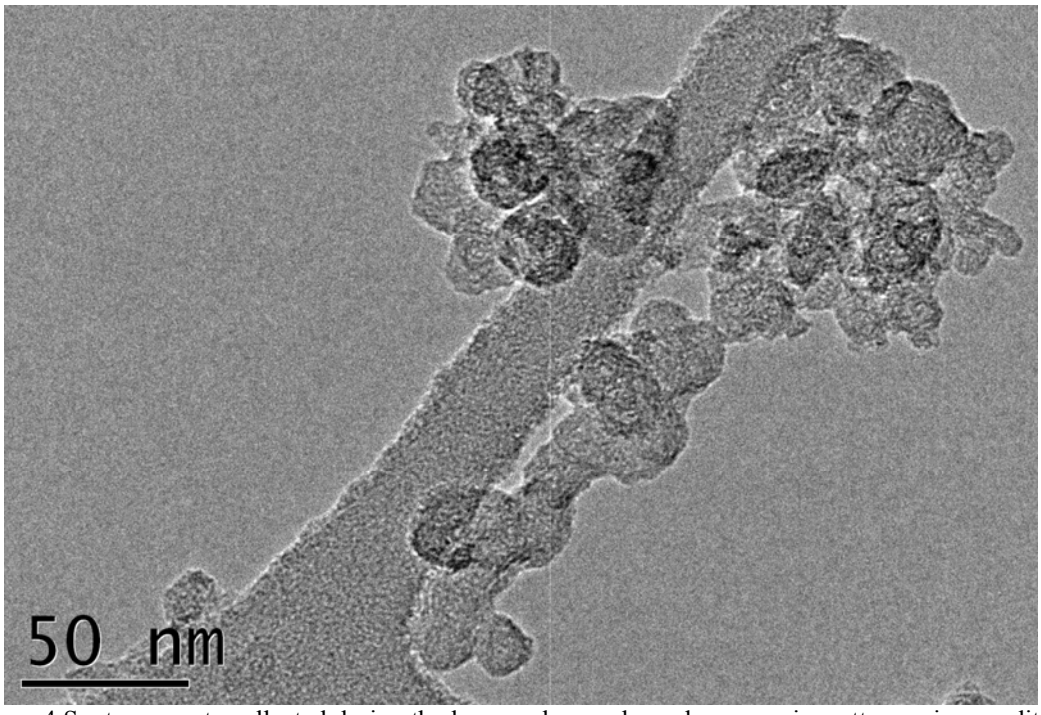

Figure 4 Soot aggregate collected during the low smoke number – low organic matter engine condition during project SAMPLE

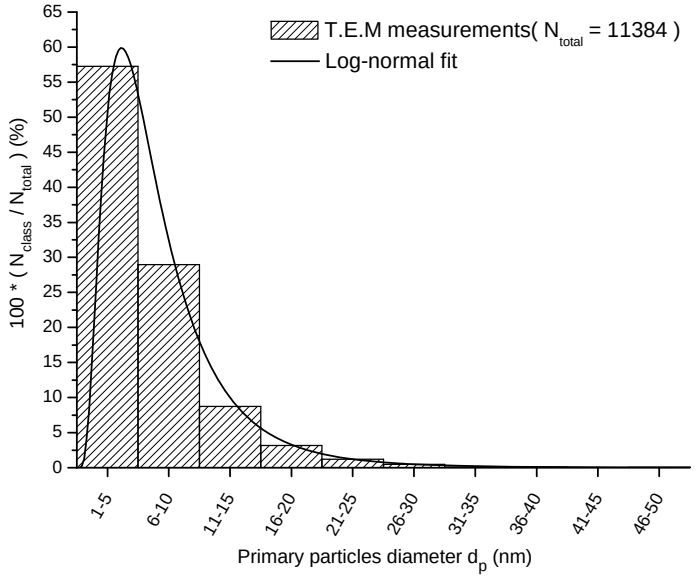

Figure 5 Soot primary particle size distributions during the low smoke number – low organic matter engine condition during project SAMPLE

Table 1 Soot primary particle size distribution parameters

	Low Smoke Number – Low organic matter
Number of diameter measurements	11 384
Type of distribution	Log-normal
Particulates mean diameter $\overline{d}_p$ (nm)	3.6 ± 0.1
Geometric standard deviation σ	1.92
Frequency of the mean diameter (%)	59.91
R^2	0.9999
k_a	1.3055
α	1.0378
Number of primary particles that compose agglomerates	$5 \leq N \leq 25000$

B - Fractal dimension of soot aggregates

Fractal dimension of soot aggregates was determined for 280 aggregates. The value determined, 1.88 ± 0.06 (figure 6), is similar to transport combustion process as automotive [Matti Maricq 2004] or biomass burning [Gwaze 2006][Schneider 2006]. The gyration diameter size distribution of those soot aggregate follow a log-normal law as commonly observed in litterature with a mean value of 52 ± 3 nm (figure 7). Table 2 summarizes values of fractal dimension and aggregate gyration diameter. However, time to time, we observed some really big spherical aggregate of soot (>500 nm) (figure 8). During the experiment, on-line techniques as SMPS or LII also

detected them. One explanation relates to the formation of a soot deposit just at the exit of the injector that broke sometimes and generate those "big" particles.

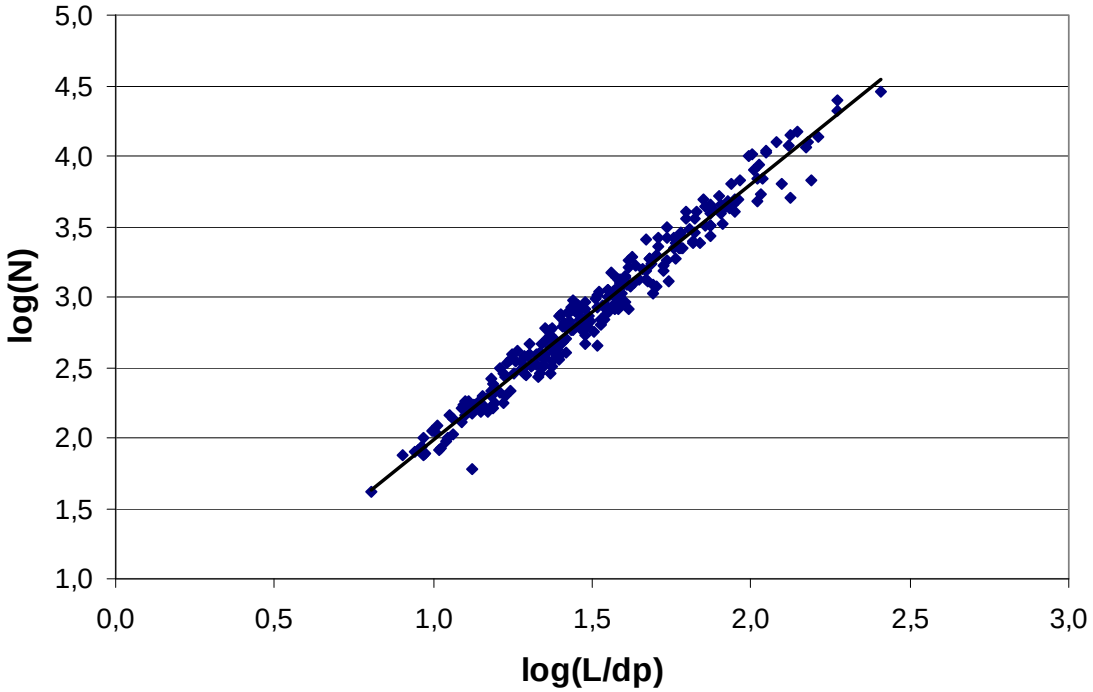

Figure 6 Soot aggregates fractal dimension determination from samples collected during low smoke number – low organic matter.

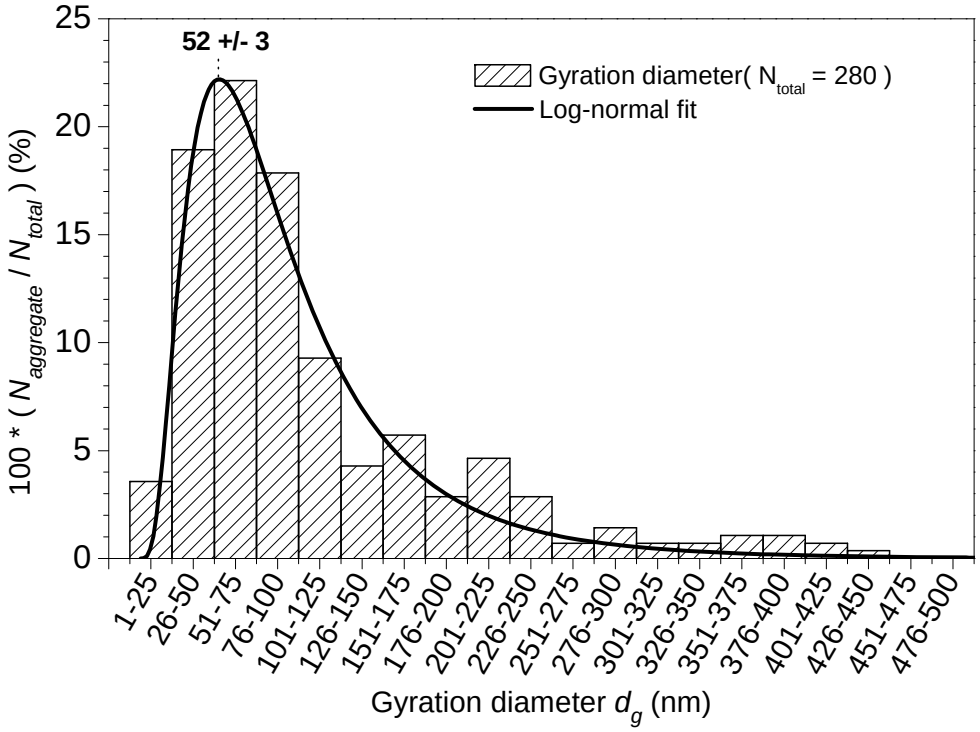

Figure 7 Soot aggregate gyration diameter size distributions during the low smoke number – low organic matter engine condition during project SAMPLE

Table 2 Fractal dimension of soot aggregates

	Low Smoke Number – Low organic matter
Number of soot aggregates studied	280
3D Fractal dimension $D_{f,3D}$	1.88 ± 0.06
R² (fractal dimension determination)	0.9708
Gyration diameter d_g (nm)	52 ± 3
Geometric standard deviation σ	1.94
Frequency of the mean diameter (%)	22.20
R²	0.9663

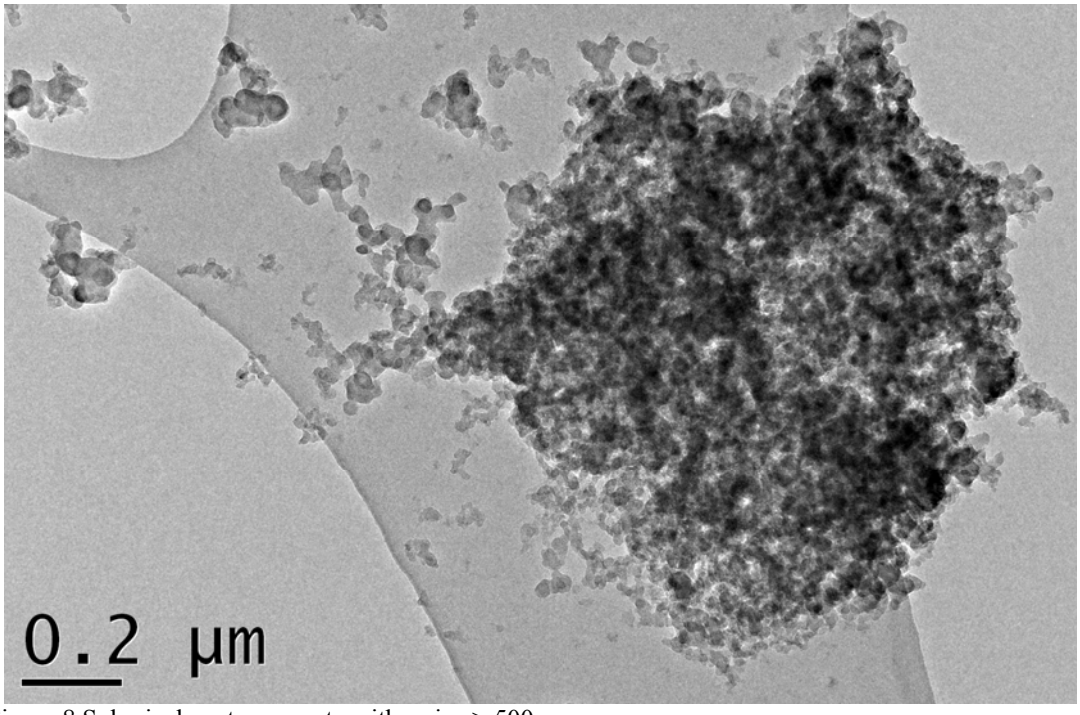

Figure 8 Spherical soot aggregate with a size > 500 nm.

4 – Conclusion

If we compare SAMPLE emitted soot primary particles to the similar ones studied in litterature [ECATS report D5.c.24 2008], we can conclude that their physical properties are closed. More than to be a representative quantitative soot source the combustor and Hot End Simulator (HES) produced also soot with similar properties to the ones emitted by aircraft engine at aggregate scale consideration as well as primary particle scale.

5 – Bibliography

[Baron 2001] Baron, P. A. And K. Willeke *Aerosol Measurement. Principle, techniques, and applications. 2sd Edition.* USA, Wiley-Interscience Ed., John Wiley & sons, Inc. (2001) ISBN : 13978-0-471-78492-0 / 100-471-18492-3 : 1129p

[ECATS report D5.c.24] ECATS report D5.c.24 (2008): Particle Emissions Measurement Report

[Gwaze 2006] Gwaze, P., O. Schmid, H.J. Annegarn, M.O. Andrae, J. Huth and G. Helas. *"Comparison of three methods of fractal analysis applied to soot aggregates from wood combustion"*. Aerosol Science 37 (2006) 820-838

[Kandler 2009] Kandler K. *"A miniature impactor for aerosol collection with emphasis on single particle analysis"*. European Aerosol Conference (2009) Karlshue, Germany

[Matti Maricq 2004] Matti Maric, M. and N. Xu *"The effective density and fractal dimension of soot particles from premixed flames and motor vehicle exhaust"*. Aerosol Science 35 (2004) 1251-1274

[Meakin 1989] Meakin, P., B. donn and G. Mulholland *"Collisions between Point Masses and Fractal Aggregates"*. Langmuir 5 (1989) 510-518

[Neer 2006] Neer, A. And U.O. Koylu *„effect of operating conditions on the size morphology, and concentration of submicrometer particulates emitted from diesel engine"*. Combustion and Flame 146 (2006) 142-154

[Schneider 2006] Schneider J., S., Weimer, F. Drewnick, S. Borrmann, G. Helas, P. Gwaze, O. Schmid, M.O. Andrae and U. Kirchner *„Mass spectrometric analysis and aerodynamic propertie of various types of combustion-related aerosol particles"*. International Journal of Mass Spectrometry 258 (2006) 37-49

[Wilson 2004] Wilson C.W. et al., *„Measurement and prediction of emissions of aerosols and gaseous precursors from gas turbine engines (PartEmis): an overview*". Aerospace Science and Technology, 8 (2004) 131-143

This page is intentionally blank.

EASA.2008.OP.13

Study on sampling and measurement of aircraft particulate emissions SAMPLE – Calibration Source Study

05 November 2009

Authors:

A. Petzold, A. Ibrahim

Institute of Atmospheric Physics, DLR Oberpfaffenhofen, 82234 Wessling, Germany

1 Introduction

During the EASA SAMPLE study techniques and methods for particulate matter measurement in the exhaust of aircraft engines at engine exit operational/flight conditions were tested and evaluated. Necessary information on instrument applicability and method characteristics under real-world conditions corresponding to engine certification measurements is provided. One major issue towards the definition of engine exhaust measurement procedures is the identification of potential aerosol sources for instrument calibration and testing in terms of quality assurance. So far there is no procedure agreed on how to calibrate instruments for particle number and particle mass.

Calibration is the set of operations that establish, under specified conditions, the relationship between the values of quantities indicated by a measuring instrument and the corresponding values realized by standards. In general, the calibration of an instrument can be performed in two ways:

1. Checking of the measuring instrument against a traceable standard, e.g. for mass, number and size.
2. Comparison of the measuring instrument with a “golden instrument”.

For particle size, there are polysterene latex spheres available which have specified size and can be used as a size standard. For particle mass concentration and particle number concentration, such standards are not available.

This report summarises tests using a commercially available laminar flame burner (CAST burner: http://www.sootgenerator.com/) which is known to be a very robust soot particle source. The main goal of these first studies was the investigation of instrument reproducibility in terms of mass and number emission.

2 Experimental Part

In the DLR laboratories a Real Soot Generator RSG miniCAST 6201-C was set up and operated at various conditions. The exhaust was sampled with a Multi-Angle Absorption Photometer (Thermo Scientific Model 5012) for the measurement of black carbon mass concentration and a Condensation Particle Counter (TSI Model 3025A) for the measurement of particle number concentrations. Both instrument principles are described in the SAMPLE Final Report.

In the CAST burner, soot particles are formed within a co-flow diffusion flame due to the hydrocarbon pyrolyse that takes place as a consequence of the heat provided by the oxidation at the flame front. The CAST burner enables the soot particles to escape from the flame without contact with oxygen. Subsequently the particle stream is mixed with a quenching gas in order to prevent further combustion processes in the particle stream and to stabilize the soot particles. The quenching inhibits condensation in the particle stream at ambient air condition. To dilute the particle stream, compressed air is supplied to the quenched particle stream. Figure 1 shows a scheme of the CAST principle. Figure 2 shows a schematic of the CAST set-up.

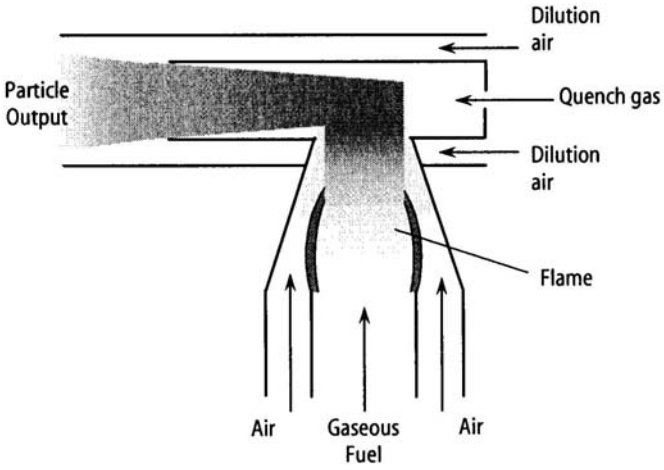

Figure 1. Working principle of th CAST burner.

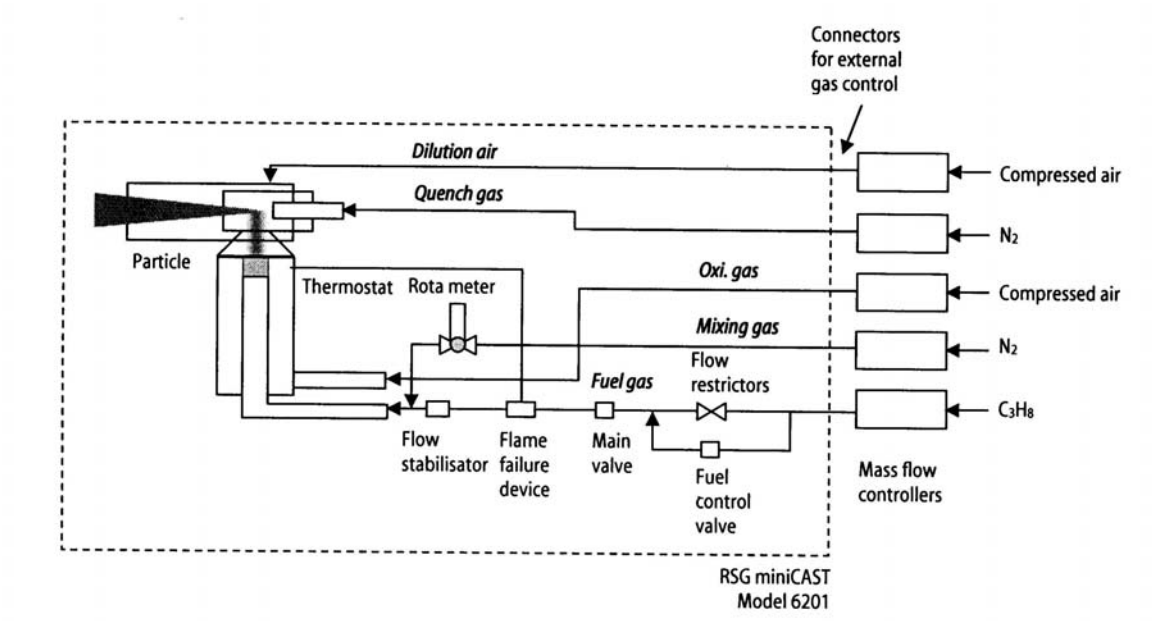

Figure 2. Schematic of the RSG miniCAST Model 6201.

The particle output provided by the miniCAST was diluted by a factor 1:100 using one Palas VKL 100s injection diluter stage. This sample dilution reduced the number and mass concentrations in the exhaust down to level measurable by the applied methods. The respective set-up is shown schematically in Figure 3, and in Figure 4 as a photograph.

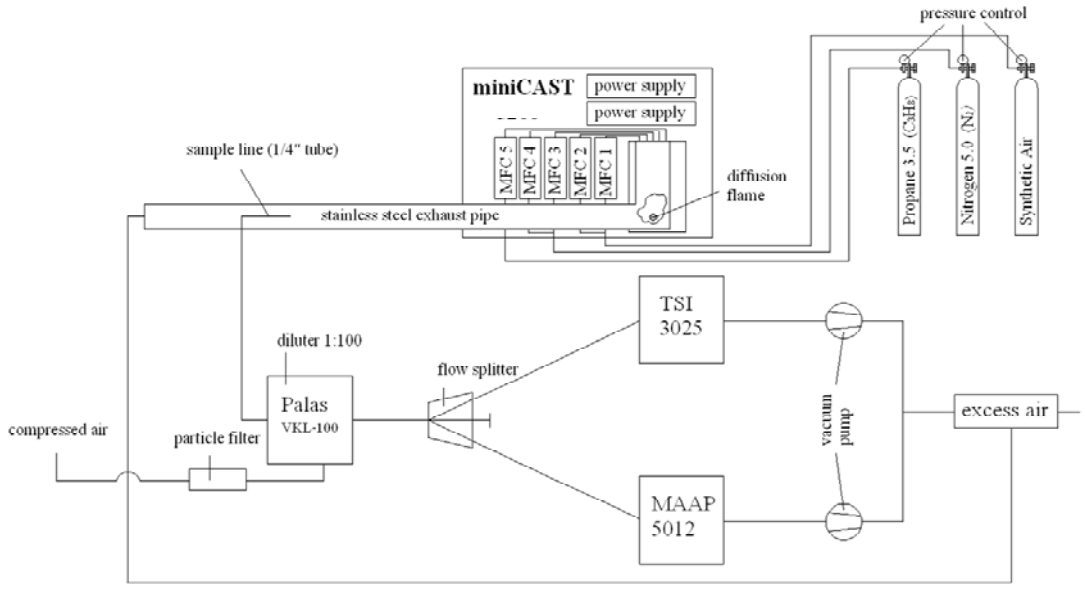

Figure 3. Experimental set-up in the DLR laboratories including the Palas VKL 1:100 dilution stage and the sampling instruments.

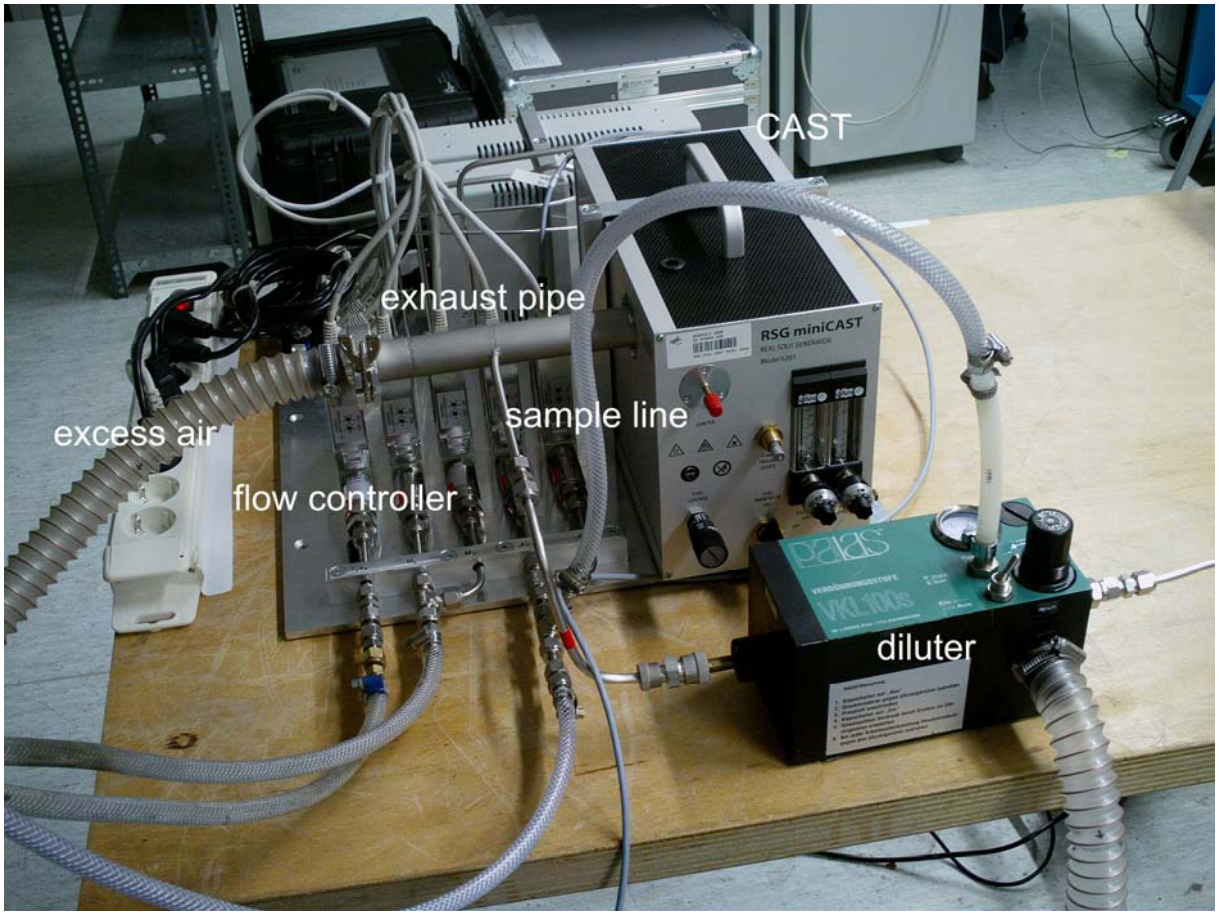

Figure 4. Photograph of the laboratory set-up.

3 Results

Table 1 summarises the operating conditions of the miniCAST burner during the tests. At stoichiometric conditions the fuel propane (C_3H_8) is characterised by an air-to-fuel ratio (AFR) of 15.5 by mass and of 23.9 by volume. For the tests, the burner was operated at fuel-lean conditions with equivalence ratios φ = 0.59 – 0.67. In principle, the burner allows the operation in the following ranges: oxidation air 0 - 1 l/min, C_3H_8 0.0 – 0.05 l/min.

Table 1 Operation conditions of the CAST burner.

miniCAST	Mass Flow (l/min)					Palas	
Condition:	Dilution Air	Oxidation Air	Quench Gas	Mixing Gas	Propane Gas	Dilution:	AFR by volume
#1	9.00	0.72	1.24	0	0.0180	1:100	40
#2	9.00	0.72	1.24	0	0.0184	1:100	39
#3	9.00	0.72	1.24	0	0.0191	1:100	37
#4	9.00	0.72	1.24	0	0.0198	1:100	36
#5	9.00	0.72	1.24	0	0.0202	1:100	36

Figure 5 shows an example of one run. The periodic variations of the number concentration are associated to the operation of the mass flow controllers. Smoothing the CPC data on a basis of 15 sec (blue line) shows the constant output of the burner. Each run lasted at least 15 minutes in order to average the periodic variation of the exhaust.

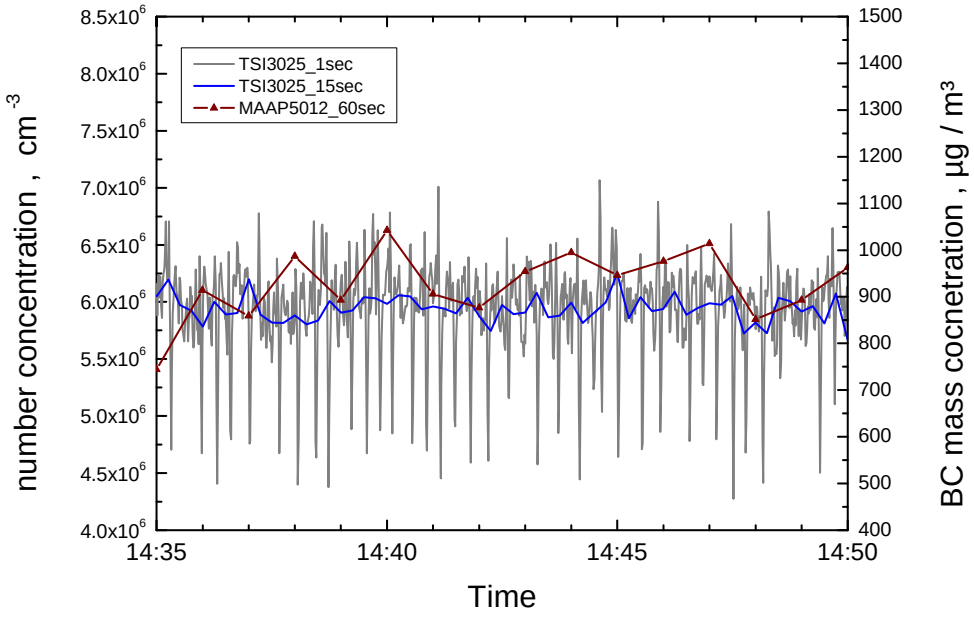

Figure 5. Example of one miniCAST run showing black carbon (BC) mass concentration and particle number concentration in the exhaust. The particle number concentration is given as 1 Hz data and as 15 sec average data.

Table 2. Average values (_av) and standard deviations (_sd) for propane flow, MAAP Black Carbon mass concentration and CPC number concentration. All concentration values are corrected for the dilution factor of 1:100.

Condition	Propane_av l/min	Propane_sd l/min	BC_av_60s µg/m³	BC_sd_60s mg/m³	CPC_av_1s #/cm³	CPC_sd_1s #/cm³
1	0.0180	3.6E-06	85	30	1.15E+06	5.88E+05
1	0.0180	5.4E-05	57	20	6.19E+05	2.88E+05
2	0.0184	5.3E-06	204	52	2.25E+06	6.55E+05
2	0.0184	5.3E-06	252	79	2.76E+06	5.05E+05
3	0.0191	3.4E-06	845	70	5.67E+06	4.35E+05
3	0.0191	3.2E-04	999	79	5.43E+06	1.02E+06
4	0.0198	1.8E-05	1631	293	7.03E+06	9.98E+05
5	0.0202	5.5E-05	1791	219	7.70E+06	8.21E+05

Table 2 compiles the results from the repetitive runs of the miniCAST burner. All values are given for ambient conditions (295 K, 936 hPa). MAAP values are recorded as 1 min average data. Number concentration values are recorded as 1 Hz data. Respective graphical representations are given in Figures 6 and 7 for Black Carbon mass concentration and particle number concentration, respectively.

As can be taken from Figure 6, the small variation of the fuel flow from 0.018 l/min to 0.020 l/min produces a factor of 20 in mass concentration output. Hence careful control of the gas flows is strictly required. The number concentration illustrated in Figure 7 does not increase in the same range, because during particle interaction in the exhaust gas, particle mass in conserved, but particle number concentration and particle size are connected by particle coagulation, i.e., at higher mass output, larger particles will form from coagulation of primary particles.

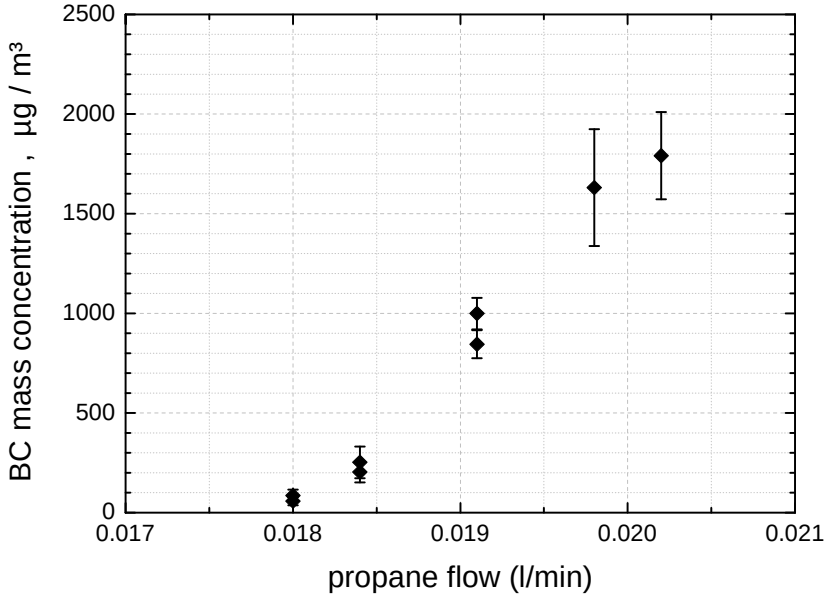

Figure 6. Black carbon mass concentration measured in the miniCAST burner exhaust by means of a MAAP.

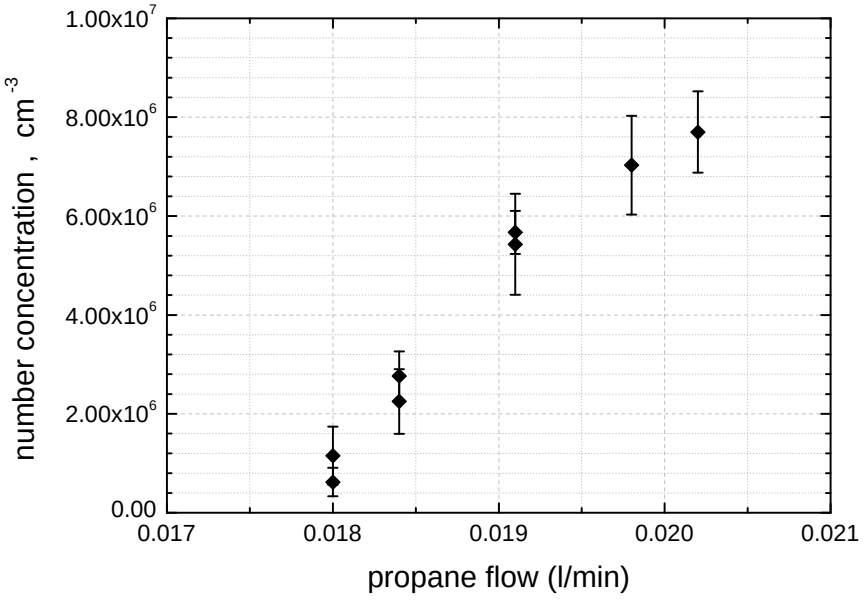

Figure 7. Particle number concentration measured in the miniCAST burner exhaust by means of a condensation particle counter of type TSDI 3025A.

4 Summary

The RSG miniCAST is capable of producing a stable and reproducible output of combustion particles with respect to black carbon mass and particle number concentration.

Repetitive measurements at the same operating condition provided similar mass concentration values. Small variations in values are indistinguishable on a statistical basis.

5 Recommendations

The RSG miniCAST is a good candidate for a portable soot source which can be used for operational checks of instruments applied for gas turbine exhaust measurements.

Further studies on the RSG miniCAST are required in to determine the generator accuracy and reproducibility by comparing two different RSGs operated at similar conditions by different organisations.

Finally, work is required to develop a ‘traceable standard’ or ‘golden instrument’ against which individual portable sort sources, such as the RSG miniCAST, could be calibrated.